



**This electronic thesis or dissertation has been
downloaded from Explore Bristol Research,
<http://research-information.bristol.ac.uk>**

Author:
Birchall, James

Title:
UE Uplink Power Distribution for M2M over LTE

General rights

Access to the thesis is subject to the Creative Commons Attribution - NonCommercial-No Derivatives 4.0 International Public License. A copy of this may be found at <https://creativecommons.org/licenses/by-nc-nd/4.0/legalcode>. This license sets out your rights and the restrictions that apply to your access to the thesis so it is important you read this before proceeding.

Take down policy

Some pages of this thesis may have been removed for copyright restrictions prior to having it been deposited in Explore Bristol Research. However, if you have discovered material within the thesis that you consider to be unlawful e.g. breaches of copyright (either yours or that of a third party) or any other law, including but not limited to those relating to patent, trademark, confidentiality, data protection, obscenity, defamation, libel, then please contact collections-metadata@bristol.ac.uk and include the following information in your message:

- Your contact details
- Bibliographic details for the item, including a URL
- An outline nature of the complaint

Your claim will be investigated and, where appropriate, the item in question will be removed from public view as soon as possible.

UE Uplink Power Distribution for M2M over LTE

BY

JAMES RICHARD BIRCHALL



Department of Engineering

UNIVERSITY OF BRISTOL

A dissertation submitted to the University of Bristol in accordance with the requirements of the degree of DOCTOR OF PHILOSOPHY in the Faculty of Engineering.

September 2018

Word Count: 34,956

Abstract

MACHINE to Machine (M2M) communications are a rapidly expanding subset of the Internet of Things (IoT)¹. Example scenarios include small wireless sensor networks, which may only transmit small amounts of data a few times a day; being constrained by a finite and small battery life. This thesis examines the use of 4G (LTE) mobile communications for M2M, and how power consumption may be optimised. Whilst 4G may not be the most efficient way to communicate, the network ubiquity makes ease of deployment a highly attractive option. With this low efficiency, every possible technique should be considered to recover system efficiency, and increase battery life.

The approach to this problem involves analysis of LTE signals, measurement and modelling of power consumption in real devices, and evaluation of candidate hardware techniques to improve efficiency. Hardware in the loop methods are used extensively, based on simulated and live networks to verify benefit.

For LTE signals, correlation is observed between the signal envelope, and degrees of freedom within the system, such as bandwidth and modulation scheme. This allows the operating point of the power amplifier to be altered to reflect the current signal characteristics without the need to continually monitor the envelope, enabling low cost efficiency enhancement.

Energy consumption of LTE modems was measured and modelled for a variety of use cases to produce information aimed at selecting appropriate transmission profiles. In order to remain energy competitive with other long range systems, LTE modems should be used in a high latency mode, accepting an increase in cold start time.

Load modulation and dynamic power supply technologies are investigated for low speed modulation based only on MAC layer information in order to increase system efficiency. Improvements of up to ten percentage points in Power Added Efficiency across a reasonable range of output power values have been demonstrated.

¹GSMA Intelligence, "Cellular M2M forecasts and assumptions : 2010 - 2020," September, 2014. [Online]. Available: <https://www.gsma.com/iot/wp-content/uploads/2016/09/GSMA-Intelligence-Cellular-M2M-forecasts-2010-2020.pdf>

Author's declaration

I DECLARE that the work in this dissertation was carried out in accordance with the requirements of the University's Regulations and Code of Practice for Research Degree Programmes and that it has not been submitted for any other academic award. Except where indicated by specific reference in the text, the work is the candidate's own work. Work done in collaboration with, or with the assistance of, others, is indicated as such. Any views expressed in the dissertation are those of the author.

SIGNED:

DATE:

Copyright

Attention is drawn to the fact that the copyright of this thesis rests with the author. This copy of the thesis has been supplied on condition that anyone who consults it is understood to recognise that its copyright rests with the author.

Contents

Preliminaries	iii
Abstract	iii
Author's declaration	v
Contents	x
List of Figures	xi
List of Tables	xv
List of Abbreviations	xvii
List of Symbols	xxi
List of Publications	xxiii
 1 Introduction & Motivations	 1
1.1 Machine to Machine Communications	1
1.2 The Drive for Efficiency	3
1.2.1 Signals Analysis	3
1.2.2 Power Amplifier Operation	3
1.3 Conclusion	5
1.4 Thesis Overview & Contributions to State of the Art	5
 2 A Technical Overview of LTE	 9
2.1 Introduction	9
2.2 LTE	10
2.2.1 Modulation	10
2.2.2 Resource Allocation	12
2.2.3 TX Procedure	13
2.2.4 Error Measurement	15
 3 Waveform Analysis for Efficiency Enhancement Schemes	 17
3.1 Current State of the Art	18
3.2 Metrics, Requirements & Tools	19
3.2.1 Metrics	19
3.2.2 ACLR	21
3.2.3 Standards Requirements	22
3.2.4 PAPR Distribution	23
3.2.5 MATLAB LTE Toolbox	23
3.3 Subframe Analysis	25

3.3.1	Modulation Scheme	26
3.3.2	Bandwidth	27
3.4	Hardware Verification	30
3.4.1	Signal Envelope	31
3.4.2	Measured Power Distribution	34
3.5	Other Measurements & Analysis	38
3.5.1	Symbol Level Analysis	38
3.5.2	Rate Constraint	40
3.6	Conclusion	41
4	Network Deployments & Power Consumption	43
4.1	Introduction	44
4.2	Power Consumption Model	44
4.2.1	Power	45
4.2.2	Duration	46
4.2.3	Idle Time	46
4.3	Current State of the Art	47
4.4	Hardware Design	51
4.4.1	Overview	51
4.4.2	Current sensing	52
4.4.3	Noise Analysis	53
4.4.4	Instrumentation Interface (LabVIEW)	56
4.4.5	Calibration	57
4.5	Base Station Emulator	57
4.5.1	Phase I Work on Connectivity	58
4.5.2	Phase I Throughput measures	59
4.6	Phase I Modelling	63
4.6.1	Objectives	63
4.6.2	Test Setup	63
4.6.3	Methodology	64
4.6.4	Power Consumption Analysis	64
4.6.5	Additional Device States	65
4.6.6	Conclusion	66
4.7	Phase II Network Based Measurements	68
4.7.1	Aims	68
4.7.2	Measurement Set-up	68
4.7.3	LabVIEW Instrumentation Interface	69
4.7.4	Network Measurement Results	70
4.7.5	Conclusion	73
4.8	Sigfox comparison	75
4.8.1	Experimental Results	78
4.8.2	LTE Versus Sigfox	80
4.9	Conclusion	83

5	Power Amplifier Dynamic Load Modulation	85
5.1	Introduction	86
5.2	LTE Physical Layer & Terminology	86
5.2.1	A Note on Plotting & Terminology	89
5.3	Current State of the Art	90
5.4	Hardware & Measurements	93
5.4.1	Circulators & Power Calibration	94
5.4.2	Dynamic Power Supply	95
5.4.3	Mechanical Impedance Tuner	96
5.4.4	Power Sensors	96
5.4.5	Base Station Emulator	97
5.4.6	UE	98
5.4.7	Entire Test Set-up	99
5.5	Practical Attempts at Improvement	99
5.5.1	What we are trying to achieve	99
5.5.2	Measurement Set-up	100
5.5.3	Results	102
5.5.4	Discussion	103
5.5.5	Continuous Wave Measurements	104
5.6	Digital Tuning	105
5.6.1	DTC Analysis	106
5.6.2	Contour diagram	110
5.6.3	Further Tuning	112
5.6.4	Discussion	113
5.7	Conclusion	115
6	Further Power Amplifier Design Techniques	117
6.1	Introduction	118
6.2	Publications	118
6.2.1	Hitting The Sweet Spot	118
6.2.2	Triple Band Power Amplifier	120
6.2.3	Asymmetrical Outphasing	121
6.3	Conclusions	122
7	Conclusions & Further Work	123
7.1	Conclusions	123
7.1.1	Summary of Research Contributions	123
7.1.2	Relevance to 5G / NB-IoT	125
7.2	Recommendations to Communications Stakeholders	126
7.2.1	Standards Bodies	126
7.2.2	Base Station Vendors / Networks	126
7.2.3	UE Manufacturers	127
7.3	Future Work	127
7.3.1	Network Measurements	128
7.3.2	Load Pull	128

7.4 Final Comments	129
A Labview Data Acquisition	131
B Python Code for Network Measurements	135
B.1 GUI	135
B.2 MQTT	135
C Matlab Code	137
C.1 Signal Power Simulations	137
C.2 Network Deployment Power Consumption	137
C.3 Load Modulation Experiments	138
D Project Plan	139
References	150

List of Figures

1.1	Growth of M2M communications.	2
1.2	M2M communications use cases.	2
1.3	Compression at high output powers.	4
2.1	A comparison of OFDMA and SC-FDMA.	10
2.2	SC-FDMA modulation.	12
2.3	LTE resource allocation grid.	13
2.4	Transport block size as a function of bandwidth and MCS.	14
3.1	PDF of an LTE signal normalised to peak power.	20
3.2	ACLR of an LTE signal.	21
3.3	LTE Toolbox environment displaying frequency and time domain signal representations.	24
3.4	Simulation of time domain waveform.	25
3.5	PAPR of variable MCS.	26
3.6	CCDF of PAPR for variable MCS.	27
3.7	PAPR of variable BW.	28
3.8	CCDF of PAPR over a variable bandwidth.	29
3.9	PAPR of variable BW - narrow band.	30
3.10	CCDF of PAPR of variable BW - narrow band.	30
3.11	Scope capture of time domain waveform.	32
3.12	VSA capture of time domain waveform.	33
3.13	Measured power distribution for MCS-10.	34
3.14	Measured power distribution for MCS-11.	35
3.15	Measured CCDF for MCS-10; Toby L210 modem, 10MHz bandwidth, E6601A analyser.	35
3.16	Measured CCDF for MCS-11; Toby L210 modem, 10MHz bandwidth, E6601A analyser.	36
3.17	Measured CCDF for 1.4MHz; Toby L210 modem, E6601A analyser.	37
3.18	Measured CCDF for 5MHz; Toby L210 modem, E6601A analyser.	38
3.19	Resource grid population.	39
3.20	PAPR over 14 symbols.	40
3.21	Configurations for limited uplink rate, data rate coloured as kB per second.	41
4.1	Factors affecting TX energy consumption.	45
4.2	UE power states.	47

4.3	Toby L210 LTE modem.	52
4.4	Data flow of power measurement apparatus, developed by the author.	52
4.5	Schematic of power measurement apparatus, including high dynamic range capability.	53
4.6	Instrumentation amplifier configuration.	54
4.7	Power measurement hardware.	56
4.8	Functional LTE test rig.	58
4.9	CCDF profile for idle, data and video transfer.	62
4.10	RX power modelling.	65
4.11	TX power modelling.	66
4.12	Transition from sleep to standby.	67
4.13	Block diagram of measurement hardware.	69
4.14	Photograph of measurement hardware.	70
4.15	Power profile - lab setup.	71
4.16	Power profile - external network.	72
4.17	Distribution of time spent transmitting.	73
4.18	Energy used per transmission - lab setup.	74
4.19	Energy used per transmission - network setup.	75
4.20	TX power distribution - external network.	76
4.21	Sigfox packet structure	77
4.22	MKRFOX1200 board.	77
4.23	MKRFOX1200 5V transmission power profile.	78
4.24	MKRFOX1200 transmission power distribution.	79
4.25	MKRFOX1200 transmission power profile.	80
4.26	MKRFOX1200 3V transmission power distribution.	81
4.27	Comparison of M2M technologies.	82
5.1	Block diagram of proposed schemes; (a) load pull, (b) load pull and DPS.	87
5.2	Envelope power distribution of a 1.4MHz LTE signal.	89
5.3	Smith chart terminology	90
5.4	Duplexing test arrangement.	94
5.5	HP 6624A power supply & Agilent E6621A base station emulator.	95
5.6	Focus 1808 iTuner.	96
5.7	Full test set-up.	99
5.8	Toby measurements as a source.	101
5.9	Skyworks PA output power sweep - 50 resource blocks.	102
5.10	Photograph of measurement setup.	103
5.11	Amplifier PAE for an output power sweep.	104
5.12	Smith chart coverage for standard and DPS load pull.	105
5.13	Optimum load pull Trajectories for CW operation.	106
5.14	Tuner insertion loss for optimum states.	107
5.15	DTC parasitics model.	107
5.16	DTC initial PCB, populated.	108
5.17	DTC series states.	108
5.18	DTC shunt states.	109

5.19	DTC series / shunt states.	110
5.20	95% peak PAE bounds for a single optimum trajectory.	111
5.21	DTI S_{11} with additional series capacitance.	113
5.22	DTI S_{21} with additional series capacitance.	114
6.1	Optimisation block diagram.	119
6.2	Optimisation results.	120
A.1	LabVIEW Data acquisition flow	133

List of Tables

2.1	LTE bandwidths.	13
2.2	LTE UE EVM limits.	15
2.3	E-UTRA ACLR constraints.	16
2.4	UTRA ACLR constraints.	16
3.1	Mean and standard deviation of subframe PAPR.	26
3.2	Mean and standard deviation of system PAPR.	28
3.3	Mean and standard deviation of NB PAPR.	29
3.4	Hardware and simulation comparison for MCS.	37
3.5	Hardware and simulation comparison for bandwidth.	38
4.1	Front end minimum detectable current values.	56
4.2	Front end detectable signals for single stage optimisation.	56
4.3	Calibration values.	57
4.4	Initial IP address setup.	59
4.5	Additional model components.	66
4.6	MKRFOX1200 performance.	79
4.7	MKRFOX1200 performance - 3V supply.	80
4.8	Toby L210 performance.	81
5.1	DTC parasitics values.	106
A.1	ADC Input Signals	131

List of Abbreviations

2G	second generation mobile communications
16-QAM	16 symbol quadrature amplitude modulation
64-QAM	64 symbol quadrature amplitude modulation
3G	3rd generation mobile communications
3GPP	3rd Generation Partnership Project
4G	4th generation mobile communications
5G	5th generation mobile communications
ACB	access class barring
ACK	acknowledgement
ACLR	adjacent channel leakage ratio
ADC	analogue to digital converter
AGC	automatic gain control
AGTI	Access Grant Time Interval
AM	amplitude modulation
APT	average power tracking
bps	bits per second
BPSK	binary phase shift keying
BSE	base station emulator
CCDF	complimentary cumulative distribution function
CMOS	complementary metal oxide semiconductor
COTS	commercial off the shelf
CQI	channel quality information
C-RNTI	cell radio network temporary identifier
CW	continuous wave
DC	direct current
DFT	discrete Fourier transform
DFT-S-OFDM	discrete Fourier transform spread orthogonal frequency division multiplexing
DHCP	dynamic host configuration protocol
DPS	dynamic power supply
DRS	demodulation reference signal
DRX	discontinuous reception
DSP	digital signal processing
DTC	digitally tunable capacitor
DUT	device under test .
EMI	electro-magnetic interference

eNB	evolved node B
EPS	evolved packet system
E-UTRA	evolved universal terrestrial radio access
EVM	error vector magnitude
FDD	frequency domain duplexing
FDMA	frequency division multiple access
FET	field effect transistor
GaAs	Gallium Arsenide
GFSK	Gaussian frequency shift keying
GSM	Global System for Mobile communication
GPiB	general purpose interface bus
GUI	graphical user interface
H2H	human-to-human
HARQ	hybrid automatic repeat request
IC	integrated circuit
IDFT	inverse discrete Fourier transform
IMD3	third order intermodulation product
IP	internet protocol
ISM	industrial, scientific and medical
LED	light emitting diode
LNA	low noise amplifier
LPWA	low power wide area
LTE	Long Term Evolution
LTE-A	Long Term Evolution advanced
M2M	machine-to-machine
MAC	medium access control
MCS	modulation and coding scheme
MEMS	micro-electro-mechanical systems
MMIC	microwave monolithic integrated circuit
MQTT	message queuing telemetry transport
MTC	machine-type-communication
NB-IoT	narrow band internet of things
NI	National Instruments
OFDMA	Orthogonal Frequency Division Multiple Access
OMN	output matching network
OSSS	orthogonal sequence spread spectrum
PA	power amplifier
PAE	power added efficiency
PAPR	peak-average power ratio
PCB	printed circuit board
PDCCH	physical downlink control channel
PDF	probability density function
PDP	packet data protocol
PL	path loss
PRACH	physical random access channel

PSS	primary synchronisation signal
PUCCH	physical uplink control channel
PUSCH	physical uplink shared channel
QAM	quadrature amplitude modulation
QoS	quality of service
QPSK	quadrature phase shift keying
RACH	random access channel
RAT	radio access technology
RB	resource block
RF	radio frequency
RFIC	radio frequency integrated circuit
RMC	reference measurement channel
RMS	root mean square
RNDIS	remote network driver interface specification
RPi	Raspberry Pi
RRC	radio resource control
RX	receiver
SC-FDMA	single carrier frequency division multiple access
SDR	software defined radio
SIM	subscriber identity module
SMT	surface mount
SNR	signal to noise ratio
SRS	sounding reference signal
SPI	serial peripheral interface
SSS	secondary synchronisation signal
TBS	transport block size
TDD	time domain duplexing
TRX	transceiver
TTI	transmission time interval
TX	transmitter
UDP	user datagram protocol
UE	user equipment
UL	uplink
UL-SCH	uplink shared channel
UNB	ultra narrow band
USB	universal serial bus
UTRA	universal terrestrial radio access
VI	virtual instrument
VNA	vector network analyser
VSA	vector signal analyser

List of Symbols

B	Suceptance
E_{in}	Input voltage noise
E_{TX}	Transmit energy consumed
Γ	Reflection Coefficient
$IP3$	Third order intercept point
N	Normalisation factor
N_b	Number of bits
NSD_{RTI}	Noise Spectral Density Referred to Input
$P_{o,sat}$	Saturated output power
$P_{o,sat}$	Saturated output power
P_{TX}	Transmit power
P_{UMAX}	Maximum transmit power
S_{11}	Reflection coefficient
S_{21}	Insertion loss
T_{TX}	Transmission time
V_{rms}	Volts RMS
X	Reactance
Z_L	Load impedance
$V_{n_{in}}$	Amplifier voltage noise at input
$V_{n_{out}}$	Amplifier voltage noise at output

List of Publications

- [1] J. Birchall, P.E. DeFalco, K. Morris, M. Beach, “Efficiency enhancement of M2M communications over LTE using adaptive load pull techniques” in *Radio and Wireless Symposium (RWS 2017)*, Jan 2017.
- [2] J. Birchall, K. Morris, M. Beach, “M2M Communications over LTE - Evaluating Energy Consumption Models” in *International Wireless Communications and Mobile Computing Conference (IWCMC 2017)*, June 2017.
- [3] P.E. DeFalco, J. Birchall, L. Smith, “Hitting the Sweet Spot: A Single-Ended Power Amplifier Exploiting Class AB Sweet Spots and Optimized Third Harmonic Termination” in *IEEE Microwave Magazine (Volume: 18, Issue: 1)*, Jan.-Feb. 2017.
- [4] E. Arabi, P.E. DeFalco, J. Birchall, K. Morris, M. Beach, “Design of a triple-band power amplifier using a genetic algorithm and the continuous mode method” in *RF/Microwave Power Amplifiers for Radio and Wireless Applications (PAWR 2017)*, Jan 2017.
- [5] P.E. DeFalco, J. Birchall, S. Ben Smida K. Morris, K. Mimis, G. Watkins “Asymmetrical outphasing: Exploiting conjugate continuous modes of operation” in *RF/Microwave Power Amplifiers for Radio and Wireless Applications (PAWR 2017)*, Jan 2017.

Chapter 1

Introduction & Motivations

WIRELESS communications for machine-to-machine (M2M) is a rapidly growing subset of the Long Term Evolution (LTE) wireless standard due to the ease of deployment and readily available access to the infrastructure. However, one of the key limitations of this technology is its relatively large power requirement, which in an energy constrained use case (e.g. a remote wireless sensor network) can mean either a short battery life, or the requirement for a large and expensive battery. This Chapter describes the use cases of M2M communications and the associated drive for efficiency associated with remote operation, motivating the research presented later. Also described is the structure of this Thesis and how the issues surrounding system efficiency have been addressed, thus enhancing the adoption of M2M wireless technologies.

Cellular M2M connections are forecast to grow to between 10 and 20 billion connected devices by 2020 [6]. This is also illustrated in Figure 1.1, where it can be seen that M2M is predicted to be the dominant use case for cellular communications in the coming years. Obviously 10-20 billion is a huge quantity of connected devices, but it is also a huge quantity of energy consumed, any possible methods for increasing the efficiency of this process should be investigated fully, as the aggregate saving in energy over all devices will be significant.

1.1 Machine to Machine Communications

M2M is generally described as any technology that allows networked devices to exchange data and perform actions without the assistance of humans. Whilst this forms the basis of this Thesis, it is important to understand that the scope of M2M communications is actually very large. When analysing and optimising communications systems, it is important to get an idea of the transmission profile of the data involved. In its most basic form, this is likely to comprise of the amount of data transmitted in bytes, and the frequency with which this

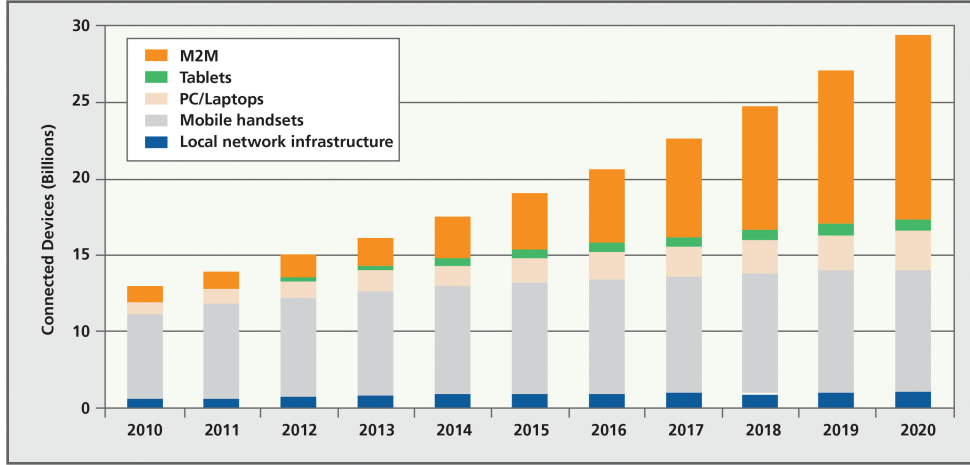


Figure 1.1: Growth of M2M communications [7].

is sent / received. More thorough analysis involves knowledge of the particular protocols involved, which will influence any overheads and acknowledgements sent and received. Figure 1.2 shows some of the potential use cases for which M2M will be leveraged. It can easily be seen that the scope of transmission profile is incredibly large, from streaming video from remote security systems, all the way down to a wireless sensor that might be required to transmit a packet of data once a day or perhaps only in response to a less frequent stimulus.

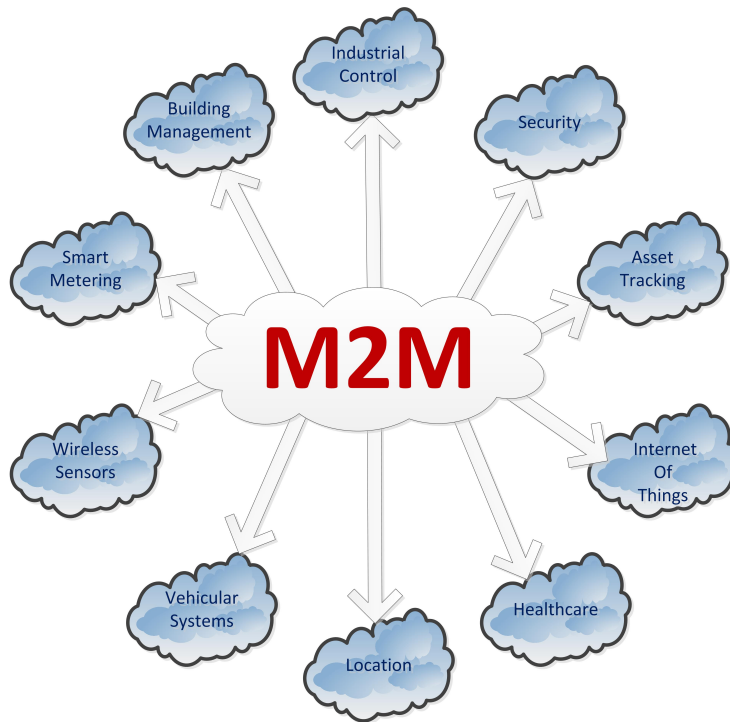


Figure 1.2: M2M communications use cases.

The focus of this Thesis is mainly on the lower end of the spectrum of use, sub 6GHz, focussing on low cost methods of efficiency enhancement for energy constrained devices, that may be required to be deployed quickly and cheaply, but with the expectation of a long battery life, i.e. deploy once, with no expectation of a battery change.

1.2 The Drive for Efficiency

1.2.1 Signals Analysis

When considering the power and efficiency of a communications system, one of the first things to consider is the characteristics of the signals involved. This involves a number of different layers, from the lowest physical to the medium access control (MAC) layer and it's random access procedures and protocols. Before these properties of signals are considered, it is important to know the particular system requirements, and what it is possible to do with the information. The main purpose is to improve some characteristic of the system, whether this be latency, power efficiency, throughput, or the overall robustness of the communications link.

Regarding machine to machine communications, any of these factors could be a targeted, however this thesis focusses mainly on the improvement of power efficiency. Beginning with the physical layer properties of the signals, LTE has four main degrees of freedom, bandwidth, timeslot (duty cycle of transmission), power level, and modulation and coding scheme. The combination of these will give a time domain signal that can be expressed in terms of its mean power, and peak-average power ratio (PAPR). Mean power will affect how much energy is consumed by the system in being brought up to a required level, whilst PAPR will influence the amount of back-off required by the power amplifier in order to maintain the integrity of the signal.

1.2.2 Power Amplifier Operation

In order to discuss how power amplifiers can be made more efficient, it is helpful to first give a brief overview of how the average power amplifier works, at what constrains the operating point. Figure 1.3 shows a generic graph of amplifier performance in terms of input vs. output power. In this case, $P_{o,sat}$ and $P_{o,sat}$ are defined as the power levels at which distortion products cause gain to be reduced by 1dB. $IP3$ is the extrapolated point at which third order distortion products will be equal in power to the desired signal output power.

It can be seen that once a certain input power has been exceeded, the useful output

power begins to plateau. This generally occurs when the desired output voltage approaches the amplifier supply voltage, causing ‘clipping’ of the output waveform. This clipping causes a rise in the amount of distortion products at the output, for example, imagine taking the Fourier transform of a sine wave that had had its peaks and troughs flattened by clipping. In terms of a real LTE system, this would cause spectral leakage into adjacent channels, resulting in interference with other devices, and the failure any compliance tests.

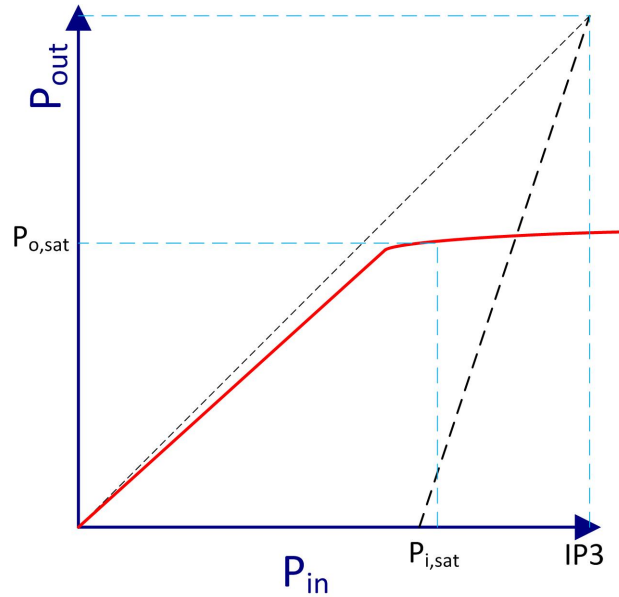


Figure 1.3: Compression at high output powers.

Considering most basic power amplifier topologies, efficiency generally increases as output power tends towards the maximum power output, therefore with a system where a constant input level is always present, and a constant level of output is always required, it is simply a matter of choosing the operating point to be as close to, but not going into, saturation for maximum efficiency with minimum distortion. The reality is far from the case, especially with wideband LTE systems, which typically have varying input powers, especially when high order modulation schemes are used, and require variable output power depending on proximity to base station. Traditionally ‘back-off’ was used, where the amplifier was always operated lower than its peak power level in order to avoid ever straying into a region that would produce distortion, however this is far from efficient, and there are many more successful techniques that can be used.

The relevance of this characteristic is that it can be seen that for maximum efficiency, the supply voltage to the power amplifier should be as low as possible without causing the amplifier to go into compression, and in fact this forms the basis of dynamic power supply systems. The closer the supply voltage can be lowered with respect to power level, the more

efficient the system can become, however the instantaneous power level of an LTE signal varies greatly over time, presenting significant design challenges with regard to measuring signal power and adjusting the system accordingly. In addition to changing supply voltage to increase efficiency, the reflection coefficient seen by the amplifier as a load can be optimised for efficiency at a certain power level, however this optimum reflection coefficient varies with power level, and so the use of a dynamically variable reactive load can be used to track signal power levels to keep efficiency optimal.

1.3 Conclusion

It has been shown that M2M is a technology likely to become ubiquitous in the coming years, with potentially billions of connected devices performing a wide range of functions. With such large numbers involved, it has never been more important to understand how energy is being consumed within a system, and explore all possible options in order to increase the efficiency with which this is done, preferably using low cost methods that allow future connected devices to operate at a price point that will encourage uptake by all stakeholders in the communications system.

1.4 Thesis Overview & Contributions to State of the Art

This thesis covers a range of topics pertaining to the drive for efficiency in M2M communications. The second chapter is a brief overview of how LTE works, in terms of the modulation schemes used, how error performance is measured and also the procedure followed by a device wishing to request resources from the network in order to transmit data. These parameters are all very relevant to the research contained in the rest of this thesis.

Chapter 3 is concerned with the physical layer signals used within LTE, with the aim of exploiting this information to increase system efficiency. Both simulated and measured results are compared in order to see how much information can be gained about the distribution of signal envelope power using only data from the MAC layer such as bandwidth and modulation scheme. The concept here is that knowledge of signal power distribution can be used to determine the operating point of many efficiency enhancement schemes for power amplifiers, such as dynamic power supplies or dynamic load modulation. Being able to achieve this without computationally intense signal processing would represent a great advantage in terms of efficiency enhancement. A correlation is demonstrated between the

PAPR of a signal and modulation and coding scheme, and the bandwidth of a signal in both simulated and measured results over successive subframes.

Chapter 4 deals with the power consumed by an LTE modem, using results in a laboratory with a base station emulator, and also on a live network. Results show that as expected, the power amplifier, and associated transmit power levels dominate uplink power consumption, however in receive mode, both received power level and data rate effect power consumption. In a laboratory setting it has been shown that there is a well defined monotonic relationship between transmit packet size and energy consumed in the transmit process, however when the same set of measurements is carried out on a real network, there are a number of confounding variables that must be taken into account. It is demonstrated that a significant number of additional network level communications can take place during a transmission, even in periods of supposed discontinuous reception. The result of this is that active transmit times increase greatly, and power consumption becomes almost invariant with regards to small packet sizes.

Chapter 5 examines the use of both dynamic power supplies and active load modulation for an LTE power amplifier. Ordinarily these schemes would require a large amount of signal processing to determine the optimal operating point, however results demonstrate that as theorised in Chapter 3, good results can be achieved using only information from the MAC layer to infer signal power distribution. Increases of up to 44% power added efficiency (PAE) over the standard case (PA only, normally biased) are demonstrated using an active load pull system, and a 27% increase in PAE is demonstrated for load pull and dynamic power supply over the dynamic power supply only case. The potential for miniaturising the dynamic load modulation method is discussed, with analysis of physically small load modulation components.

Chapter 6 details additional work on radio frequency (RF) power amplifiers completed in collaboration with other authors. The appendices contain LabView code, used for the acquisition of data used in Chapter 4, Python scripts for interfacing with LTE modems for results in Chapters 3 and 4, and also Matlab scripts for processing data used throughout the thesis.

Chapter 2

A Technical Overview of LTE

2.1 Introduction

THIS chapter contains background material on the processes involved in Long Term Evolution (LTE) (4th generation mobile communications (4G)) communications systems. The pertinent subjects that are covered involve the underlying modulation schemes, the processes used to connect to a base station and request resources for transmission, and also the methods by which errors in signal quality are measured. These are all subjects that underpin work presented in the rest of this thesis.

2.2 LTE

2.2.1 Modulation

There are two macro modulation schemes currently used in the LTE standard. Orthogonal Frequency Division Multiple Access (OFDMA) is used for downlink data from the evolved node B (eNB) to the user equipment (UE), whilst single carrier frequency division multiple access (SC-FDMA) is used for uplink data transfer. Within these macro schemes, the data is first modulated with an M-QAM scheme within the shared channels; this is limited to quadrature phase shift keying (QPSK), 16 symbol quadrature amplitude modulation (16-QAM), and 64 symbol quadrature amplitude modulation (64-QAM), however binary phase shift keying (BPSK) may also be used in the physical uplink control channel (PUCCH), and Zadoff-Chu reference signals are also used in the primary synchronisation signal (PSS), physical random access channel (PRACH), PUCCH, physical uplink shared channel (PUSCH) and sounding reference signal (SRS)

The modulation for the uplink channel was chosen as SC-FDMA, due to the fact that the peak-average power ratio (PAPR) of the output signal is much lower than the OFDMA alternative, allowing a relaxation in the normally rigorous design constraints applied to the power amplifier (PA) in a mobile device. Ordinarily a signal with a high PAPR would require a complex and usually inefficient amplifier device (i.e. operating with a high degree of back off) in order to amplify the signal in a linear fashion, minimising any distortion products that could interfere with users in adjacent channels. The lower PAPR of SC-FDMA reduces the amplifier requirement specification. The absolute size of the difference in PAPR depends on many factors, which are discussed in Chapter 3.

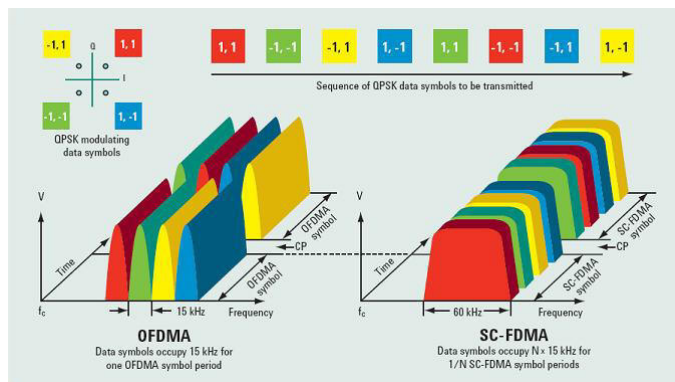


Figure 2.1: A comparison of OFDMA and SC-FDMA [8].

Figure 2.1 shows the fundamental differences between OFDMA and SC-FDMA; note that although 4 sub carriers are shown for simplicity, in reality the minimum of 12 in a single resource block would actually be used. The OFDMA scheme shows four subcarriers,

each transmitting a single symbol in parallel over a single symbol period, followed by the cyclic prefixes of the next symbols and repeat. SC-FDMA differs in that instead of sending the four symbols in parallel, they are sent in series, at four times the rate, over four times the bandwidth. The aggregation of this bandwidth is where the “Single Carrier” prefix comes from. The parallel transmission of multiple signals is what contributes to the high PAPR of OFDMA, transmission in series with SC-FDMA results in a much lower PAPR, closer to that of the original symbols. It is worth noting that this effect is also additive for OFDMA; an increase in the number of sub carriers increases the PAPR towards that of Gaussian noise (∞ dB), whilst increasing the bandwidth of SC-FDMA has little increase in the PAPR over that of the original symbols [9] .

It may seem like the apparent shorter symbol times used in SC-FDMA would actually reduce resistance to multipath fading, however the amplitude and phase of the waveforms are kept constant over multiple symbol periods, yet different symbols are still transmitted. This is achieved in the same way that two sine waves of constant amplitude and phase but different frequency can be summed into a time varying waveform. The difference between OFDMA and SC-FDMA is that in the former, data symbols directly modulate the subcarriers, whilst this is not the case with SC-FDMA.

The process for creation of the SC-FDMA waveform is illustrated in Figure 2.2; symbols already modulated into an appropriate IQ form (eg.by QPSK) enter in a serial stream, whereupon they are split up into M parallel streams, where M represents the number of sub-carriers available to the device over the current symbol period. Particularly in SC-FDMA, M is also equal to the number of symbols to be transmitted in a single symbol period. This time domain waveform is then passed through an M point discrete Fourier transform (DFT) in order to produce a frequency domain output, which will give M frequency bins spaced at 15kHz, with each sub-carrier being held at constant amplitude and phase for an entire symbol period. The DFT output is at baseband, and must be shifted to the required part of available spectrum; this is done simply by copying the M bins into the larger N bins of the system channel bandwidth, either 1.4, 3, 5, 10, 15 or 20MHz. If N is much larger than M, the M bins from the UE can be placed in any vacant location in N in order to facilitate the frequency division multiple access (FDMA) part of the scheme. The N bins are then converted back into the time domain via an inverse discrete Fourier transform (IDFT), output in serial, and have a cyclic prefix added before being transmitted [10].

It is worth noting that the current LTE system allows QPSK, 16-quadrature amplitude modulation (QAM) and 64-QAM to be used in the uplink, and whereas an OFDMA system would require the same amount of PA back-off to be used regardless of modulation depth, SC-FDMA requires an increase in back-off for each increase in depth, due to the additional

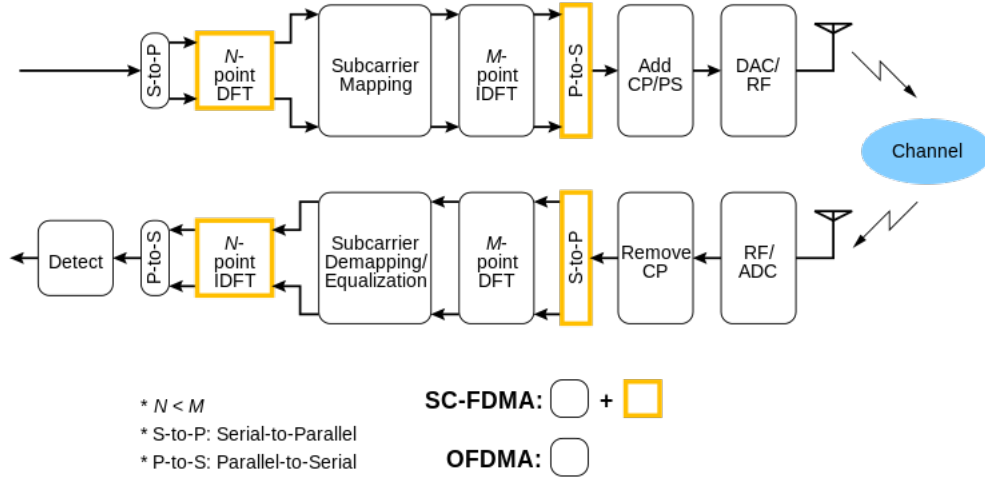


Figure 2.2: SC-FDMA modulation [11].

amplitude levels involved affecting the PAPR.

2.2.2 Resource Allocation

Resource allocation in LTE uplink is best viewed as a grid in order to visualise the two main degrees of freedom with which a user can be allocated resources. Figure 2.3 shows an example grid from a MATLAB simulation. The x-axis is the time domain, with the resolution being a single symbol, of duration $71.4\mu\text{s}$. There are seven symbols in a slot of 0.5ms , fourteen symbols, or two slots in a 1ms subframe, and ten subframes in a 10ms frame. Regarding the frequency domain, the smallest unit is a single subcarrier of width 15kHz . A single resource element, as annotated in the figure is one symbol wide in the time domain, and 1 sub carrier wide in the frequency domain. In reality, the smallest unit that would be allocated to a user will be a single resource block. This unit is seven symbols wide in the time domain (0.5ms) and twelve sub-carriers (180kHz) wide in the frequency domain.

Common LTE system bandwidths are shown in Table 2.1. The system bandwidth will generally be set by the amount of spectrum a particular operator has available at a specific frequency. The maximum resource block allocation is also shown in the table, resource allocation to a particular user will be between one and the maximum available, with the actual number being determined by proprietary algorithms in the base station.

Figure 2.4 illustrates how the data capacity of each subframe varies with both bandwidth and modulation and coding scheme. It may be noted that there are two plateaus along the modulation and coding scheme (MCS) index axis, where the system moves a higher modulation scheme but a lower coding rate, resulting in the same transport block size.

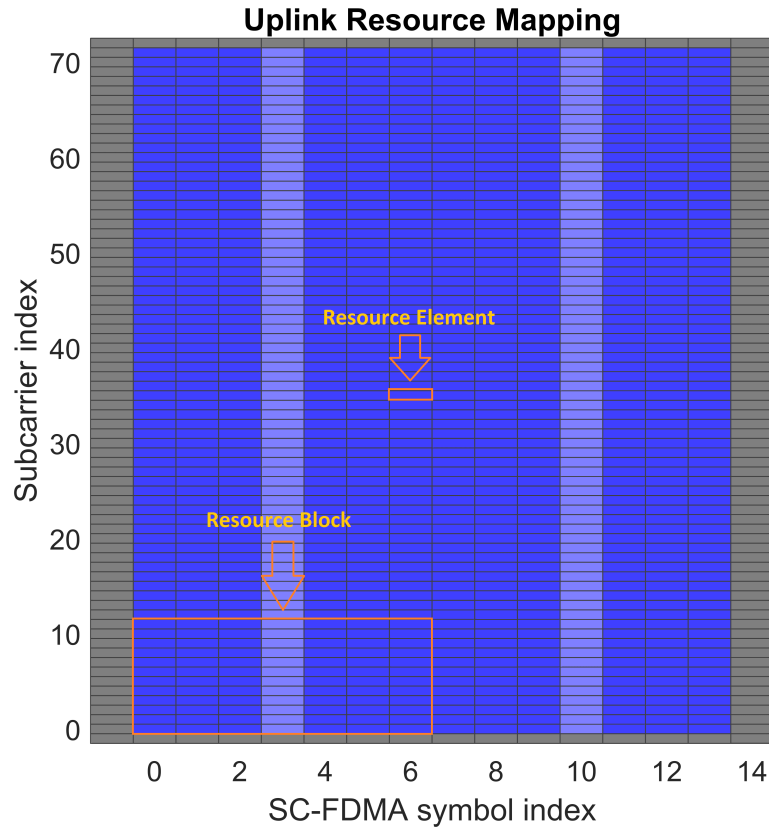


Figure 2.3: LTE resource allocation grid.

Bandwidth	Resource Blocks
1.4 MHz	6
3 MHz	15
5 MHz	25
10 MHz	50
15 MHz	75
20 MHz	100

Table 2.1: LTE bandwidths.

2.2.3 TX Procedure

When considering energy consumption, it is useful to look at how data is transmitted on each level of the communications system. The reason this is exceedingly important for the machine-to-machine (M2M) scenario is that the duration of the process of establishing a network connection in order to request resources can be comparable to the duration of the user data itself, thus having a significant implication on the amount of energy required to complete a transmission.

If it is assumed that the UE is already in the connected state, then the main steps

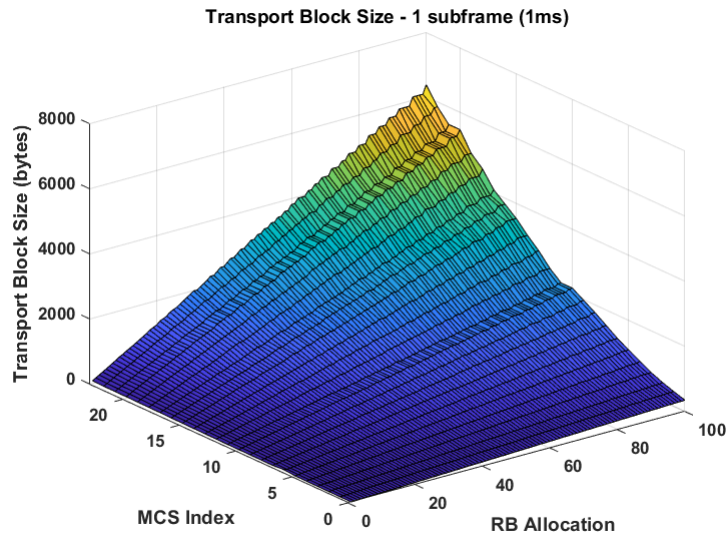


Figure 2.4: Transport block size as a function of bandwidth and MCS.

towards transmission of data in the PUSCH channel are referred to as the random access channel (RACH) procedure or random access procedure, this is described below. Note that for brevity the cold start procedure of waking up a device and making a new connection to a network is not described, as this much more complex, it is however shown in measurements made in Chapter 4, where the duration can be seen as even more significantly power consuming.

- Establish / Re-establish radio resource control (RRC) connection - a preamble is transmitted by the UE on the PRACH so that the eNB can estimate how far away the UE is and what value of timing advance to use so that future UE transmissions will be received in the correct time slot. UE gives an indication of the amount of data it has to transmit.
- Random access response - Timing advance parameter is sent from the eNB to the UE. uplink shared channel (UL-SCH) resource assignment is given to the UE for the next stage. cell radio network temporary identifier (C-RNTI) is assigned.
- First transmission on the PUSCH, contention resolution may occur if required.

It can easily be seen that this type of always on, broadcast based synchronisation is not always efficient for uplink, and in fact, several discontinuous reception (DRX) and sleep modes are used to save energy. In order to minimise use of the PRACH and minimise collisions, there is a requirement that RACH procedures should only happen when necessary, and be specific only to a particular UE.

Parameter	Unit	Level
QPSK	%	17.5
16-QAM	%	12.5
64-QAM	%	8

Table 2.2: LTE UE EVM limits [12].

2.2.4 Error Measurement

During the creation, amplification and transmission of wireless power signals, there always exists the possibility of generating distortion products, particularly in hardware dealing with high signal powers and through poor radio frequency (RF) channels. There are many ways of measuring performance in terms of error creation & generation, the two main characteristics relevant for an LTE system are error vector magnitude (EVM) and adjacent channel leakage ratio (ACLR). The particular significance of these parameters is demonstrated in Chapter 5, where particular techniques are applied to power amplifiers in order to increase efficiency. Certain techniques, such as the use of dynamic power supplies can cause the signal of interest to be distorted, potentially corrupting the informational content, and causing interference to other users. Constant measurement of the following parameters ensures that only techniques that allow equipment to function correctly, and to specifications will be used.

2.2.4.1 EVM

If a received symbol is pictured on a constellation diagram, the EVM is basically defined as the distance between the ideal received symbol, and the symbol that has actually been received [12]. A more accurate definition would be the ratio of mean error vector power to mean reference power, as described in Equation 2.1. Note that this measurement is made after the IDFT in the receive chain, as described in Section 2.2.1, and any timing and frequency offsets have already been corrected.

$$EVM(\%) = \sqrt{\frac{P_{error}}{P_{reference}}} \times 100\% \quad (2.1)$$

The particular limits set in the 3rd Generation Partnership Project (3GPP) specifications for EVM are given in Table 2.2. Note that the minimum requirement decreases with constellation size. This is because as the constellation size increases, distance between constellation points decreases, thus a smaller error vector is tolerable before a particular symbol in error conditions appears as an incorrect symbol. Maintaining an appropriate minimum EVM ensures quality of service is sufficient for all degrees of freedom in the system.

2.2.4.2 ACLR

A further method of quantifying distortion products is Adjacent Channel Leakage power Ratio (ACLR). This is perhaps the most easy to visualise and understand in terms of power amplifier performance. In the same manner as the traditional two-tone test can give an indication of how close to saturation a power amplifier is by measuring harmonic distortion products, ACLR gives an indication of the relative RF signal power in the spectrum outside of the intended signal as a metric for distortion produced, and the interference this might cause for other users.

ACLR is defined the ratio of the filtered mean power in the band of interest to the filtered mean power in an adjacent channel frequency. As compatibility with legacy universal terrestrial radio access (UTRA) systems is desired, ACLR requirements are defined in terms of adjacent UTRA and evolved universal terrestrial radio access (E-UTRA) channels. These figures can be seen in Tables 2.4 and 2.3.

	Channel BW / $E - UTRA_{ACLR1}$ / Measurement BW				
	1.4MHz	5MHz	10MHz	15MHz	20MHz
$E - UTRA_{ACLR1}$	30dB	30dB	30dB	30dB	30dB
Measurement BW	1.08MHz	4.5MHz	9.0MHz	13.5MHz	18.0MHz

Table 2.3: E-UTRA ACLR constraints [12].

	Channel BW / $UTRA_{ACLR1/2}$ / Measurement BW				
	1.4MHz	5MHz	10MHz	15MHz	20MHz
$UTRA_{ACLR1}$	33dB	33dB	33dB	33dB	33dB
$UTRA_{ACLR2}$	-	36dB	36dB	36dB	36dB
E-UTRA BW	1.08MHz	4.5MHz	9.0MHz	13.5MHz	18MHz
UTRA BW	3.84MHz	3.84MHz	3.84MHz	3.84MHz	3.84MHz

Table 2.4: UTRA ACLR constraints [12].

It may be noted that the UTRA bandwidths refer to a 5MHz UTRA system in co-existence with an E-UTRA frequency domain duplexing (FDD) system. Different limits would apply for use with an E-UTRA time domain duplexing (TDD) system, though this is not in use in the UK. Two figures are given for compliance, as it is desirable that the E-UTRA system work without interfering with two successive UTRA channels. These limits are generally used as they are the more stringent.

Chapter 3

Waveform Analysis for Efficiency Enhancement Schemes

THIS chapter addresses the signal structure of the Long Term Evolution (LTE) uplink channel, and how knowledge of certain parameters can be exploited to enhance system efficiency. As a functional overview, the power amplifier for an LTE system will be biased in such a way as to achieve a reasonable degree of efficiency whilst creating a minimum amount of distortion products. When biasing to avoid distortion, the peak excursions of the signal are generally taken into account in the form of peak-average power ratio (PAPR), and where the biasing is fixed, the worst case PAPR will be the value considered. As the uplink signals have many degrees of freedom in terms of resource allocation, the PAPR of a signal will change depending on factors such as bandwidth and modulation and coding scheme. This chapter addresses the change in PAPR distribution over these parameters, with the aim of being able to leverage this information in order to alter the bias of a power amplifier in order to increase efficiency, using only the resource allocation information in the medium access control (MAC) layer.

3.1 Current State of the Art

One of the biggest obstructions to a highly efficient radio frequency (RF) system is a range in required transmit power, both in terms of signal excursion around a mean power, defined by the PAPR, or in terms of a change in mean power, usually brought about by the use of adaptive transmit power systems, whereby Transmit power (P_{TX}) is modulated in response to the transmit channel.

In order to mitigate the inefficiencies brought about by these factors, two main tactics are generally deployed; When a new modulation scheme is developed for a communications system, this can be selected on the basis of a low PAPR, or research can address the optimisation of PAPR. An alternative strategy is to use efficiency enhancement schemes such as those described in Chapter 5. An example of modulation scheme optimisation is given in [13] where variations in single carrier frequency division multiple access (SC-FDMA) schemes are assessed for optimum PAPR and also how using multi-band filter bank techniques can offer a more isolated frequency slots than the discrete Fourier transform spread orthogonal frequency division multiplexing (DFT-S-OFDM) currently used.

The efficiency enhancement schemes described generally require either an accurate measurement of the magnitude of the signal, the more accurate this is, the greater the benefit to efficiency. Assessing the magnitude of a high speed signal envelope can be a computationally complex task, adding to the energy consumption of the modem. Any ability to do this without direct measurement and digital signal processing (DSP) is likely to enable the production of low cost and efficient transmitters.

[14] describes the development of a PAPR aware amplifier which uses a form of load modulation to increase backed off amplifier efficiency in response to the RF signal passed into the power amplifier (PA). A power detector coupled into the mixer is fed into a comparator, where an appropriate threshold can be set in order to switch between load modulated states. The power involved is lower than required for LTE at 8.9dBm, given that typical transmit power may be as high as 23dBm measured at the antenna port, which can require PA output power levels of up to 28dBm in order to deal with losses in switches and filtering. Achieving a power added efficiency (PAE) of 25.5% at 8.9dBm is sufficient to validate the PAPR aware approach, as for comparison, the commercial off the shelf (COTS) amplifier used in Chapter 5 achieves a PAE of less than 5% at the same power level.

[15] describes how the DG.09 probability density function can be used to give a better approximation of power consumption within a mobile device. DG09 is a statistical distribution of transmit power levels released by the Global System for Mobile communication (GSM) association in order to help user equipment (UE) vendors predict battery life under normal use. Previous measurements have centred around 'static' power figures, i.e. a fixed transmit

power for a single communications transaction, whereas the reality is, there is quite a large distribution in instantaneous signal power, as will be seen in this chapter, especially with data centric communications being pushed up to higher order modulation schemes by base stations keen to maximise throughput. The contents of this chapter is aimed at describing a multitude of LTE power distributions, which change shape with bandwidth, modulation and coding scheme (MCS) and overall power level.

Attempts have been made to numerically calculate the distribution of PAPR in SC-FDMA. [16] describes an approximation for calculating this distribution quite well, although results are analysed qualitatively rather than quantitatively. The limitations here are that a-priori knowledge of the symbols used is required, which makes for a very computationally resource intensive activity.

In summary; whilst there is plenty of work on how to optimise PAPR, there is very little done on approximating figures of PAPR in the context of how it varies across the degrees of freedom in a communications system. The ultimate goal would be leveraging this as an easily implementable control for a dynamic power supply or active load pull for a power amplifier. The research that follows attempts to address this lack of knowledge, and prove that knowledge of resource allocation can go a long way towards providing knowledge of signal power characteristics of use to the system designer.

3.2 Metrics, Requirements & Tools

During the course of any piece of work on signals analysis, it is vital to know what is required, how it is quantified, and how this is measured, especially in the context of a system as complex as LTE, these quantities will be described below.

3.2.1 Metrics

It is important to use appropriate metrics to quantify how the signals produced in a system will effect the performance of any components downstream, whilst the bulk of these are described in Chapter 2, the elements important to this research are reviewed below:

In terms of defining signal powers and distributions, root mean square (RMS) envelope value is the RMS average power of the envelope, and a good way to define a particular system operating point. Peak envelope power (PEP) is the maximum possible value of the signal envelope, this will obviously have an impact on how much our amplifier is backed off. A more widely used measure, that covers the properties of a particularly modulated signal is the ratio of this to the average signal power, aptly named peak to average power ratio.

PAPR, defined as:

$$PAPR_{dB} = 10 \log \left(\frac{\max[x(t)x^*(t)]}{E[x(t)x^*(t)]} \right) \quad (3.1)$$

As power is the main quantity of interest, peak power is defined by maximum value from the time domain signal multiplied by its conjugate, and mean power is the average of the time domain signal multiplied by its conjugate. There are statistical methods of describing the signal envelope, which are sometimes harder to use analytically, but give a better indication of how the power is distributed in a signal. Probability density function, probability density function (PDF) simply shows how the envelope power is distributed. An example of this is show in Figure 3.1 for an LTE signal.

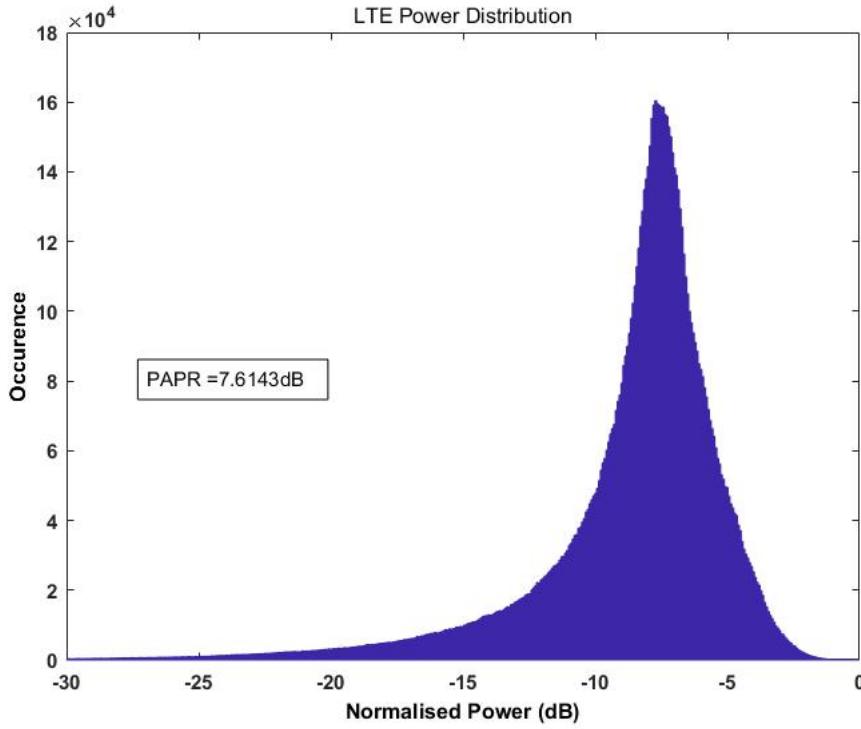


Figure 3.1: PDF of an LTE signal normalised to peak power.

Further to this complimentary cumulative distribution function (CCDF) is also used to display signal characteristics, and is defined as:

$$CCDF = 1 - CDF \quad (3.2)$$

This is the probability $P(x > c)$, where x is the signal power and c is a a particular level. This gives useful information about the envelope peak characteristics . Throughout, these figures will generally be normalised to the peak envelope power. The benefit of using

a CCDF plot is that the use of a logarithmic scale on the y axis allows easy visualisation of the low probability, peak signal powers that can sometimes be obscured on a linear scale.

3.2.2 ACLR

Whilst adjacent channel leakage ratio (ACLR) is covered more comprehensively, along with error vector magnitude (EVM) in the previous chapter, a brief overview is important here in order to understand better the goals of this work. A typical measurement of ACLR is shown taken on an Agilent E6601A Wireless Communications Test Set in Figure 3.2. The large blue column in the centre of the diagram is the signal of interest transmitted by the UE, in this case a continuous uplink transmission of random data over a 10MHz bandwidth. In order to share wireless spectrum with other users efficiently, it is important to ensure that when a device transmits in a certain allocated bandwidth, the signal is confined largely to the bandwidth in question.

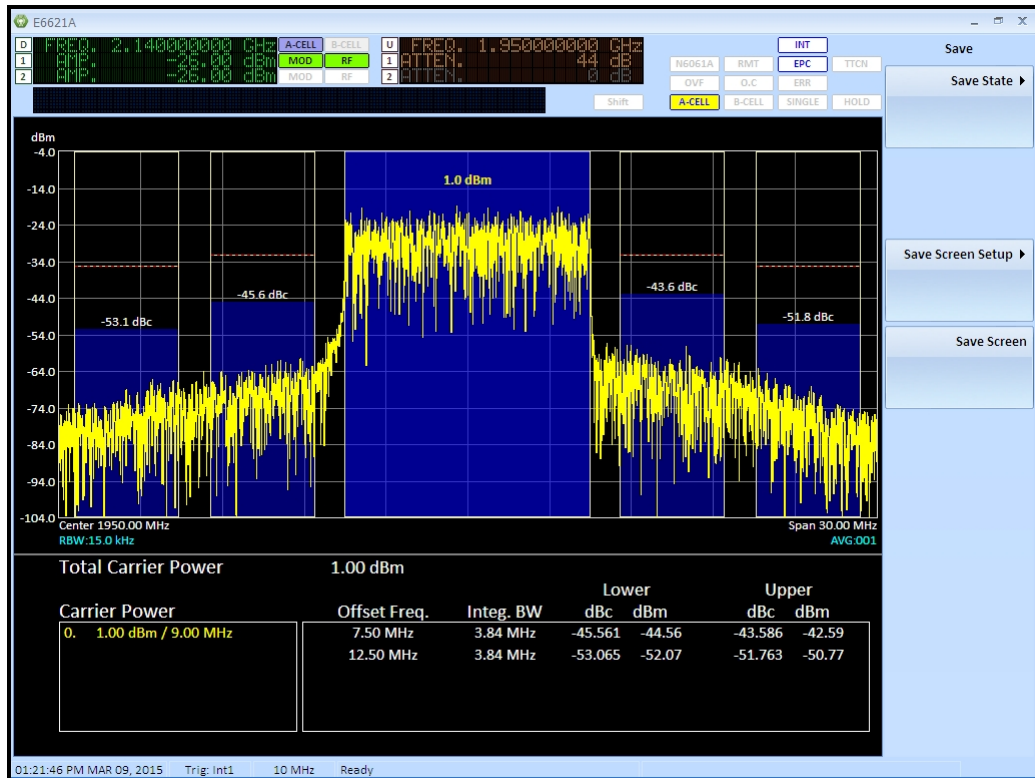


Figure 3.2: ACLR of an LTE signal.

Due to limitations in real amplifier performance and filtering technologies, especially over the large range of frequencies specified in the LTE standards, some leakage into other parts of the spectrum is inevitable. The smaller blue bands in Figure 3.2 show the signal strength at a specified frequency separation away from the band of interest. The magnitude

of the signal power in these adjacent channels forms the basis of the ACLR measurements and corresponding minimum requirements in the LTE specifications. The specific limits for ACLR performance are described in the previous chapter, but what is important here is to understand the mechanisms that affect ACLR.

The most common cause of leakage into adjacent channels is the production of distortion products, generally by the power amplifier. This occurs when the input signal contains components of sufficient magnitude to push the amplifier into saturation, distorting the output. This problem can be alleviated most realistically by increasing the power supply of the amplifier, thus increasing the threshold at which waveform clipping occurs, though at the cost of reducing the efficiency of the amplifier. The methods proposed in this thesis surround changing the supply and bias of the amplifier in line with the characteristics of the signal, in order to increase efficiency, without violating the minimum standards of ACLR.

3.2.3 Standards Requirements

When analysing signals in the context of amplifier and system design for a specific application, it is obviously essential to know what the requirements of the system are, in this case, the LTE test requirements. Whilst there are many parameters that can be used to assess amplifier performance, the most relevant in the LTE spec are the EVM and ACLR measurements described previously. This section will focus on the method and applicability of ACLR, as the link between an amplifier being pushed into saturation and the results of an ACLR test are most readily seen.

TS1 36.521-1 Section 6.6.2.3.4.2 [17] details the test procedure for ACLR measurement. The UE is connected to the test equipment and instructed by the base station to transmit using padding bits (random data) on the uplink (UL) reference measurement channel (RMC). The UE is then instructed to keep increasing its transmit power levels in order to Maximum transmit power (P_{UMAX}). The power is measured both in the bandwidth of interest, and also the adjacent evolved universal terrestrial radio access (E-UTRA) and universal terrestrial radio access (UTRA) bands, using the appropriate filtering methods, the ACLR can then be calculated for each case. This test is then repeated over a number of bandwidths and modulation schemes as detailed in Table 6.6.2.3.4.1-1 of the previously mentioned document.

One of the key pieces of information here is that the duration of this test is over 'at least one subframe' or 1ms, which is in fact a very small duration for the test. As will be described in subsequent sections, the output power distribution of LTE may vary considerably from subframe to subframe. Additionally, as described in TS136.508, the padding data used in the ACLR measurement is set by the UE, i.e. the manufacturer may decide which data should be used for padding, and in theory it would be possible to choose a set of values that

would work advantageously in an ACLR test. What can be surmised from this information is that the ACLR test metrics may not be the best way of defining the performance of an amplifier for an LTE system, and that there may be better, more analytical ways of doing this.

3.2.4 PAPR Distribution

Much of the work that follows in this chapter concerns the difference in PAPR between different operating conditions, but at what point can a difference in signal PAPR be leveraged to improve efficiency? To put this into context, consider Equation 3.3, which gives the peak voltage of a pure sine wave of Power P dBm, into a 50 Ohm load. A sine wave of power 23dBm would have a peak voltage excursion of 4.46V, whereas at 2dB lower, a sine wave of power 21dBm would have a peak voltage of 3.54V. If this is taken in the context of the additional supply voltage required to prevent distortion, an amplifier supplied with 4.46V, yet producing an output swing of only 3.54V would be very inefficient.

Whilst this comparison is obviously more complex for SC-FDMA over a pure sine wave, the argument still stands; If power amplifier supply voltage is set for worst case scenario PAPR, then when the signal to be amplified is of a lower PAPR, the system will not be operating in the most efficient way.

$$v_{pk} = 10^{\frac{P(dBm)-10}{20}} \quad (3.3)$$

3.2.5 MATLAB LTE Toolbox

The main tool used for simulation and analysis of waveforms was the MATLAB LTE toolbox [18]. This offers a wide range of functionalities from generating test signals for UE and evolved node B (eNB), all the way up to simulating realistic end to end communications over various RF channels with full hybrid automatic repeat request (HARQ) processes. Real signals can be captured using a software defined radio (SDR) and decoded by the toolbox, and candidate 5th generation mobile communications (5G) waveforms can be evaluated in a realistic system.

The main functionality used in this piece of work is the ability to generate a range of uplink signals with all the required system degrees of freedom, and then analyse these as appropriate. Figure 3.3 shows the main interface of the toolbox. A typical process would consist of starting with an empty LTE resource grid, a set of random data is generated, and then converted into the appropriate symbols. The resource grid is populated with both data symbols and demodulation reference signals to aid decoding, before being converted into a

realistic time domain waveform envelope. Appropriate resource grids and spectrograms of the signal are easy to plot in order to further analysis.

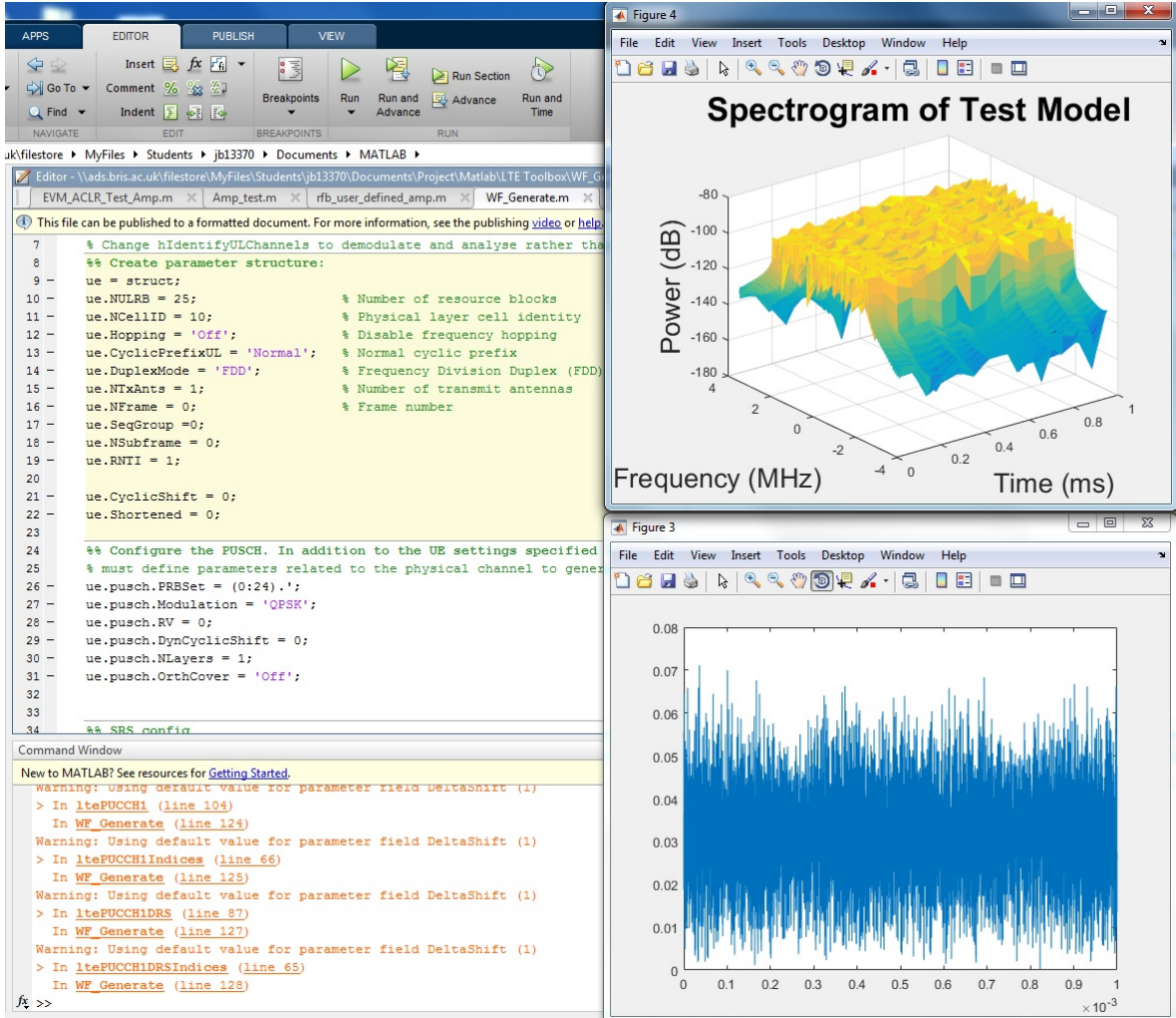


Figure 3.3: LTE Toolbox environment displaying frequency and time domain signal representations.

An example time domain waveform is shown in Figure 3.4. This waveform is from a single generated subframe, using quadrature phase shift keying (QPSK) modulation in the physical uplink shared channel (PUSCH) over a 10MHz bandwidth. It may be readily observed that the signal exhibits a kind of periodicity with respect to peak signal excursion, with two notable slots of lower peak voltage. These are the kind of characteristics that may be utilised for power amplifier enhancement scheme design, and calculating signal metric from the waveform is a relatively trivial task. The one major advantage from using simulations is that many thousands of iterations can be run with little operator input, in order to gain a better idea of how the system performs in response to certain criteria.

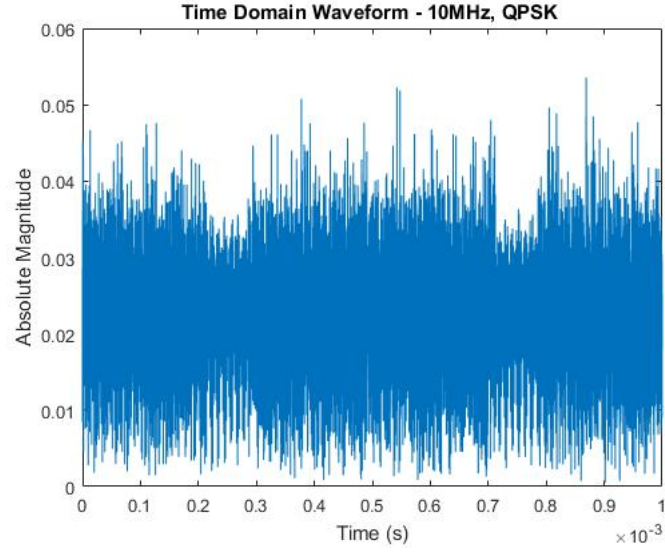


Figure 3.4: Simulation of time domain waveform.

3.3 Subframe Analysis

The LTE System Toolbox provided by Mathworks for MATLAB provides an excellent opportunity to simulate and analyse LTE waveforms in order to extract any useful parameters for determining ways to enhance the efficiency of a design. The entire toolbox covers end to end simulation and design verification, but it is the signal generation that is of most interest. Most of the available documentation and examples are centred around eNB waveforms, i.e. using Orthogonal Frequency Division Multiple Access (OFDMA) waveforms, but with some effort directed towards rewriting some of the underlying code, most of the examples and plotting functions can be updated to use SC-FDMA for UE analysis.

The first stage of a simulation is to create a structure for the UE and allocate various parameters to this, for example number of uplink resource blocks ($ue.NULRB = 6$) and the method of duplexing ($ue.DuplexMode = 'FDD'$). Once these have been set, the parameters for a particular transmission must be set, in particular for the work is the PUSCH. Similarly the structure is filled out to set the particular amount of resource blocks granted to a transmission and the modulation scheme used.

Once the basic parameters have been set up, a blank subframe of the appropriate size is generated from the initial configuration. Random data is generated, of a least the minimum size to populate a single transport block in this scenario, this can then be used to generate both the PUSCH symbols and the respective demodulation reference signal (DRS) symbols, together with indices to map these onto the resource grid. The final steps take the grid of symbols and modulate them with SC-FDMA to produce a time domain waveform that can be analysed.

3.3.1 Modulation Scheme

One of the first areas to look at is an obvious one; the effect of modulation scheme on PAPR. There should be a discernible difference between the use of QPSK and 16 symbol quadrature amplitude modulation (16-QAM) due to the fact that 16-QAM has more amplitude levels than QPSK, thus the ratio of peak excursion to mean power should be higher. In addition to this, if QPSK symbols are modulated using only phase shifts, rather than passing through the middle of the constellation, then the modulation should be constant envelope, giving a PAPR of zero. Of course, all of this must be taken in the context of the fact that SC-FDMA modulation is applied on top of this, with the associated subcarrier mapping and inverse discrete Fourier transform (IDFT), which will have an effect on the envelope of the waveform.

The results below show the simulation of 100,000 subframes filled with pseudo random data, evaluated for mean power and PAPR. Figure 3.5 shows the distribution of subframe PAPR, and it is immediately clear to see the large variation between both modulation schemes. The numerical parameters for this plot are given in Table 3.1; it can be seen there is a large difference in mean PAPR of just over 2dB.

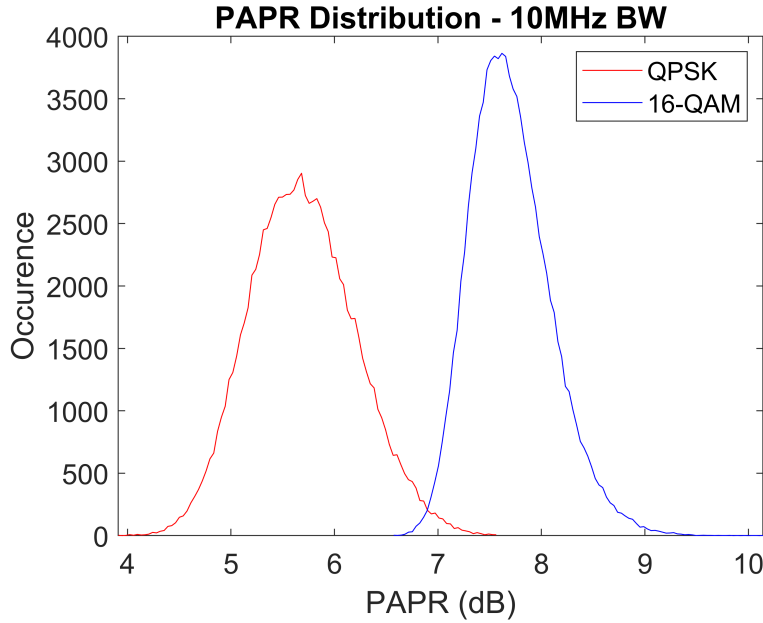


Figure 3.5: PAPR of variable MCS.

Modulation Scheme	Mean PAPR (dB)	Std. Dev. (dB)
QPSK	5.69	0.51
16-QAM	7.70	0.39

Table 3.1: Mean and standard deviation of subframe PAPR.

In order to analyse these results better, a CCDF plot is created of the PAPR data, shown in Figure 3.6. The plot illustrates the fraction of time that the PAPR of the signal is above a given level; The x axis is the PAPR, and the y axis is the fraction of occurrence, from 1 (100%) at the top of the axis, to 0.0001 (0.01 %) at the base. An example of interpreting this plot would be that considering the red QPSK curve, there is a point plotted at 6.9dB PAPR and 10^{-2} (1%), this means that over the set of simulations, the PAPR in a subframe exceeds 6.9dB, 1% of the time.

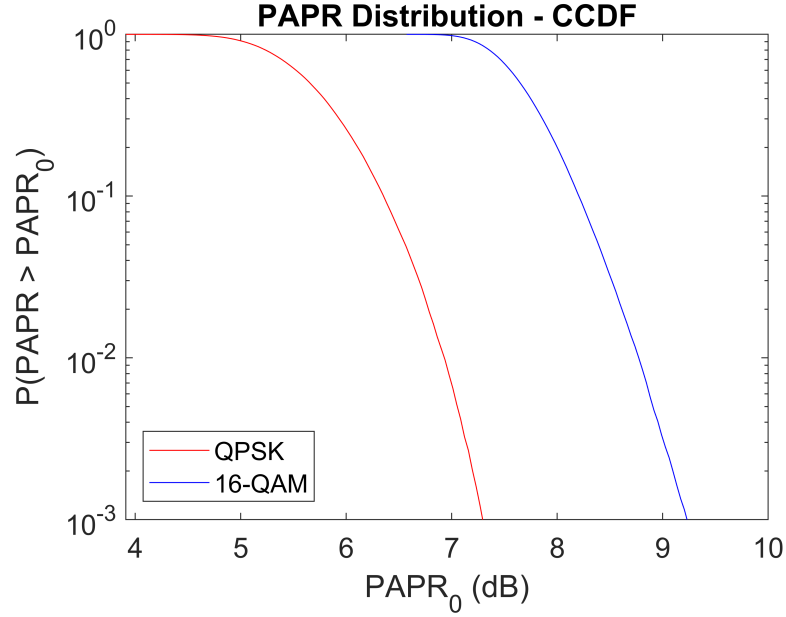


Figure 3.6: CCDF of PAPR for variable MCS.

3.3.2 Bandwidth

The simulations described above produce an output in the form of a PAPR figure for each subframe produced. By way of analysing these results, it can be observed that the distribution of PAPR over the number of iterations in the simulation. Figure 3.7 shows the results of this simulation. It can be seen that interestingly, there is a very observable trend with respect to the effect of bandwidth on PAPR. Some of the key metrics can be observed in Table 3.2. The mean PAPR ranges from 6.19dB with 6 resource blocks allocated, up to 7.03dB with 100 resource blocks. This is quite a significant difference, and something that could very likely be leveraged for the purposes of efficiency enhancement. One of the more interesting results is the effect on Standard Deviation. As allocated bandwidth increases, the spread of PAPR values decreases from 0.44dB at 6 RB to 0.31dB at 100RB. This is quite an interesting result, and is most likely due to the interaction of subcarriers averaging

Bandwidth (RB)	Mean PAPR (dB)	Std. Dev. (dB)
6	6.19	0.44
25	6.64	0.36
50	6.84	0.33
75	7.03	0.30
100	7.03	0.30

Table 3.2: Mean and standard deviation of system PAPR.

out mean subframe PAPR.

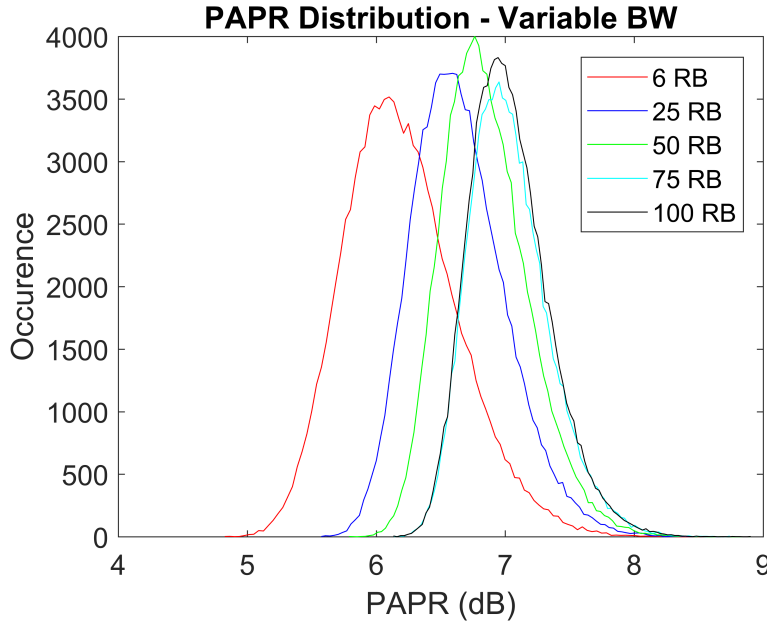


Figure 3.7: PAPR of variable BW.

Figure 3.7 illustrates the results from varying only bandwidth over the range of a conventional LTE system (1.4 to 20MHz). It can be observed that there exists a significant variation in PAPR between the various bandwidths, and a monotonically increasing relationship between PAPR and system bandwidth. Considering the mean values, it can be observed that an allocation of 6 RB (1.4MHz) has a mean value of 6dB PAPR, whereas increasing the allocation to 100RB (20MHz) results in a mean value 7dB, which is significant.

3.3.2.1 Narrowband Effects

Although not so likely for the standard LTE case, it is worth examining the effect of reducing the resource block allocation below 6RBs to emulate the conditions in a narrower band LTE system, where the maximum possible bandwidth is 1.4MHz (6 resource blocks).

Figure 3.9 illustrates the distribution of PAPR over bandwidths of 1 to 6 resource blocks.

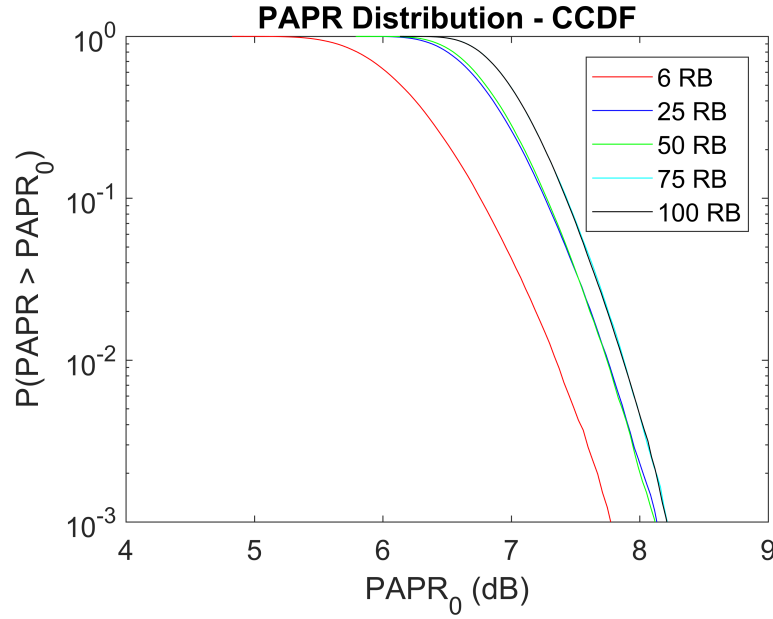


Figure 3.8: CCDF of PAPR over a variable bandwidth.

Bandwidth (RB)	Mean PAPR (dB)	Std. Dev. (dB)
1	5.70	0.51
2	6.02	0.48
3	6.14	0.46
4	6.18	0.44
5	6.19	0.44
6	6.19	0.44

Table 3.3: Mean and standard deviation of NB PAPR.

As could reasonably be expected from a much smaller step in bandwidth, there is more of a similarity observed between plots. These results are further enumerated in Table 3.3. This shows a range in mean PAPR of 0.495dB, not a huge amount, but enough to afford benefits if leveraged by an adaptive system. Again, standard deviation decreases with an increase in bandwidth, most likely due to the interaction of subcarriers minimising overall variation in signal envelope.

The results from this simulation are summarised in Table 3.3. The suggestion here is that the small difference in PAPR distribution is perhaps not enough to warrant using this in a dynamic efficiency enhancement system, although if a resource allocation of 1RB was at all likely within this system, it might just be justified to do so.

Again, the CCDF shown in Figure 3.10 illustrates that there is little potential in differentiating between RB allocations 2-5, though there is a discernable difference between this and an allocation of 1 resource block (RB).

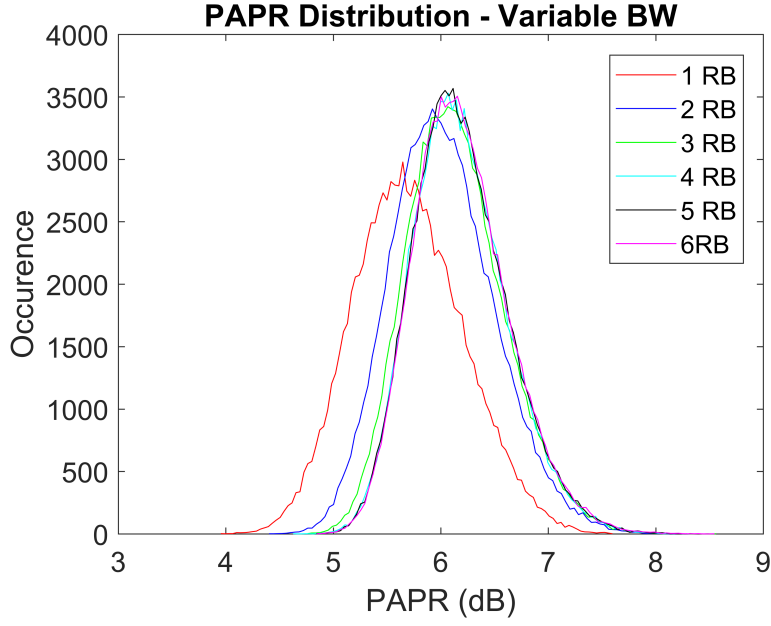


Figure 3.9: PAPR of variable BW - narrow band.

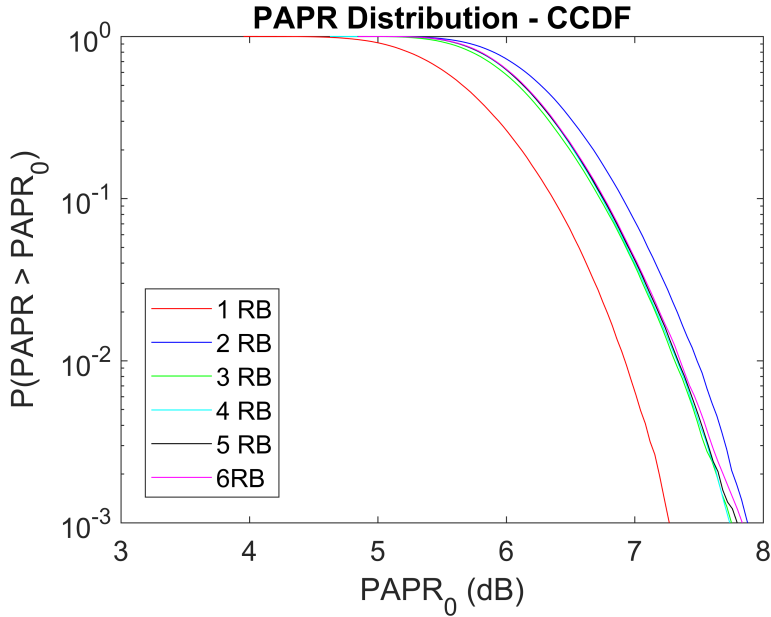


Figure 3.10: CCDF of PAPR of variable BW - narrow band.

3.4 Hardware Verification

Whilst simulations can greatly aid the understanding of amplifier power consumption, and optimal biasing points, some form of verification is generally necessary in order to give weight to any optimisation suggestions that may arise from these. A couple of options were explored in terms of achieving this.

3.4.1 Signal Envelope

The first option selected to analyse signal power was via direct sampling of the UE whilst connected to a base station emulator. RF power was measured using a power splitter to couple off half of the transmitter output power, which was then fed into measurement hardware. Initial testing used the Rohde & Schwarz ZVL network analyser in spectrum analyser mode. It was quite easy to extract data using this method, however the sample rate was too low. The minimum resolution required would be able to capture one symbol of an LTE packet with appropriate triggering for synchronisation, and unfortunately the ZVL was not able to do this at a sufficiently high sampling rate.

The next option involved using a high speed oscilloscope to directly sample the RF waveform; this required some additional setup in terms of connecting the trigger signal output from the PXT base station emulator to the trigger input of the oscilloscope in order to synchronise the recording of the signal with the actual packet transmitted. The idea here was then to use matlab code to analyse the power characteristics of the signal. One of the limitations of this method is that because the sampling rate required for accurate measurement at RF is so high, the resulting data file is very large, so much so that the internal memory of the oscilloscope was only large enough to store half a subframe, not enough for a useful analysis. One useful point however is that the oscilloscope can be useful for observing characteristics such as power amplifier ramp up at the start of a frame, and transition in between subframes.

Figure 3.11 shows a scope capture at a much coarser time resolution. Obviously this means that there is likely to give a heavy aliasing effect on the signal, so any spectral analysis of the data is pointless, though it does offer another interesting method of observing communications between the eNB and the UE. The green trace indicates the subframe synchronisation pulse from the base station emulator (BSE), and the blue trace is a trigger signal from a Raspberry Pi that indicates that it is sending a packet of message queuing telemetry transport (MQTT) data. The red trace is the signal coupled from the cable between the UE and BSE, and so shows the communications in both directions, which is another limitation of this technique. It can be seen that there are some network level communications before the blue trigger signal drops, and then three subsequent bursts of activity, which will correspond with the UE making a request for resources, a resource grant being sent, and finally the transmission of the UE packet.

The final method trialled was use of a Rohde & Schwarz vector signal analyser to down-mix the signal into its baseband I & Q components, this required the trigger input plus synchronisation of the 10MHz reference signal output from the PXT to the reference input of the vector signal analyser (VSA) in order to ensure accuracy of the measurement in a

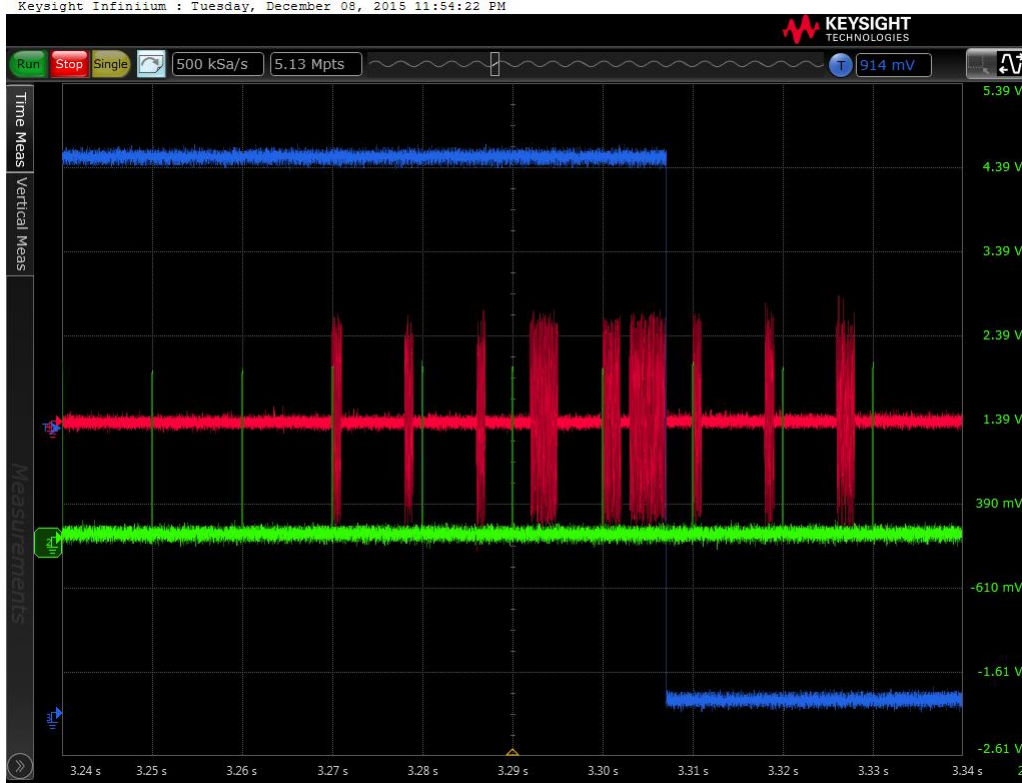


Figure 3.11: Scope capture of time domain waveform.

tight bandwidth. The output files produced were of an appropriate size to be recorded and analysed, with an duration of one subframe being of a reasonable size for later analysis. The recorded files were then processed with a matlab script which reconstructed a polar signal from the I & Q components, and then produced plots of the spectrum involved, and a measure of PAPR.

Figure 3.12 shows the time domain plot of the RF signal captured in this manner. In order to properly isolate a subframe of data, the BSE was set to instruct the UE to transmit a stream of random data for test purposes. The resource allocation process was configured so that only every other subframe was used, in order that a single subframe could be isolated and triggered on for a complete capture. It can be noted that there are two areas, corresponding to the width of a symbol within the waveform of a lower overall amplitude. These correspond to the demodulation reference signals, made up of a Zadoff-Chu sequence with a lower PAPR, which were demonstrated in the simulated subframe analysis. It can easily be seen that in a dynamic power supply system, supply voltage could be dropped for these signals, as the peak excursions are much lower than the symbols carrying user data.

Further analysis consisted of looking at the distribution of signal power level for each captured point in the subframe, this was simply done using a histogram function of appro-

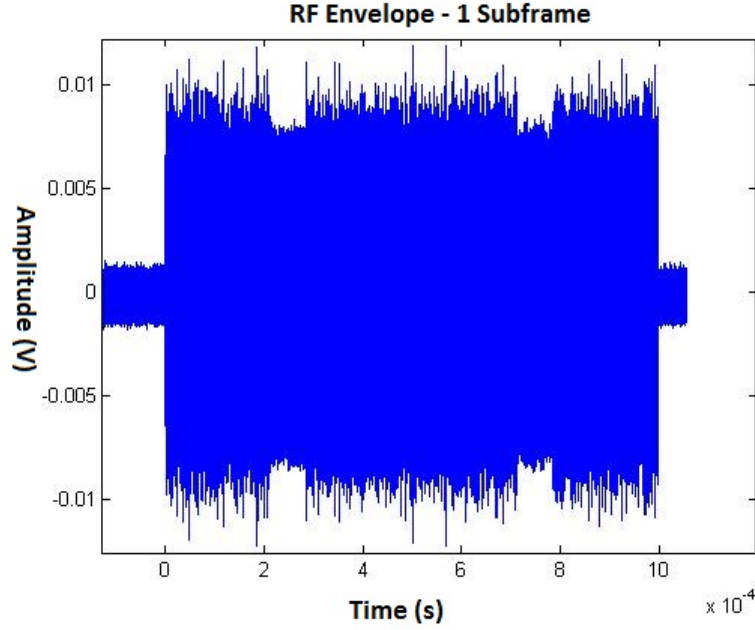


Figure 3.12: VSA capture of time domain waveform.

priately small bin size. Figure 3.13 shows the result of this analysis using LTE MCS-10, which uses QPSK modulation. The PAPR for this particular subframe was 7.6143dB, which is within the range of the simulations, although certainly at the top end. It should be noted that the plot shows the power distribution normalised to 0dB, so the mean power level is actually 0dB minus the PAPR, so a normalised -7.6143dB.

Figure 3.14 shows a repetition of this procedure for LTE MCS-11, which uses 16-QAM modulation. As was demonstrated in the simulations, it can be seen that the PAPR of the signal distribution is much higher at 8.5944dB. Again, this is towards the top end of the simulated range, but still within this. One of the more interesting features to note is that whilst the distribution of signal power in the QPSK case could be said to be approximately normal, although with a slightly negative skew. The distribution in Figure 3.14 is much more unique, with a bulge above the mean power level, and a significantly negative skew below this.

A limitation is this technique is still the requirement to process a large amount of data. In order to trigger correctly, capture data, and then process every value to calculate PAPR, a time of at least 15 minutes is required. Multiplied by the 100,000 iterations used in simulations for each MCS and bandwidth and this method rapidly becomes unfeasible.

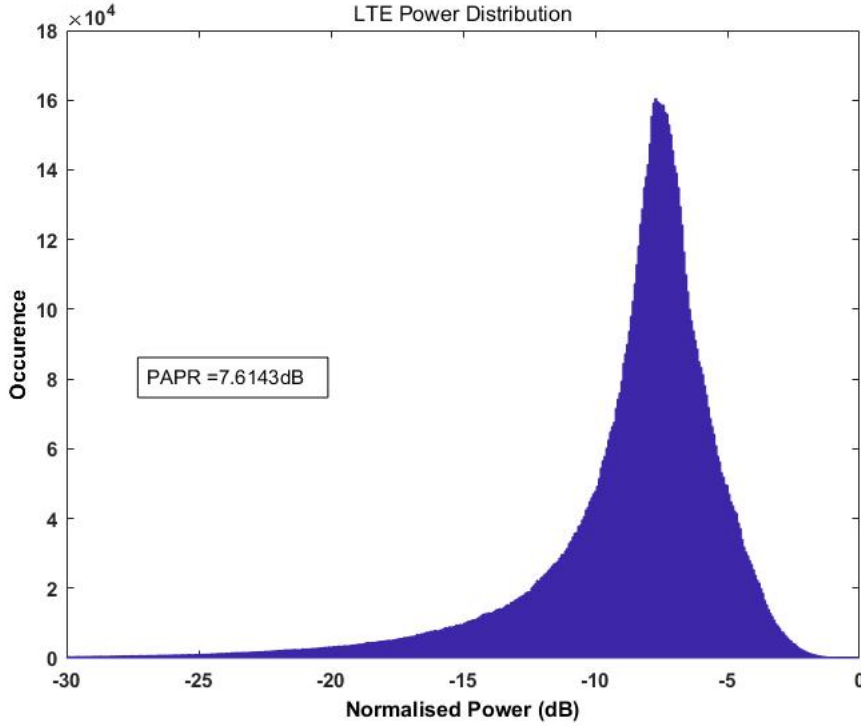


Figure 3.13: Measured power distribution for MCS-10.

3.4.2 Measured Power Distribution

In order to try and gain a better idea of how signal power distribution can be better measured, the additional functionalities of the base station emulator were analysed in detail. It was found that within the spectrum analyser test kit, a CCDF function was present. In order to test this out, a UE is connected to the BSE, both electrically and on the network, and instructed to transmit random data over the shared channel. When this has been set up, the spectrum analysis tools are started, and CCDF of signal power can be plotted as a distribution over 10^6 points. By varying the bandwidth and modulation scheme of the signal, it is possible to compare these results to the initial simulations.

3.4.2.1 Modulation Scheme

Figure 3.15 shows the first CCDF plot produced. This uses a similar set of parameters to the first set of simulations with a bandwidth of 10MHz and QPSK modulation. This plot is slightly different from the simulated results, as the value on the x-axis is the mean signal power, rather than the PAPR used in simulations. The yellow curve is the plot of signal power distribution from the UE, whilst the cyan plot is a standard Gaussian distribution for reference. For the duration of these experiments, the power at which the

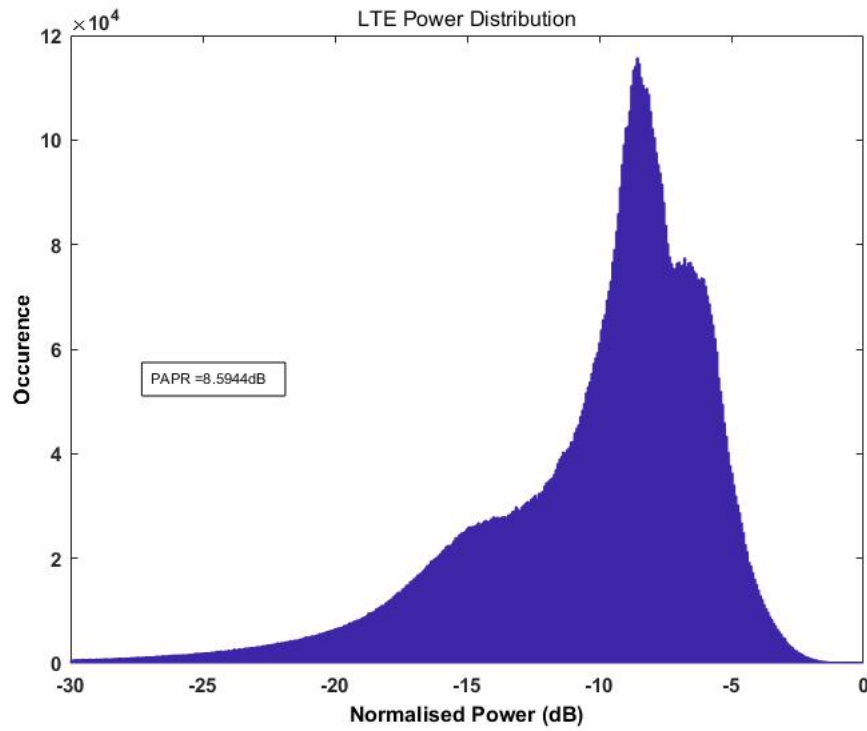


Figure 3.14: Measured power distribution for MCS-11.



Figure 3.15: Measured CCDF for MCS-10; Toby L210 modem, 10MHz bandwidth, E6601A analyser.

UE was transmitting is fixed in a closed loop in the MAC layer at 0dBm. Obviously this can fluctuate a bit, so comparisons will always be in dB relative to mean power level.

It can be seen from the figure that the peak power level, or PAPR is 7.78dB, which is in agreement with the measurements taken from the VSA. One really important feature to note

is that although the peak signal excursion relative to the mean is 7.78dB, the breakdown on the right hand side shows that the signal only ever exceeds the 7.38dB point for 0.0001% of the time. From this it can be seen that PAPR isn't necessarily a particularly good measure of a signal, as it is so heavily influenced by outliers. It can easily be seen from the figures where some of the inefficiencies in an LTE system lie. Even if an amplifier was biased to produce no distortion at the mean power, 41.04% of the signal excursions are below the mean power, and thus being amplified inefficiently, and this is before the requirement for backoff from the PAPR at 7.78dB.



Figure 3.16: Measured CCDF for MCS-11; Toby L210 modem, 10MHz bandwidth, E6601A analyser.

Figure 3.16 shows the equivalent results for the case using 16-QAM modulation. Straight away it can be seen that peak excursion is much higher, 9.01dB compared with 7.78dB in the QPSK case. A better method of comparison would be to look at the excursions above 0.1 and 0.01% In this comparison for 0.1% the value is 5.52dB and 6.26dB for QPSK and 16-QAM respectively and 6.67dB and 7.53dB for the 0.01% limit. In both limits it can be seen there is a significant difference in peak signal excursions about the mean.

Unfortunately the fact that the simulations are based on PAPR distribution rather than signal power distribution mean a comparison is only possible using the maximum value of simulated PAPR distribution and the measured peak signal relative to the mean. The results from this comparison are shown in Table 3.4. It can be seen that there is a good agreement between the figures for QPSK, but a rather large gap between the values for 16-QAM of over 1dB. This is quite a significant difference, and could be for a variety of reasons, although the most likely explanation is that as the acPAPR metric is so heavily influenced by a single outlying value, and the hardware measurement has been based on a statistically rare peak

value.

Modulation Scheme	Simulated Peak PAPR (dB)	Measured Peak (dB)	Difference (dB)
QPSK	7.58	7.78	-0.2
16-QAM	10.16	9.01	1.15

Table 3.4: Hardware and simulation comparison for MCS.

3.4.2.2 Bandwidth

Similarly for bandwidth, measurements can be taken using the BSE to analyse signal power CCDF. Figure 3.17 shows the results for a 6RB (1.4MHz) bandwidth. It can be seen the PAPR in this case is a relatively modest 6.45dB, which is to be expected with a small bandwidth and low modulation scheme. Similarly to previous results, 41% of the signal power is below the mean, and only 0.1% is over 5.7dB.

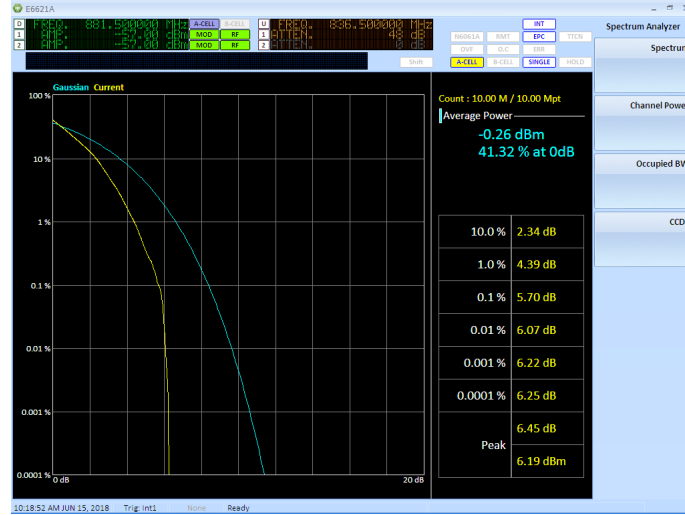


Figure 3.17: Measured CCDF for 1.4MHz; Toby L210 modem, E6601A analyser.

Regarding the results for a 25RB (5MHz) it can be seen that the PAPR is higher, as expected, at 7.28dB. Interestingly, in comparison with the results from 1.4MHz, the distribution of signal power is different, with higher, low probability signal excursions, but lower power thresholds for distributions over 10%, 1% and 0.1%, suggesting an interesting skew to the power distribution.

A comparison with simulated results can be seen in Table 3.5. These results are very interesting, in that whilst the trend of a larger bandwidth means a larger PAPR, there are significant discrepancies between simulated and measured behaviours. It is believed that again, this is due to the heavy influence of outliers on the PAPR metric, and in future, a better comparison of simulated signal power distribution would be appropriate.

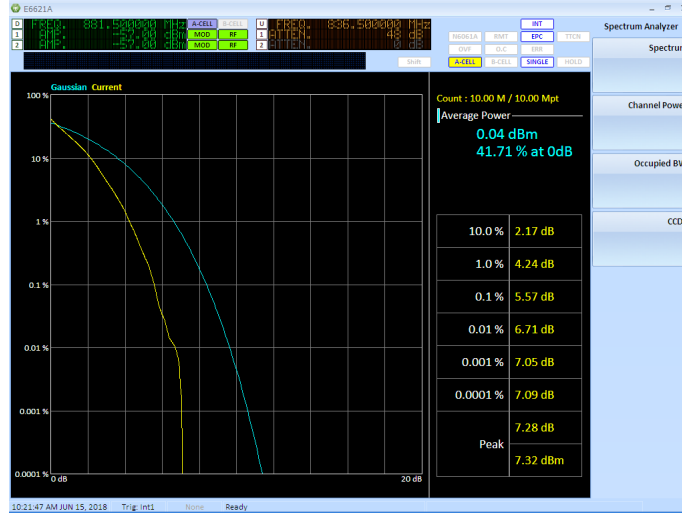


Figure 3.18: Measured CCDF for 5MHz; Toby L210 modem, E6601A analyser.

Bandwidth	Simulated Peak PAPR (dB)	Measured Peak (dB)
1.4 MHz	8.55	6.45
5 MHz	8.83	7.28

Table 3.5: Hardware and simulation comparison for bandwidth.

3.5 Other Measurements & Analysis

During the course of this research on simulated signal analysis and becoming familiar with the functionality of the base station emulator, there were a few offshoots that are still worthy of inclusion due to their potential use. The two topics covered are the distribution of signal PAPR on a symbol-by-symbol basis and also how the peak uplink rates of LTE Cat-0 and Cat-1 might affect signal properties.

3.5.1 Symbol Level Analysis

The previous part of this work has focussed on the change in PAPR over an LTE subframe, this is largely because considering the duration of a subframe, and the frequency of changes to the MAC layer, low cost and efficient techniques can be utilised to increase efficiency. This is a far cry for the other end of the spectrum, which might for example require a supply voltage modulated at 20MHz as part of an envelope tracking system. Whilst not approaching this level of complexity, there is some merit in looking at the PAPR on a finer resolution with respect to time, in this case how it varies from symbol to symbol within a subframe.

Figure 3.19 shows a typical resource grid from the shared channel for an uplink trans-

mission within an LTE system. The x-axis is the symbol number, in this case showing the 14 symbols that make up a subframe, and the y-axis is the sub-carrier index, or frequency axis, in this case there are 72 sub-carriers which make up 6 resource blocks bandwidth (1.4 MHz). What can be seen immediately is that there are two different types of symbols in the subframe; the standard PUSCH symbols, which contain the user data transmitted over the shared channel, and also the demodulation reference signals used to decode the subframe. There are two DRS symbols per subframe, at symbols 4 and 11 if indexed to 1, and these are always in the same position.

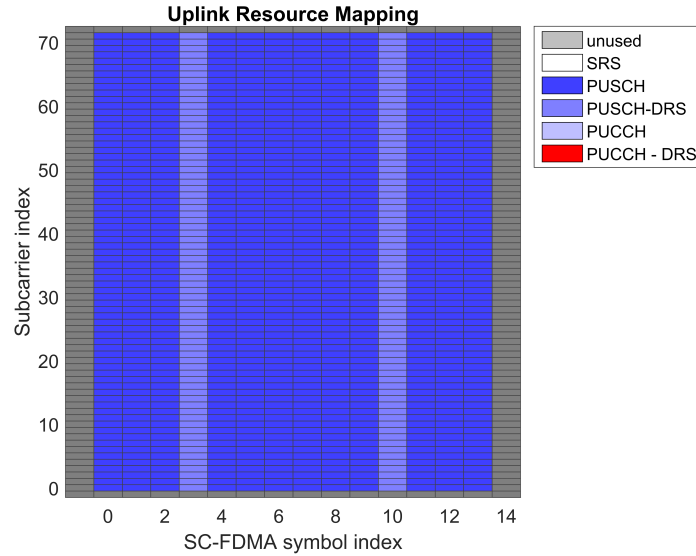


Figure 3.19: Resource grid population.

Increasing the temporal resolution of analysis, PAPR can be analysed on a per-symbol basis, as is illustrated in Figure 3.20. It can be seen that there are two regions within the waveform where the peak levels are noticeably lower than the rest. This is because there are two out of the fourteen symbols within this subframe are demodulation reference signals, modulated with a Zadoff-Chu sequence, possessing a much lower PAPR than the rest of the waveform, which will use QPSK or 16-QAM as directed by MAC layer information. In order to verify this feature, we can see an plot in Figure 3.12 where the capture of a real signal using a VSA demonstrates the same, lower amplitude characteristics around symbols 4 and 11.

The implication of these results is that a basic dynamic power supply (DPS) system could be implemented, that drops the supply voltage by a certain percentage for the duration of symbols 4 and 11 within every shared channel subframe. There would be no requirement for any signal analysis, and the power supply would have to be modulated at the symbol rate of 14kHz, which is still a relatively minor requirement compared to a 20MHz envelope

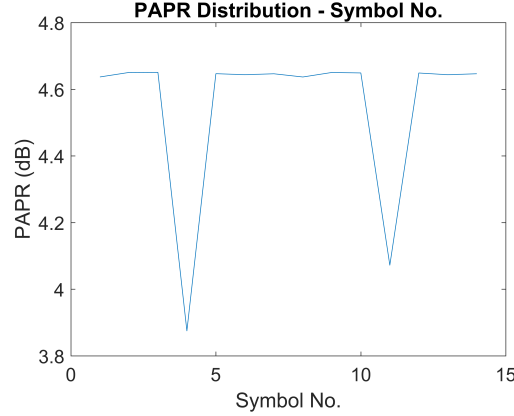


Figure 3.20: PAPR over 14 symbols.

tracking system.

3.5.2 Rate Constraint

During the course of this work, the concept of machine type communications began to be incorporated within the LTE specifications. In particular the case for Cat-0 and Cat-M1 are of much interest to the low cost, low rate communications application. One of the key parameters for Cat-0 & Cat-M1 devices is a restriction in uplink data rate to 1MB/s. Using previously gathered data on uplink data rates a table was produced to present rate versus the two parameters that primarily affect this; bandwidth allocation and modulation and coding scheme.

Figure 3.21 shows all combinations of resource allocation that result in a rate of just over 1MB/s or less. One of the most important conclusions that can be drawn from this is that only two of the acceptable combinations use MCS 11 and 12. This is significant because MCS 11 & 12 use 16-quadrature amplitude modulation (QAM) rather than QPSK, and as has been shown in 2.1, this increase in modulation scheme causes a rise in PAPR of around 1dB, increasing the amount of back off that must be applied to an amplifier design, thus reducing potential efficiency. The upshot of this is that it should be possible to apply this QPSK only constraint to a LTE based machine-to-machine (M2M) system, and produce a much more efficient design.

In the time between this research being initially conceived and the date of thesis completion, Cat-0 and Cat-M1 have of course been formalised into the 3rd Generation Partnership Project (3GPP) specifications, release 13 in 2015 [19]. Both in fact do make use of both QPSK and 16-QAM. Whilst the reasons for this are most likely enhancing capacity and throughput, it may be observed that an opportunity has been missed to lay the groundwork for a more efficient overall device architecture.

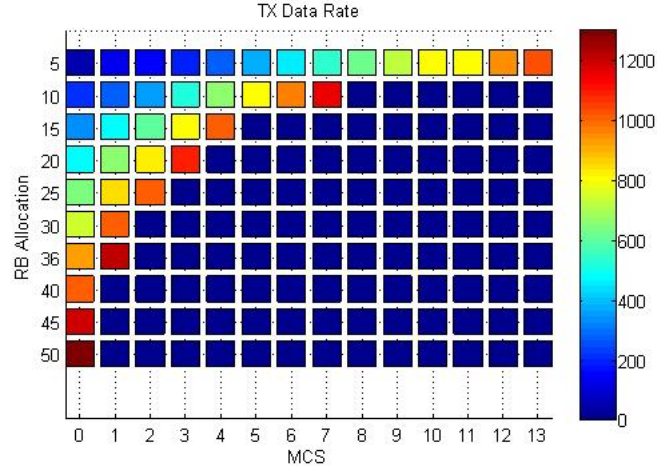


Figure 3.21: Configurations for limited uplink rate, data rate coloured as kB per second.

3.6 Conclusion

One of the key points from this chapter is that the distribution of signal power in an SC-FDMA uplink signal, changes significantly with parameters that are recorded in the MAC layer such as bandwidth, modulation scheme, and obviously transmitted signal power. The range of PAPR variation within these scenarios is generally significant enough to mean that enacting a dynamic power supply system for the power amplifier is a viable way of increasing the system efficiency. Systems such as dynamic power supply and load modulation traditionally require a large amount of signal processing, in order to respond to relevant signal characteristics, however this chapter has illustrated how MAC layer information can be used to do this with virtually no additional computational overhead.

One of the limitations in determining the correct biasing point and supply voltage for a practical amplifier is that performance will always be based on test waveforms specified in the LTE standards, it would unfortunately take a larger program of work on this topic in order to understand better the relationship between test waveforms and the distribution of signal power likely to be seen in the course or normal operation of a modem, especially as the data used for test waveforms may be manufacturer specific.

One of the interesting conclusions that can be seen is that PAPR is not necessarily a good metric for signals as far as modelling power consumption and proposing efficiency enhancements is concerned. This is because is a metric that is heavily reliant on outliers, as far as signal parameters are concerned. One single excessively high signal power level will increase the PAPR metric for the entire measurement interval. The problem with this is that if further analysis is done, to determine how efficient a system can operate efficiently

for a given PA biasing condition based on PAPR, we don't have enough information to determine the system efficiency.

A much better solution to this problem is to consider the probability density function of signal power levels as a whole. This gives the opportunity of selecting a biasing point based on a fraction of the power distribution that we can accept the production of distortion products. A starting point to this would be to use measurements of real LTE signals and categorise them with respect to n x standard deviations to mean ratio, with n most likely being in the 3 to 5 range. Work would be required using power amplifiers backed off by this ratio, to analyse the effect of n on likelihood of distortion products, and the impacts these might have on real network uses. By using standard deviation in the ratio of the performance metric rather than peak signal power, the effect of outliers on the metric is drastically reduced.

$$Ratio_{dB} = 20 \log \left(\frac{\mu + n\sigma}{\mu} \right) \quad (3.4)$$

An example of this is shown in equation 3.4, where μ is the mean signal level over a sufficiently large number of samples, σ the standard deviation, and n an integer, again, likely between 3 and 5.

Chapter 4

Network Deployments & Power Consumption

THIS chapter is concerned with measurements and modelling of Long Term Evolution (LTE) (4G) systems. Here, work is presented using both laboratory based measurements and those taken using a live network in order to further validate observations and enhancements proposed later in this thesis. Detailed consideration is given to the factors that determine how power is consumed within a piece of user equipment on an LTE network, with particular emphasis on machine-to-machine (M2M) applications, and suggestions are made as to how this can be improved.

4.1 Introduction

With the predicted dramatic increase in M2M communications, it is of particular interest to this thesis to examine cases such as wireless sensor networks, which are likely to be remote and battery powered. It is important to form an idea of what kind of battery life we can expect for a given application. This chapter concerns itself with measures of power consumed both within closed laboratory environments and on active networks, including observations to explain the differences in between these results. Hardware was designed to measure the wide dynamic ranges of current consumption observed in cellular communications before deploying this in a laboratory scenario to characterise a particular modem, indicating transmission power consumption is dominated almost entirely by the transmit power level, and thus the power amplifier and associated systems whilst power consumption during the receive process is proportional to both the data rate and the received signal power. Supporting work on live networks illustrates how simple small transmissions may consume much more energy than predicted due to issues with base station algorithms.

4.2 Power Consumption Model

LTE lends itself to a wide variety of use cases due to the highly adaptive nature of the transmission and reception data rate and power output. The amount of data transmitted in one transport block of duration 1ms, varies from 2 to 5477 bytes, (assuming modulation and coding scheme (MCS) index is limited to 20)[20] depending on the modulation and coding scheme used and the amount of bandwidth allocated to the user equipment (UE). In realistic terms, a minimum resource block allocation would increase this lower limit to 19 bytes.

This research has focussed on M2M scenarios where data packet size is likely to be comparable to associated overheads such as the random access channel (RACH) process, as will be seen later in the chapter. The total amount of energy consumed in these transmissions is a function of two main factors, the amount of RF transmission power needed to effectively communicate with the base station, and the duration over which this takes place.

Figure 4.1 illustrates the factors affecting power consumption. The quality of the RF channel including signal to noise ratio (SNR) dictates a metric called channel quality information (CQI). CQI then be used by the base station (evolved node B (eNB)) to set the required transmission power the UE must use, and the MCS supported. MCS in turn can be combined with the bandwidth allocated to give transport block size (TBS), the amount of data that can be transmitted in a 1ms subframe. In order to further explain this model, this can be split into two sub processes; Power and duration.

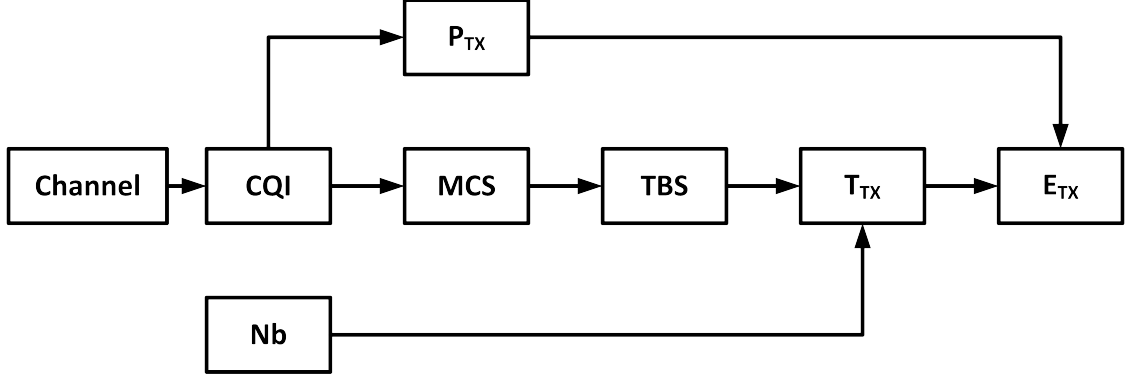


Figure 4.1: Factors affecting TX energy consumption.

The additional acronyms used in the diagram are Number of bits (N_b), Transmission time (T_{TX}), Transmit energy consumed (E_{TX}) and Transmit power (P_{TX})

4.2.1 Power

A thorough analysis of LTE transceiver performance is given in [21], summarised in Equation 4.1. This models transceiver power consumption as the sum of power consumed by baseband transmit and receive processes (P_{TxBB} & P_{RxBB}) and radio frequency (RF) transmit and receive processes (P_{TxRF} & P_{RxRF}).

$$\begin{aligned}
 P_{tot} = & m_{idle} \cdot P_{idle} + m_{idle}^- \cdot \{ P_{con} + m_{Tx} \cdot m_{Rx} \cdot \\
 & P_{Rx+Tx} + m_{Rx} \cdot [P_{Rx} + P_{RxRF}(S_{Rx}) \\
 & + P_{RxBB}(R_{Rx}) + m_{2CW} \cdot P_{2CW}] \\
 & m_{Tx} \cdot [P_{Tx} + P_{TXRF}(S_{Tx}) + P_{TXBB}(R_{Tx})] \}
 \end{aligned} \tag{4.1}$$

Similar modelling processes have shown that total power consumption on the transmit side is based almost entirely on the RF output power, with the transmitter (TX) data rate having very little effect, due to the large energy consumption of the power amplifier and associated systems. The RF power level itself is well described in [22] and [23], shown in equation 4.2. This shows UE power level is set by the eNB, dependent on reference power P_0 and path loss (PL) as expected, but with additions for resource block allocation (M), MCS (Λ_{TF}) and closed loop operation (f). [24]. Whilst path loss is hard to generalise for an LTE system, due to the variability in path loss exponent and particular density of base stations, depending on environment, a worst case figure for a low rate link would be 163.4dB [25], In reality, particularly within urban and suburban environments, path loss would be

expected to be considerably lower than this.

$$P_{Tx} = \min(P_{max}, P_0 + 10\log_{10}(M) + \alpha \cdot PL + \Lambda_{TF} + f) \quad (4.2)$$

4.2.2 Duration

In the first approximation, transmission duration can be calculated as packet size, divided by transport block size, which would be valid for the continuous transmission case. The only parameter that would be required for a model would be a derivation of MCS as a function of SNR; with higher MCSs (higher order modulation and less forward error correction) being used over more stable channels.

Modelling the likelihood of a particular MCS being prescribed can be particularly challenging, as this is usually done with proprietary algorithms in the eNB. These algorithms are most likely aimed at maximising metrics such as throughput or latency.

One of the biggest differences with machine type communications over user-centric traffic is the duration. If uplink data can fit into a single subframe, the amount of time and energy spent transmitting the request for resources will be approximately the same duration again. In addition to this, there are many other LTE system overheads that can throw off a data based power consumption model.

4.2.3 Idle Time

Once the UE has successfully transmitted data, there is a sequence of power states the devices passes through before true idle mode, the state diagram in Figure 4.2 illustrates this.

Once transmission on the physical uplink control channel (PUCCH) has occurred in the active state, an inactivity timer begins to count down to a more efficient operating mode. When this timer has expired, the device enters 'Short discontinuous reception (DRX)' mode, where resources are no longer assigned, and reception of control information from the eNB is periodic rather than continuous, in order to reduce energy consumption. Similarly, a short cycle timer is initiated. Upon expiry of this, the UE enters the 'Long DRX' state, which simply increases the length of the period between waking to receive system messages.

Once the system inactivity timer has expired, the UE enters the 'radio resource control (RRC) Idle' state, where it is no longer connected to the network, but continues to be able to receive paging data in a DRX scheme. The idea behind this scheme is that power consumption reduces as the mode of the device moves from the top of the diagram to the bottom, but the latency for a new transmission increases. Ideally this state machine should

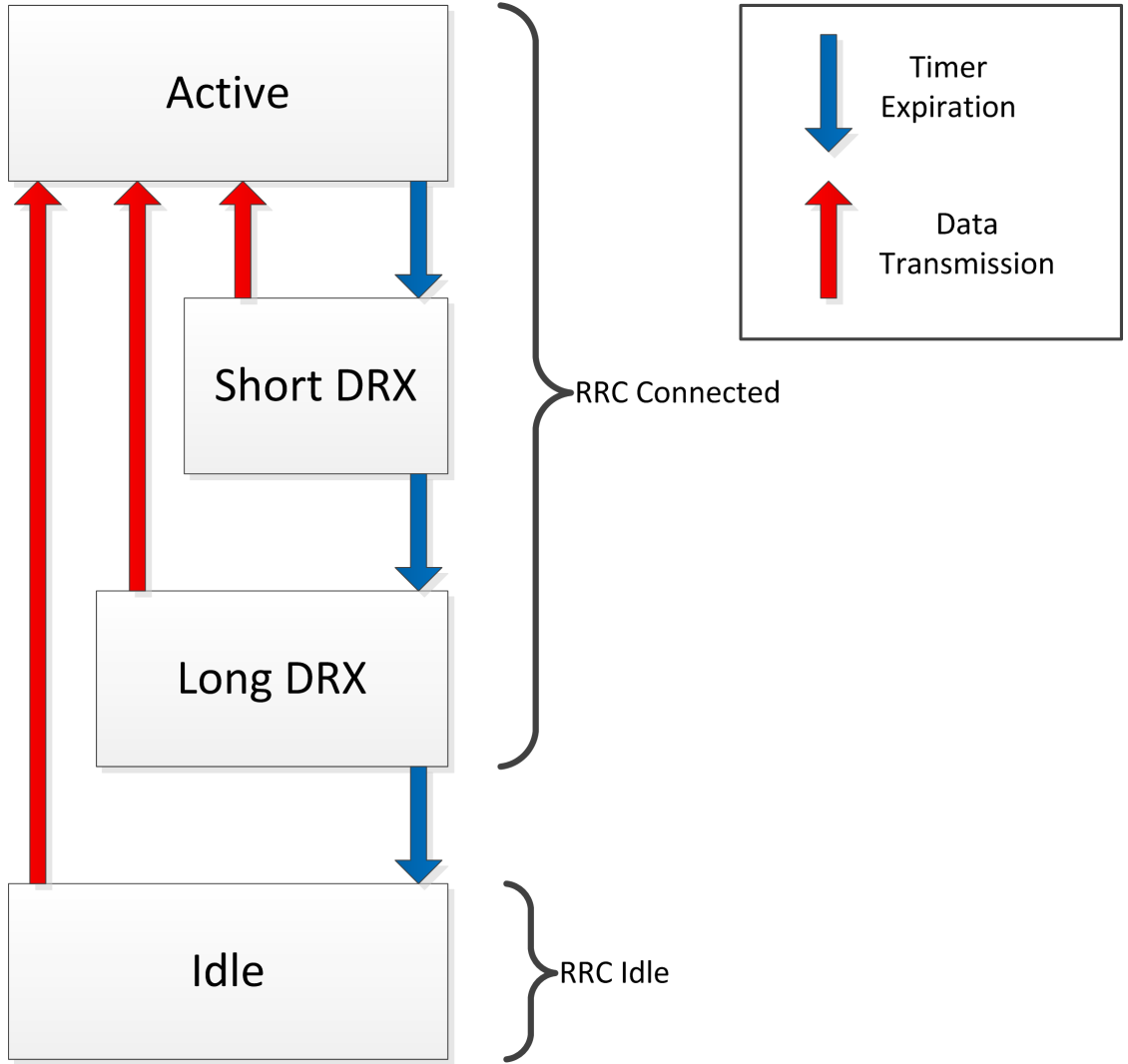


Figure 4.2: UE power states [26].

make for an easily characterisable system, however this has not been found to be the case in network measurements conducted by the author. Significant research exists surrounding the optimisation of various DRX parameters, however this tends to be far from trivial due to the varied nature of network traffic, access schemes and customisation by network operators.

4.3 Current State of the Art

Previous work surrounding modelling of uplink and downlink LTE power consumption between (UE) and (eNB) tends to focus on long term measurements, proportional to activity in the baseband and RF blocks of the transmit and receive chains [21], [27]. These models are generally valid and representative for systems transmitting or receiving large amounts of

data ($\approx 1\text{MB/s}$) continuously. Where packet size is small in comparison with overheads, such as sensor node reports transmitted as infrequently as daily or less, these models become less accurate.

More realistic work looking at periodic updates has been done in [28]. This work considered infrequent transmission in smart phones, typical of the packets generated by background processes. These are characterised in terms of traffic type, then processed by a model that takes into account the effect of the subsequent DRX process upon power consumption. One of the interesting conclusions are that as far as smartphone traffic is concerned there are generally only two types of traffic related to background application processes, which makes modelling much simpler. Another useful outcome is that the DRX inactivity timer has a much smaller effect on the sleep ratio of a device than the DRX long timer and the on duration timer. However, this work still lacks a comparison with live network measurements for verification but provides insight into the processes within LTE that can influence power consumption.

DRX and the optimisation of its parameters for low power have been well examined in [29]. This work considered how the transmission time interval (TTI) size affects power consumption together with the DRX parameters. This is a slightly artificial scenario as in LTE, the TTI is fixed at 1ms, as unlikely to deviate from this without a major system overhaul. Further, [29] suggests that 10 ms would be the optimum TTI for efficiency enhancement with minimal effects on latency. Some conclusions are made on the power saving efficacy of short and long DRX processes, however again these are done in the context of benefits in a variable TTI environment.

A good analysis of LTE UE power consumption has been completed in [30], where the use of LTE for M2M applications such as smart grid access is evaluated. The proposal here is that with short bursts of M2M traffic, the system within the coverage of a particular eNB is no longer limited by the data capacity of the network, but is instead limited by the signalling constraints in the RACH and uplink and downlink control channels. The paper finds that for ideal operation, M2M traffic on an LTE network required a fundamentally different approach to access. The limitations specified for small payloads are within the physical downlink control channel (PDCCH) or physical random access channel (PRACH) if the overall system bandwidth is sufficiently large. For larger UE payloads, the limitations are as expected, in the physical uplink shared channel (PUSCH). Again, additional signalling within access procedures is identified for large reductions in theoretical capacity of the system. The modelling of the LTE system and procedures is excellent, and would be worth incorporating into actual power consumption models rather than just system capacity.

An excellent overview of the challenges involved in M2M over LTE is presented in [31].

This addresses some of the key challenges in modelling system performance and energy consumption; namely the large and diverse range of applications, each with their own requirements in terms of traffic profiles, latency and energy consumption. In addition to this, the huge number of devices that are forecast to be network connected is sure to put a strain on any infrastructure. A large part of this work is dedicated to proposing enhancements to the existing LTE system in order to facilitate the growth of these M2M use cases.

Regarding developments that have been made in this field, a review of some of the advanced features in 3rd Generation Partnership Project (3GPP) release 13 plus forthcoming developments in narrow band internet of things (NB-IoT) is given in [32]. To summarise some of the main changes to the 3GPP specifications; Release 12 introduced a new UE category - Category 0, which has a much more relaxed set of communications requirements, these are discussed in Chapter 2. Going further, in release 13 a wider range of improvements were implemented. These include narrowband operation and reduced transmission modes, a useful summary is provided in [33].

Regarding the actual type and profile of traffic within the network, an excellent analysis is presented in [34]. This work compares and contrasts data connected from a cellular network in the United States, paying attention to the differences between smartphone data and M2M traffic. One of the limitations of this study, is that the data collected is from 2013, and only over second generation mobile communications (2G) and 3rd generation mobile communications (3G) networks. As the use cases and uptake of M2M communications are continually evolving, so are the patterns of data produced, however some useful conclusions can still be drawn. Not surprisingly this work finds that there are considerable differences between smartphone traffic and that from M2M devices, particularly in the increased ratio of uplink to downlink traffic. Some interesting insights come from the breakdown of device type classes. An example of the largest proportions would be 18% as asset tracking devices, and 51% as fleet management solutions, a very high combined proportion. In addition to this, the report states that while smartphone traffic seems to track the diurnal cycle of peoples waking hours, M2M traffic is more likely to track working hours. This is something that could provide strong opportunity for optimisation in a system where scarcity of resources becomes a factor; Whilst it is understandable that fleet management systems must be active most during working hours, it would be advantageous for metering type applications to make use of the less congested night time periods for the uplink of data, thus easing some of the pressures on the communications system.

More extensive work on traffic issues in M2M over LTE is presented in [35]. This argues that M2M traffic's temporal distribution appears to be more evenly distributed than as described in [34], however it is likely that there are large differences once this is broken down

into particular use cases. Some good methods of modelling M2M traffic are put forward, using beta distributions and Markov chains. Mention is made of a study on machine-type-communication (MTC) over Global System for Mobile communication (GSM) that suggests highly synchronised M2M communications are more likely to negatively influence the user experience in human-to-human (H2H) communications as opposed to less synchronised access schemes [36]. An example of this happening would be large network of environmental sensors, all attempting to upload data at a particular and exact time of day, blocking access to other users. It is presumed that this could become exponentially worse with large numbers of highly coordinated sensors connected to an LTE network, as collisions within the RACH procedure combined with the finite resources available to an eNB have the potential to clog the system up quite effectively.

An elegant solution to these types of problems is proposed in [37] using a technique called access class barring (ACB). This is a congestion control scheme aimed at getting UE to spread their access request through time so as not to overload signalling layers. This is currently implemented in Long Term Evolution advanced (LTE-A). The basis of ACB is that a UE may randomly delay its RACH attempt proportional to a barring rate and barring time provided by the eNB. Whilst this procedure does work, it is good to see that the paper notes that power consumption is something that must be taken into account here, supporting the aims of this thesis. Considering the case where instead of waking up to transmit a small packet of data; using an ACB scheme to delay this process could cause a notable increase in energy consumption due to the total 'awake time' in the process, obviously a negative result. Taking into consideration a much more nodally dense area, the standard LTE RACH procedure might result in a jamming effect on signalling layers, and a vastly increased 'awake time' for each node, however this is likely to be mitigated by an ACB scheme. It is presumed that the optimum way forward would be to work a dynamic ACB scheme into the eNB, with the ability to modulate barring rate and barring time with the average traffic for a particular time of day.

Similar methods of performance enhancement for an integrated system are mentioned in [38], in particular, proposing a method called Access Grant Time Interval (AGTI). The principle of AGTI is that a certain proportion of an LTE frame is reserved for a particular traffic type, e.g. M2M, with the rest being reserved for more conventional H2H traffic. Particular sub-groups are formed depending on the particular quality of service (QoS) requirements of the technology. A dynamic AGTI scheme is proposed, where slot allocations of particular sub-groups are monitored, and the fraction of resource allocation is modulated accordingly, in order to maximise system performance.

To summarise, there has been a good deal of work done on this subject area in attempting

to model power consumption in cellular networks, however this tends to focus on power intensive continuous transmissions. Additionally, very few pieces of work use measurements on live networks. This is presumable because sufficient degrees of freedom exist over factors affecting power consumption to make modelling a far from easy task. This chapter address the need for this by comparing both lab based, and real network M2M style transmissions in an attempt to see how easily power consumption can be modelled, and whether there are any additional important factors that must be taken into account.

4.4 Hardware Design

4.4.1 Overview

In order to measure and model the power consumption of a particular system, appropriate instrumentation must be purchased or constructed in order to provide an accurate measurement of the appropriate parameters. In terms of measuring power consumption, there are two main areas to focus on, direct current (DC) and RF. DC power consumption refers of course to the energy consumed by the supply lines into the device under test (DUT), and is not simply a static value, but will in fact possess higher frequency components proportional to the rate at which internal processes occur in the DUT and the amount of capacitive power supply decoupling used to remove these components from the power supply lines.

In order to gain a comprehensive idea of what is going on in LTE uplink communications, a variety of different parameters must be measured. Figure 4.4 shows the basic flow of data and control signals used in phase I laboratory measurements used to achieve this. The bottom row of the figure shows the actual data flow during a transmission; Data flow occurs from right to left, with the furthestmost left block being a Raspberry Pi used to generate data, typically for initial experiments, this could be a constant flow of data as a throughput test, video streaming or small packets from a wireless sensor network. The Raspberry Pi client then connects to an LTE network using a suitable modem, in this case a Ublox Toby L210, illustrated in Figure 4.3. The network infrastructure is provided by a Keysight E6621A PXT base station emulator, in turn this has another Raspberry Pi connected to it, in order to function as a server, accepting data and providing a measure of throughput. Figure 4.8 gives a photo of the full set-up .

The top part of the figure illustrates the measurements that will be taken, each of which will be described further in this chapter. Power supply measurement will produce a detailed record of DC power consumption of the modem, spectrum analysis will record the RF output power and other characteristics, whilst physical layer protocols may also be logged in order to gain a better idea of the data transmission processes involved.



Figure 4.3: Toby L210 LTE modem.

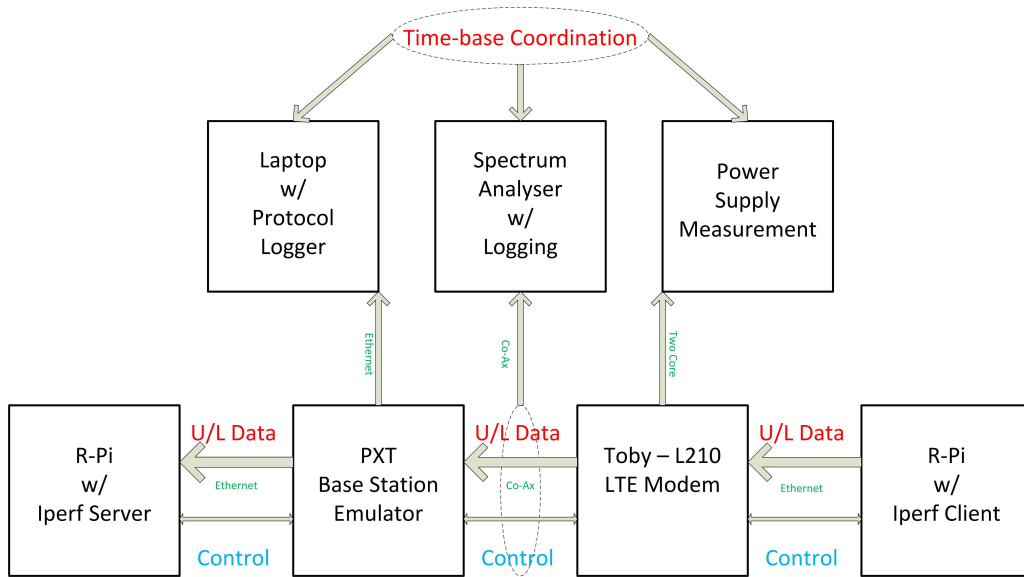


Figure 4.4: Data flow of power measurement apparatus, developed by the author.

4.4.2 Current sensing

The initial design for the current sensing hardware was based on the current sense resistor technique, as previously used in relevant work such as [39]. This was expanded slightly to take into account the potentially high dynamic range of the input current across all radio access technology (RAT) modes, which could vary from $15\ \mu\text{A}$ when powered down to 2.5A at peak GSM transmit power [40] corresponding to a dynamic range of 104dB. Whilst it would be possible to design a single stage of sensing and amplification to deal with the peak

current of 2.5A, the sensitivity at the lower end of the scale would suffer, i.e. 104dB is an exceptionally large dynamic range for a single stage, thus a multi stage design was used, as illustrated in Figure 4.5. Three stages were chosen to provide an acceptable amount of dynamic range and low noise performance over the available number of analogue to digital converter (ADC) inputs. Later work used a single stage current to voltage conversion, as confining the modem to a single RAT (LTE) dramatically reduces the peak current consumption and thus dynamic range requirement.

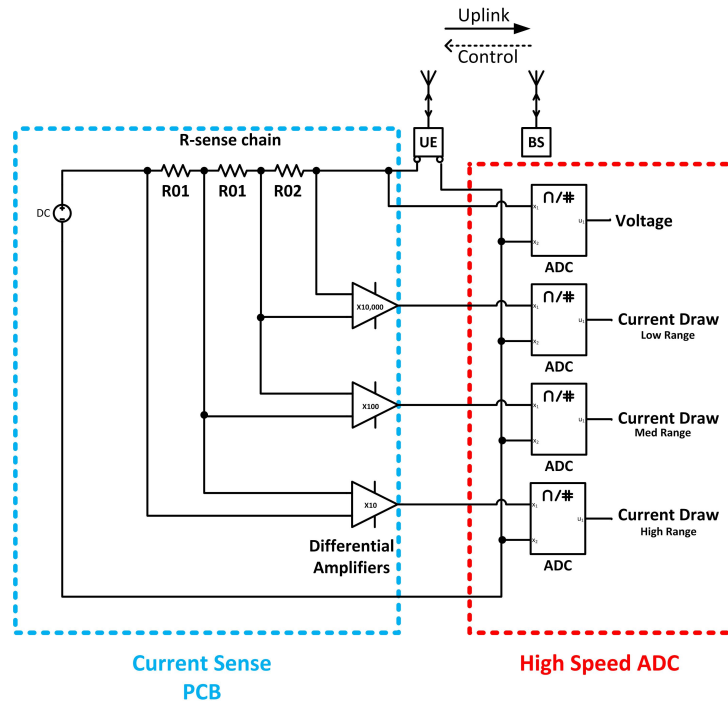


Figure 4.5: Schematic of power measurement apparatus, including high dynamic range capability.

4.4.3 Noise Analysis

As the voltages dropped over successive current sense resistors are very small, it is worth conducting a noise analysis of the system to ensure that the lower limits of each measurement range can be measured, rather than obscured by the noise floor. A large number of parameters are evaluated to take into account thermal noise, current noise and device noise in order to ensure that the prospective hardware's minimum detectable signal rating is sufficiently small.

The amplifier chosen for this work was the Analog Devices AD625 [41]. This was selected due to the excellent low noise performance, and availability of suitable form factors for low volume prototyping. A summary of the topology used for the noise analysis is shown in

4.6, minus the current sense resistor that would be inserted in between inverting, and non-inverting inputs. Note the addition of the series resistors, 'R' and the filter capacitors. These obviously have the effect of reducing the bandwidth of the system and increasing the noise floor due to the series resistive elements, however these filtering components were considered important to reduce the effects of RF interference, especially in this use case, as recommended by the datasheet [41].

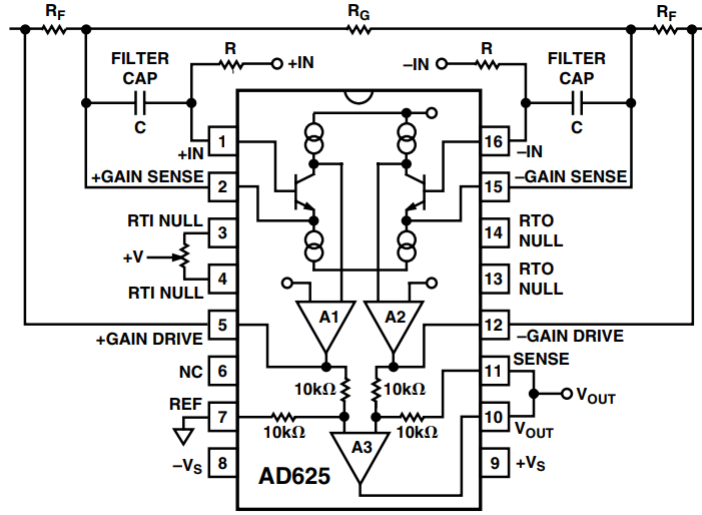


Figure 4.6: Instrumentation amplifier configuration [41].

Several noise parameters must be evaluated; firstly the thermal noise, calculated with equation 4.3. Note that the resistance in this case is for a single leg of the input, i.e. half of the sense resistor plus one of the resistors in the input filter. This gives the total amount of voltage noise in Volts per \sqrt{Hz}

$$E_{n_{rb}} = \sqrt{4kTR} \quad (4.3)$$

Current noise is simply the current noise parameter for the particular amplifier multiplied by the resistance that input current flows through. This is expressed separately for both the inverting and non-inverting input as $I_{nn} \cdot R$ and $I_{np} \cdot R$ respectively, again with units of Volts per \sqrt{Hz} .

The three noise parameters above are then combined as per Equation 4.4 to form an expression for total noise present at the input of the amplifier, Input voltage noise (E_{in}) as Volts per \sqrt{Hz} .

$$E_{in,i} = \sqrt{(I_{np} \cdot R)^2 + (I_{nn} \cdot R)^2 + 2 \times (E_{n_{rb}})^2} \quad (4.4)$$

Amplifier voltage noise at input ($V_{n_{in}}$) is the input stage noise of the amplifier and Amplifier voltage noise at output ($V_{n_{out}}$) is the output stage noise, these are both parameters from the datasheet. Total noise spectral density, is generally referred to the input, (Noise Spectral Density Referred to Input (NSD_{RTI})), thus $V_{n_{out}}$ is divided by gain before being combined with the previous parameters as shown in Equation 4.5. As is usual, this is expressed as Volts per \sqrt{Hz} .

$$NSD_{RTI} = \sqrt{(V_{n_{in}})^2 + (E_{in.i})^2 + \left(\frac{V_{n.o}}{Gain}\right)^2} \quad (4.5)$$

As input filtering is present at the input of the amplifier, the bandwidth of the system depends on the roll-off of this simple filter expressed in Equation 4.6.

$$BW_{noise} = \frac{1}{2\pi \cdot R_{filt}C_{filt}} \quad (4.6)$$

Finally, noise present at the output is calculated by multiplying all the noise figures referred to the input by the gain, and again by the square root of the noise bandwidth to give a final figure of noise present at the output in Volts RMS (V_{rms}).

$$E_{n.out} = Gain \times NSD_{RTI} \times \sqrt{BW_{noise}} \quad (4.7)$$

$$Min.det.I_{noise} = \frac{E_{n.out}}{Gain \cdot R_{sense}} \quad (4.8)$$

$$Min.det.I_{ADC} = \frac{V_{ADC_LSB}}{Gain \cdot R_{sense}} \quad (4.9)$$

Table 4.1 shows the gain of each stage, together with the minimum detectable signals due to both noise and ADC resolution. It can be seen that the smallest detectable signal in Stage 1 is due to noise, which is acceptable, as this is the hardest parameter to improve in a high gain design. In order to reduce this further, gain could be increased, however this will typically also increase the effect of any noise sources pre-output, i.e. thermal noise, current noise, and device input noise. Additionally, high gains will tend to produce issues with slew rates, reducing the operational bandwidth of the system.

In order to provide support for measurements in the field, a scaled down design was produced in order to facilitate DC analysis on the move. One single stage of current to voltage conversion was used, which occupies less space, and also together with supply voltage measurement only requires two ADC channels, reducing the size of data files created. The noise analysis for this is provided in Table 4.2. A gain of 41 was selected in order to give

	Gain	Effective BW (Hz)	Min Det. I ADC (A)	Min Det. I Noise (A)	Min Det. I (A)
Stage 1	10052	1.89×10^4	7.59×10^{-7}	3.90×10^{-5}	3.90×10^{-5}
Stage 2	1001	2.65×10^4	1.52×10^{-5}	9.25×10^{-5}	9.25×10^{-5}
Stage 3	100	2.65×10^4	1.52×10^{-4}	9.33×10^{-5}	1.52×10^{-4}

Table 4.1: Front end minimum detectable current values.

performance that was an acceptable trade-off between dynamic range an noise performance.

	Gain	Effective BW (Hz)	Min Det. I (A)	Max Det. I (A)
Stage 1	41	1.2×10^5	1.67×10^{-5}	1.09

Table 4.2: Front end detectable signals for single stage optimisation.

Once component values had been selected, an appropriate PCB was designed, this was manufactured and populated to form the test rig shown in Figure 4.7.

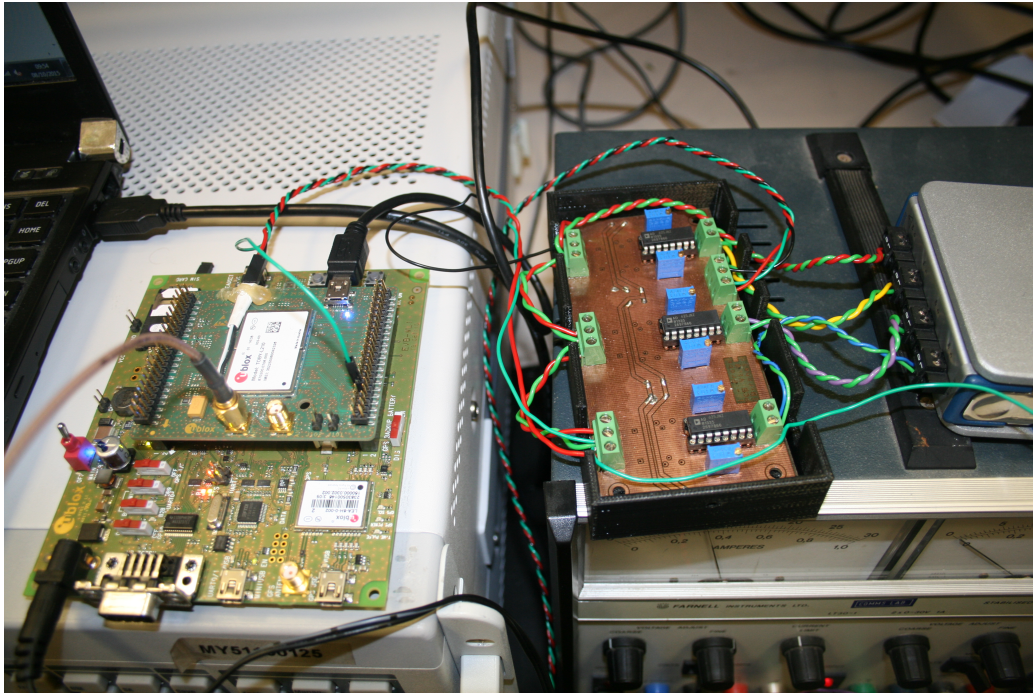


Figure 4.7: Power measurement hardware.

4.4.4 Instrumentation Interface (LabVIEW)

The LabVIEW code was originally designed with a large amount of functionality, to acquire data from the four analogue channels, perform an auto-ranging operation and provide any

filtering operations that might be required, whilst providing a graphical output of all of these stages. This functioned well for lower sampling rates, but it soon became clear that when high temporal resolutions were required, operation using a laptop was limited to around 10kS/s. In order to rectify this, a more slimmed down virtual instrument (VI) was written, which would simply acquire data from the ADC and store in an appropriate form. With these simplifications it was possible to record data from all four channels at 100kS/s for as long as required. The functionality of the LabVIEW code is further discussed with images in Appendix A.

4.4.5 Calibration

Calibration was carried out in order to make the most accurate measurements of DC power consumption, this was done using a set of precision resistors and a voltage source measured with a calibrated voltmeter, with the output being modulated in order to vary current flow. The current measurement device was placed in series with this circuit, with data from current consumption stored by the LabVIEW VI, along with recorded values of supply voltage and the resistor used. A Matlab script was later used to average the 1s of stored data for each current, these were then plotted against the true supply current, and linear regression were applied in order to obtain calibration data for future use, as shown in Table 4.3.

Action	Gradient (A/V)	Intercept (A)
Stage 1	0.00486	-0.00025
Stage 2	0.09498	+0.00140
Stage 3	0.81101	-0.00039

Table 4.3: Calibration values.

4.5 Base Station Emulator

Attempting to measure energy consumption in real world communications systems can become incredibly challenging due to the large number of confounding variables that can affect the result. Not least of these are factors such as the time varying nature of the wireless channel and differing levels of resource contention throughout the day with an operational cellular network.

The best way to ensure that initial measurements are consistent enough to generate a base model is to conduct them in a laboratory environment. This alone is a far from trivial task, as in the cellular case, equipment is required to provide almost all of the functions of

a base station, or eNB for an LTE network. The technical complexity of this equipment generally restricts its use to equipment vendors, however for the duration of this research, the lab was fortunate enough to have the long term loan of an Agilent / Keysight E6621A combination spectrum analyser and base station emulator.

Whilst the spectrum analyser functionality does not require much description, the base station emulator (BSE) offers emulation of the revision 9 LTE standard with end to end IP testing. This means that data can be streamed from a server networked with the BSE, through an LTE interface to user equipment and vice versa. The E6621A offers time domain duplexing (TDD) and frequency domain duplexing (FDD) options, variable power, frequency, MCS, bandwidth and resource grant / allocation. Test functionality allows measurement of error vector magnitude (EVM), adjacent channel leakage ratio (ACLR) and throughput during streaming tests.

A completed set-up of the emulated LTE networks with instrumented UE is shown in Figure 4.8.

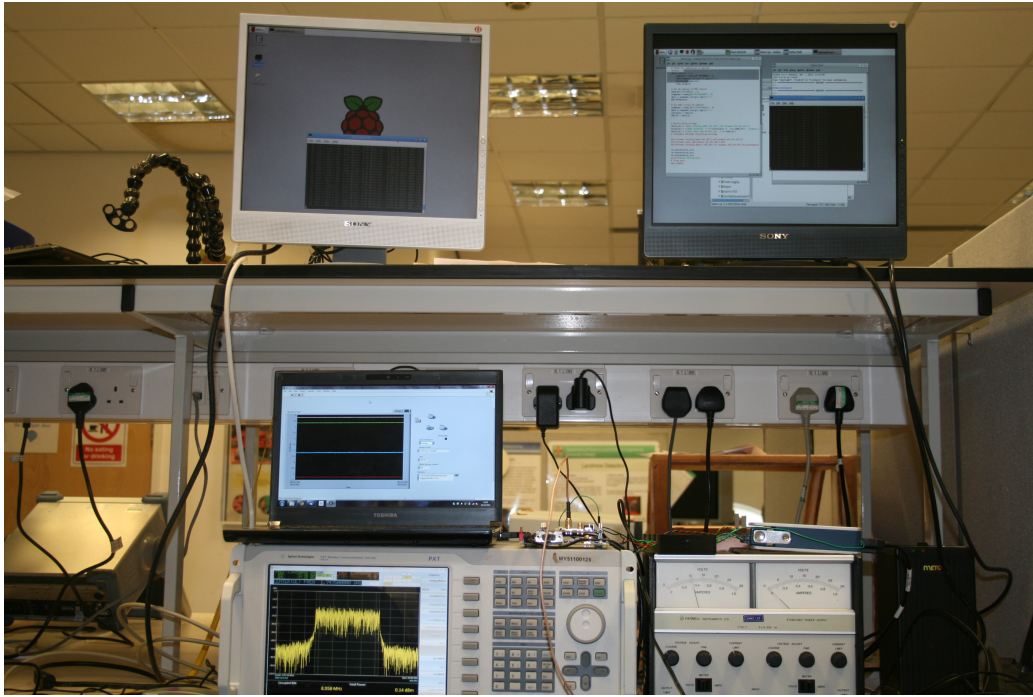


Figure 4.8: Functional LTE test rig.

4.5.1 Phase I Work on Connectivity

To begin with, there are some challenges in getting a piece of equipment this complex to the stage where it can be interfaced with commercial off the shelf (COTS) user equipment. As the functionality is lower than a full LTE system, certain security measures must be taken.

Device	Own IP	Gateway IP
Server RPi	192.168.2.1	192.168.2.2
BSE	192.168.2.2	192.168.2.1
UE	192.168.1.51	-
UE RNDIS	192.168.1.1	-
Client Pi	192.168.1.10	192.168.1.1

Table 4.4: Initial IP address setup.

Unlike 2G cellular communications, where authentication is uni-directional, i.e. only the UE must prove it is a genuine device with a registered subscriber identity module (SIM) card via a security procedure. LTE has a bi-directional authentication procedure, where both the UE and eNB must prove they are genuine to each other. In order to overcome this for the laboratory scenario, a special test SIM card can be used which will provide the requisite amount of authentication between the BSE and UE for both to function.

Once security procedures have been taken care of, there are a number of other parameters, mostly relating to the physical layer that must be taken care of. As a cellular link generally involves variable link budgets, the power transmitted by the BSE must be at a reasonably similar level to that in a real world scenario, and also appropriate to the power level that the UE will be asked to transmit at.

4.5.2 Phase I Throughput measures

To start investigating the throughput of an LTE link, a network emulation was implemented similar to the theory described in the previous section. The server connected to the back of the base station emulator was a Raspberry Pi (RPi). This was given a static IP address, as no dynamic host configuration protocol (DHCP) is available in this setup. The gateway IP of the RPi was set to be the IP address of the base station emulator, so ensure all outgoing messages from the RPi are passed to the BSE

Similarly to the RPi, the BSE is given a fixed IP address on the same subnet as the server, with its gateway IP set the the address of the server RPi, so ensure any messages passed out of the ethernet interface are given only to the server. The BSE also required additional settings in the form of an evolved packet system (EPS) bearer. This is similar to the packet data protocol (PDP) context used by 3G networks, and allows a data session to be set up, and an internet protocol (IP) address allocated to the UE. The most important setting here is just to pick the IP address allocated to the UE, this is chosen to be on a different subnet to the server and BSE to avoid any problems in packet routing. A summary of these setting is shown in Table 4.4.

The Toby L210 LTE modem is configured to act in remote network driver interface specification (RNDIS) mode. This enables the modem to be plugged into a client RPi using a universal serial bus (USB) interface, but have this function as a networked IP interface, which greatly facilitates creation of appropriate code to send data over the network. This setup of the virtual networking functions will be greater examined in the section on code creation for data transmission. In addition to the IP address assigned to the modem by the BSE, the modem also has a separate IP address for the RNDIS interface with other devices.

A second RPi is used to take on the function of a network client in this test setup. The responsibilities of this system are to initialise the LTE modem and connect to the network offered by the BSE and then proceed to upload various different types of data so that the results can be analysed. Code for the client RPi was written in python, due to the ease of use and availability of similar examples for this platform. The client RPi is given a static IP address on the same subnet as the modem, and uses AT commands to obtain the additional information required to initiate data transfer on the network. A short summary of this code is shown below. '*PDP_IP*' and '*USB_IP*' are IP addresses obtained previously using AT commands to the modem. This was automated in such a way as to take into account the fact that the PDP IP address would change when connected to a real world LTE network.

```

1 Cntxt_str = 'sudo ifconfig usb0 192.168.1.149 netmask 255.255.255.0 '
2 Alias_str = ('sudo ifconfig ' + str(interface) + ' '+str(PDP_IP)+ ' netmask
    255.255.255.255 pointopoint ' + str(USB_IP) + ' up')
3 Gatew_str = ('sudo route add default gw ' + str(USB_IP))
4
5 os.system(Cntxt_str)
6 os.system(Alias_str)
7 os.system(Gatew_str)

```

Listing 4.1: Python IP Initialisation

The most basic of throughput measurements can be actuated very simply on the BSE using the 'fixed MAC padding' mode, which effectively tells the UE to transmit a stream of pseudo-random data continuously over the entire bandwidth and time slot allocation is has been given. This is fine for measurements involving RF metrics, such as analysis of the ACLR and EVM of the transmitted signal, but does not tell us very much about the system performance, as fixed medium access control (MAC) padding only involves data transfer at the MAC layer level between UE and eNB.

Three scenarios were used to perform a more realistic metric of network performance; idle, data, and video. Idle is simple the power consumption of the modem alone connected to the network, with few network level communications between the UE and eNB occurring. Data

transfer was facilitated using the 'iperf' [42] network throughput measurement software. This was run on both the client and server hardware, with the link throughput tested only in the UE uplink direction. Video transmission used the raspivid application [43], which sets up a webcam server on the client RPi. The server can then access this webcam and instruct it to stream video. Video is quite a complex data type to quantify in terms of power consumption, as the in addition to video quality, the type of codec used to encode the data has a dramatic effect on the bandwidth requirements. The most basic methods simply transmit a sequence of photographs, however more advanced systems only transmit information when the images captured by the camera change, i.e. motion is detected. This means that the amount of data transferred, and thus energy expended can be proportional to the amount of movement occurring in front of the video camera.

```

1 raspivid -o - -t0 -n -hf -w800 -h400 -fps24 | cvlc -vvv stream:/// dev/stdin
   -sout
2 '#standard {access=udp, mux = ts, dst = 192.168.2.230:8160}' :demux = h264

```

Listing 4.2: Python Video TX Initialisation

Settings:

- output to stdout not file
- timeout 0 - continue running
- no preview
- horizontal flip
- 800 x 400 image size
- 24 fps
- console vlc video player

```

1
2 omxplayer -o hdmi udp://192.168.1.51:8160

```

Listing 4.3: Python Video RX Initialisation

Once each of the previously described scenarios was set up, it was allowed to run for 1 minute using a fixed supply voltage, with data on DC power consumption being recorded via the high speed ADC and labview interface. Figure 4.9 shows the results from this initial

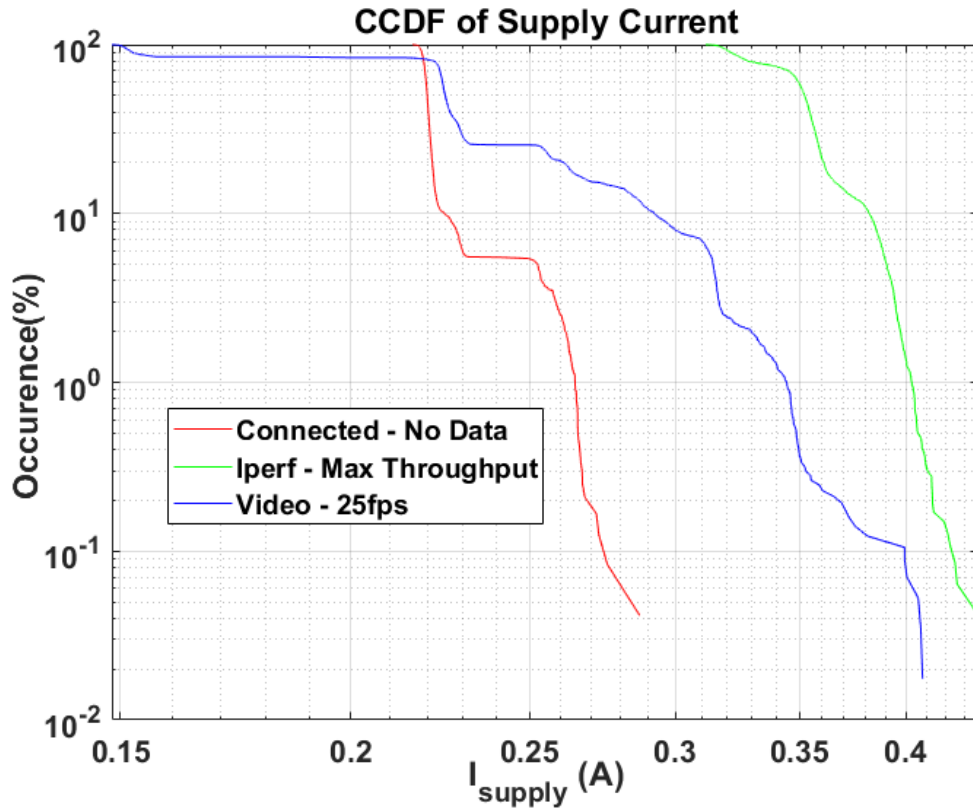


Figure 4.9: CCDF profile for idle, data and video transfer.

experiment in the form of a complimentary cumulative distribution function (CCDF) profile. It can immediately be seen that there is a large difference in the amount of current consumed for each activity. As expected, the idle process consumes the least amount of energy, which can be described as proportional to the area under the CCDF. Peak current consumption is around 2.85A, which is likely to correspond to high power signalling to the eNB, with lower power states requiring less active communications. It can be seen even the minimum current requirements are high, as this is a continuously active transmission, with no DRX operations that would reduce this.

The iperf activity consumes the most amount of energy, which is fitting, as its purpose is to transmit data at the maximum capacity of the system. It can be seen from the plot that the minimum amount of current consumed is 0.315A, which is a significantly large figure, which would be likely present challenges if it were part of a remote system with a finite energy source. Video is positioned in between, justified by its moderate data transmission requirements, it is perfectly possible to transmit acceptable quality video at rates that are very low in comparison to maximum LTE throughput.

Video transmissions can be complex to model due to the varied functionalities of the

coding applied; in its most basic form, this will just involve sending a stream of complex images, though more advanced systems will only transmit the difference between subsequent frames. This can have the effect of system power consumption being proportional to the activity that appears in from of the camera. In this particular example, it can be seen that the CCDF plot covers almost the entire range of the axes, with periods of peak power consumption likely to represent when a hand was waved in front of the camera to simulate motion, and lower usage due to the resting state. Further it can be also seen from the CCDF plots that the video process appears to occupy lower power states than the idle alone. It is suggested that this might be due to outlying and infrequent processes, indicative of the need to extend the period over which these measurements are taken.

4.6 Phase I Modelling

4.6.1 Objectives

Whilst the previous section covers procedure on how to gain a reasonable idea of how power consumption changes with different use cases, it does not provide a model that enables us to predict energy usage for a wider range of cases. Before this can be done, it is important to review the mechanisms that affect this consumption. In the most simplistic fashion, this depends on the rate at which data is transmitted, how long the communications process lasts for, and what power the UE transmits at. For the purposes of a very simple model, we can ignore the transmission duration, and perform continuous steady state measurements, that will yield a wattage per process rather than an absolute energy. This leaves only transmission power and data rate as independent variables to be changed for basic modelling.

4.6.2 Test Setup

The test setup was reasonably similar to the previous section, using the Toby modem and base station emulator, however no client and server are used to generate data, this is done using only the fixed MAC padding mode on the BSE in order to generate a more application agnostic model. The basic premise involves creating two separate models, one each for transmit and receive processes. Each process will have RF power changed. TX power is changed by altering the desired closed loop figure in the MAC layer. For power level received by the UE, this is done by changing the output power level of the BSE. Data rate in both cases could be changed by varying the system bandwidth, the time slot allocation, or the modulation and coding scheme. In this case the MCS is changed, as this will likely be a function of the channel in which the device operates rather than the other two parameters,

which will be most likely to be a function of proprietary algorithms on the eNB. Changing MCS also most represents a change in baseband processing power, and thus allows another degree of freedom to be modelled.

4.6.3 Methodology

Once the appropriate DC power measurement hardware has been connected to the UE, and the UE has been connected to the BSE, the test can begin. Due to the large state space of variable power output and MCS, it would be incredibly time consuming to measure every possible permutation. A reasonable compromise is setting one to a mid-point value, and varying the other, for example setting MCS 10 and doing an output power sweep, and after that setting $P_{out} = 10dBm$ and sweeping MCS. For each measurement point, 5 seconds of data are recorded, which are then averaged to give a mean value of power consumption. The above process results in two intersecting curves, which can be extrapolated to give a 3D surface defining power consumption over the various operating conditions. In a similar method, the receiver power consumption was measured and modelled. Validation of this method of extrapolation is given in [21].

4.6.4 Power Consumption Analysis

Figure 4.10 shows the initial results from the receiver measurements. It can easily be seen that both the baseband processing, proportional to data rate, and received power level contribute equally to the overall power consumption of the system. Whilst it is obvious that the higher the data rate, the more baseband processing power is utilised, and more energy is consumed, the RF power level may require more explanation. The plot shows that power consumption decreases with and increases in received signal power level. This is because lower receiver (RX) power levels require greater amplification by the low noise amplifier (LNA) and any further automatic gain control (AGC) stages in order to bring them up to an easily decodable level. The larger the amount of gain required, the more power is consumed by the associated circuitry within the modem. An assumption would be that the variation in power consumption with gain would be very small, which in fact it is, but so is the variation in baseband processing power, giving the particular characteristics to this plot.

The low amount of baseband processing power is illustrated in the TX measurements shown in 4.11. It can be seen here that the overall system power consumption is dominated by the RF output power, to such an extent that variation due to baseband processing seems negligible by comparison. This result is fairly unsurprising due to that fact that the power

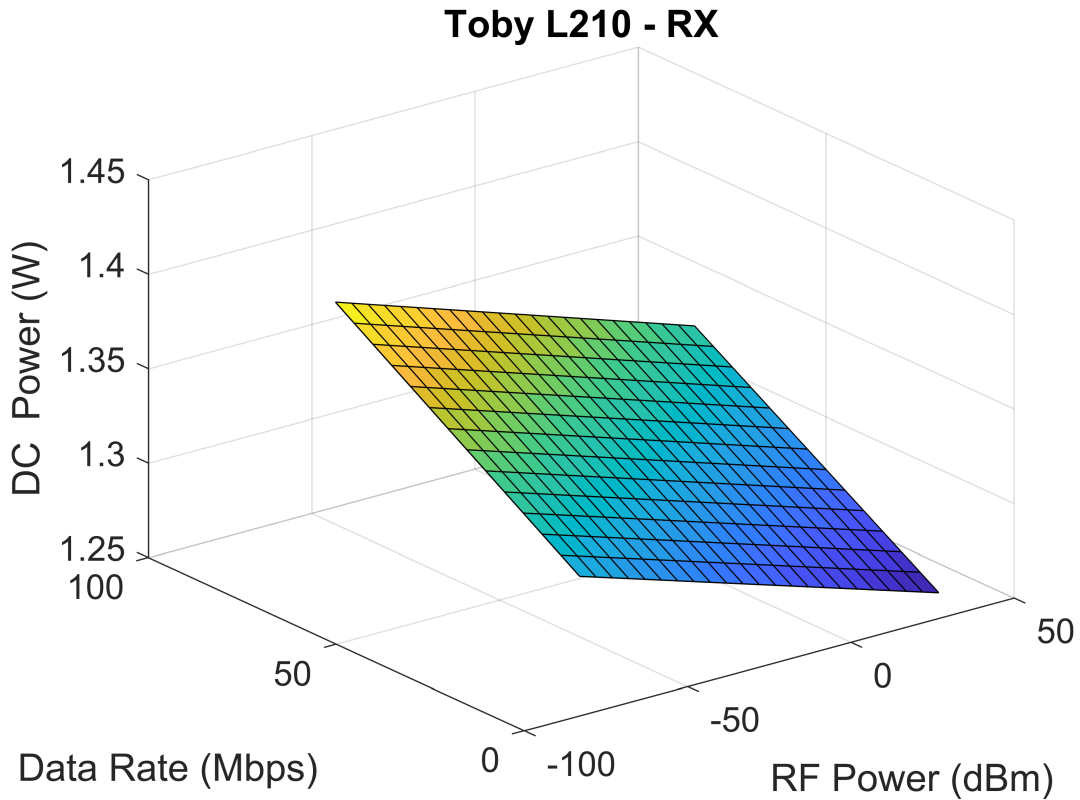


Figure 4.10: RX power modelling.

amplifier producing this RF output power is widely regarded as the most power hungry component in most RF transceivers.

4.6.5 Additional Device States

As the initial work on modelling power consumption was constrained to continuously transmitting or receiving scenarios, the logical extension is to begin to look at the transition in between various device states that more readily describe how a piece of user equipment would be used in a real world deployment. An example of this would be a coordinator node in a wireless sensor network which spends much of the day in a low power sleep state, waking up occasionally in order to transmit data over LTE. When calculating average power consumption, it is important to take into account not only the power consumption of each state, but also the average power used over the transition time between states, which can be significant.

Figure 4.12 shows the power profile of the Toby modem when it wakes from a deep sleep state, entirely disconnected from the network, to a state connected to the network and ready to transmit data. At 1.2s to transition between states, this can be a significant

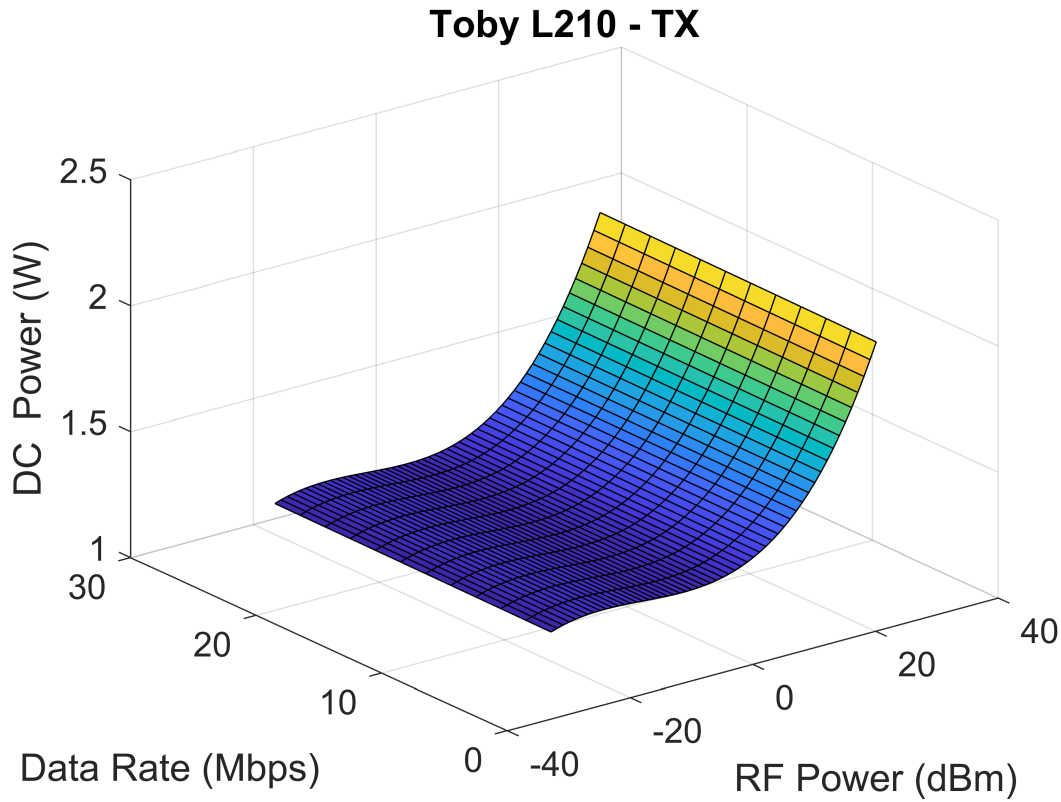


Figure 4.11: TX power modelling.

amount of power consumed over the course of multiple transmissions within a day. Over many iterations, these results were summarised in Table 4.5.

Action	Avg. Power Consumption (W)	Duration (s)	Energy (J)
Cold Start	0.729	18.25	13.3
Sleep	0.166	-	0.166t
Standby	0.988	-	0.988t
Sleep - Standby	0.969	1.23	1.19
Standby - Sleep	0.338		

Table 4.5: Additional model components.

4.6.6 Conclusion

To conclude, it can be seen that power consumption in an LTE transceiver can be decomposed to separate processes related to RF and baseband activity for both the transmitter and receiver. In the receiver both processes contribute equally to the rate of energy consumption, and in the transmitter, the RF processes, particularly that of the power amplifier

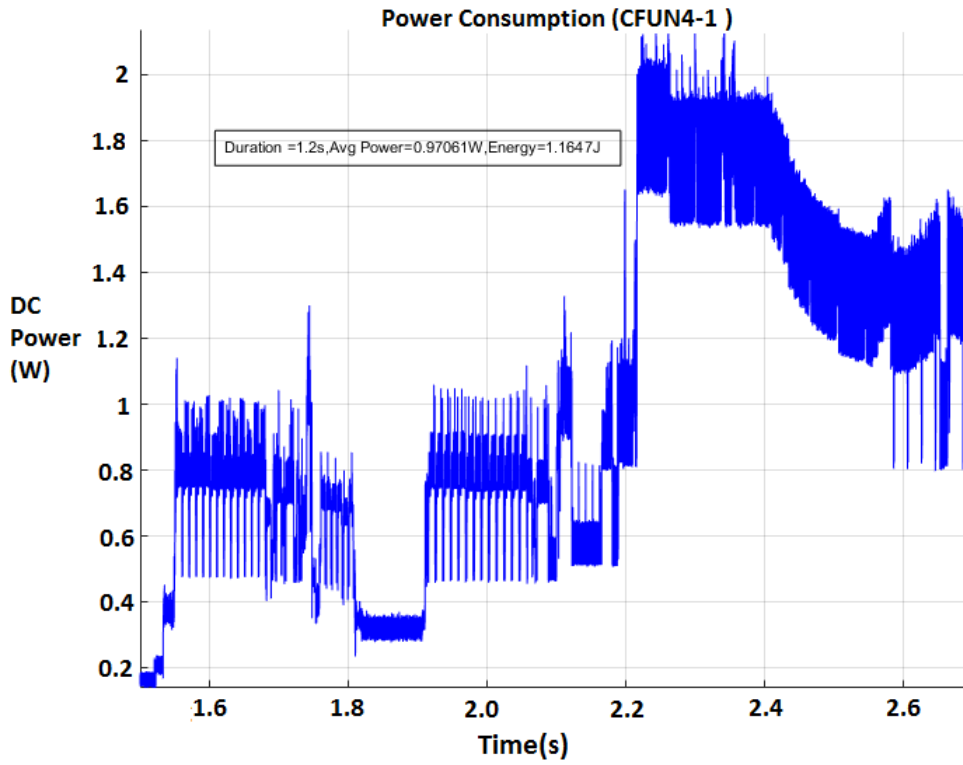


Figure 4.12: Transition from sleep to standby.

dominate all energy consumption. Comparing the two plots, it can be seen that when separated, the RF power amplifier (PA) is one of the most energy hungry subsystems of the transceiver. The implication of this is that the PA should be targeted for any future work on efficiency enhancement, or at least studying the feasibility of efficiency enhancement. The opportunity for efficiency enhancement however does not lie solely with the hardware in this case. As future work will describe, the format in which information is sent also has a dramatic effect on how much energy is used to do this.

Interestingly, much research effort has been focussed on reducing the latency of future 5G systems, not just in order to facilitate more advanced applications such as the tactile internet and remote surgery, but also because faster communications require less time to be forfeit waiting for responses in an actively receiving mode, which can consume surprising amounts of energy.

4.7 Phase II Network Based Measurements

4.7.1 Aims

The previous section has described how basic modelling in a controlled laboratory environment can give a reasonable model of how power is consumed within an LTE modem. As alluded to in the Power Consumption Modelling section at the beginning of this chapter, the reality can be quite different due to a number of factors. Whilst the environment and RF channel will play a part here, these can be modelled with the variable TX power and MCS as previously shown. The trade-off with the variables at play in an environment is generally down to resource contention. As more users are present in an area, the demand for the radio resource increases, and the eNB must use resource allocation algorithms to decide how these resources are shared out. Modelling here is extremely challenging as resource allocation algorithms are often proprietary, and vary from base station to base station and network to network.

Particularly in the case of small M2M packets, there is the issue that the communications required to establish a data connection with the eNB are of a similar size and duration to the payload itself, which must obviously be taken into account in these cases. The best way to try and understand how these factors effect the consumption of energy is to make some initial measurements, and compare them to the simulated results on the BSE. From this comparison it should be possible to gain an idea of how resource allocation takes place. The likelihood is that for packets below a certain size, the emphasis is on speed of transaction, so the maximum required resource block (RB) allocation is given in order to minimise the amount of subframes required to transmit the payload.

4.7.2 Measurement Set-up

The equipment used for measurement is shown in figure 4.13. Current consumption is achieved using a simple series resistor fed through a low noise instrumentation amplifier into an ADC, which also measures supply voltage, combined to give DC power consumption. RF output power is measured using a 20dB directional coupler fed into an envelope detector, then through a pre digitisation low pass filter, and finally an ADC before being logged.

Experiments consisted of using an appropriate source to generate user datagram protocol (UDP) packets, from a terminal appropriately fire-walled in order to block any system level communications interfering with measurements. The waveforms for supply voltage, supply current, and RF output power were recorded for the duration of the transceiver active process. UDP packet size was varied between 2^3 and 2^{15} bytes of data using a graphical user

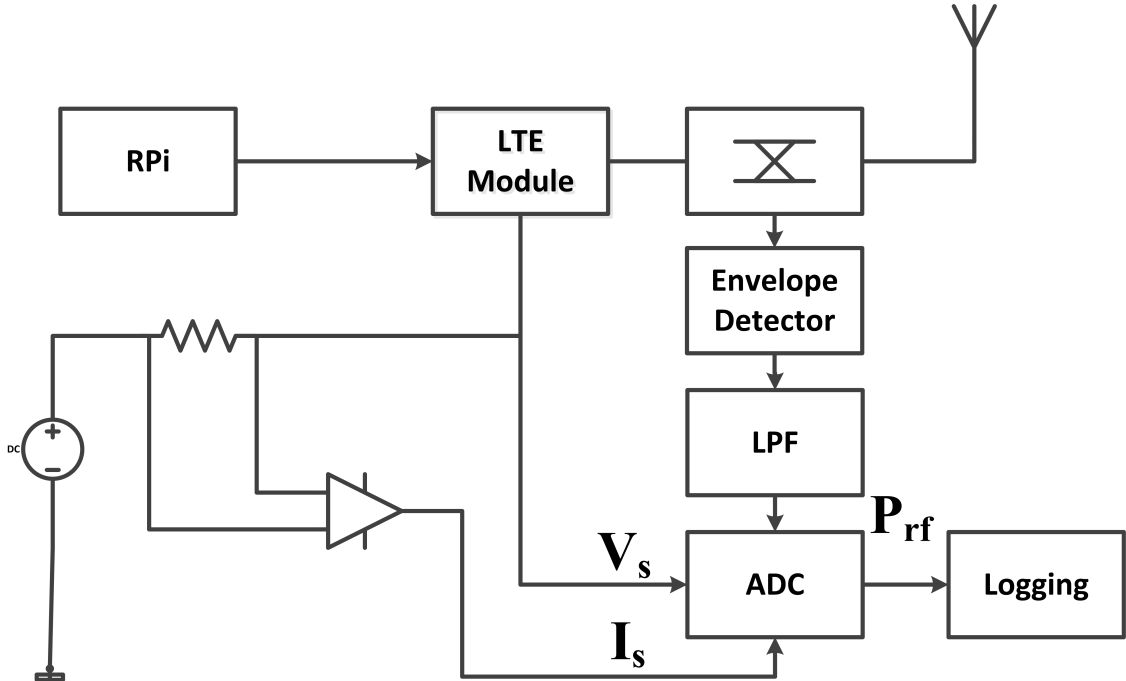


Figure 4.13: Block diagram of measurement hardware.

interface (GUI), the construction of which is described in the appendices.

The first scenario was recorded in a lab based scenario with a base station emulator. This gave baseline performance comparable with prior work. A second experiment was carried out on a live LTE network in order to assess the effects of additional protocol overheads in a real environment.

4.7.3 LabVIEW Instrumentation Interface

Once an appropriate analogue front end was designed to record a high dynamic range of current, the next challenge is to get this information into a state where it can be viewed in real time, and stored for further analysis. The obvious tool to do this is a high speed ADC, which will convert the analogue voltages into digital values to be stored on a computer. The National Instruments NI-9222 ADC was chosen to perform this function as it offers a maximum sample rate of 500kS/s on each of the four differential input channels, with a resolution of 16 bits covering an input range of ± 10 volts.

The interface in between the ADC and computer is a high speed USB one, and the data is recorded using the National Instruments (NI) LabVIEW interface. LabVIEW is a graphical programming environment, designed to create 'virtual instruments', where data can be acquired, processed, displayed and stored with a minimum of effort. The optimised nature of this National Instruments setup means that high sample rates can be used over a

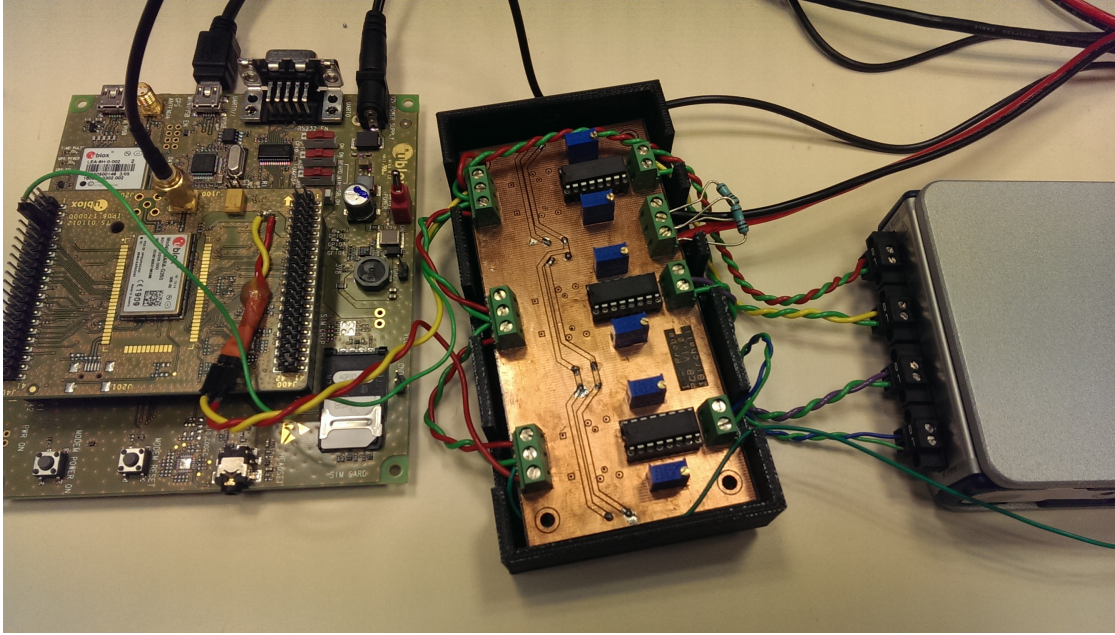


Figure 4.14: Photograph of measurement hardware.

long period, with few buffering issues. Data flows in LabVIEW are further discussed in the appendix.

4.7.4 Network Measurement Results

To begin with, a comparison can be drawn between the power profile of the ideal transmission using the base station emulator, and the real world equivalent using an actual network. Figure 4.15 is the ideal scenario; Two peaks can be observed in the RF envelope, corresponding to the process of requesting resources from the base station for the first peak, and transmitting the UDP packet for the second peak. Increases in DC power consumption in between the two peaks correspond with the reception and decoding of resource grants and acknowledgements from the base station. It is important to note that this entire process takes no longer that 20ms.

Figure 4.16 shows an equivalent transmission on a standard LTE network, DC power consumption has been omitted for clarity. The most important thing to note is the large increase in activity in the RF transmitter; a duration of 10.5 seconds in comparison to the 20ms of the ideal case. As mentioned in the subsection on measurement set-up, appropriate firewalling is used to ensure no extraneous transmission from the UDP source, so all activity beyond transmission of the UDP data is a direct result of communication between the UE and eNB / network.

In order to ensure that is is not an infrequent occurrence, Figure 4.17 shows the dis-

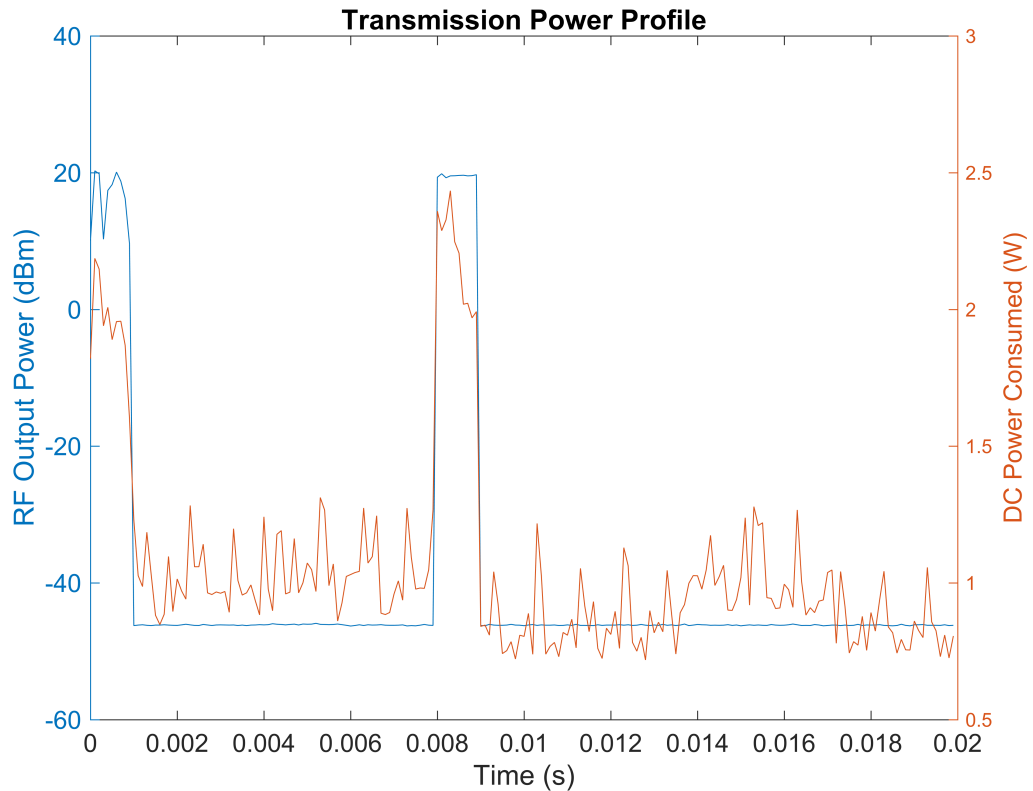


Figure 4.15: Power profile - lab setup.

tribution of the time spent transmitting for all packet sizes from 8 to 32768 bytes over 10 iterations of each set. It can be seen that the RF activity time is independent of UDP packet size. The likelihood here is that the transmission time is determined by the RRC activity timer. Once the UDP transfer has been completed, additional network traffic is transmitted until the timer expires and the UE enters the RRC idle state.

To gain a better idea of the processes contributing to this additional energy consumption, it is helpful to compare the the ideal emulated case with the real deployment. Figure 4.18 shows energy consumption and transmission in proportion to the amount of data transmitted. It can be seen that there is a strong correlation between packet size and both RF energy transmitted, and DC energy consumed. The flat portion at the beginning of each data series corresponds to where the transport block size is less than one subframe, thus a complete transmission consists of a request for resources, followed by a transmission of data, and since we have not entirely filled a transport block over these values, transmission time is set at the lower bound of 1 subframe (1ms) and the energy consumption is consistent with this. Using higher modulation schemes will increase potential transport block size, and thus the range of UDP packet size over which transmission energy consumption is invariant. This

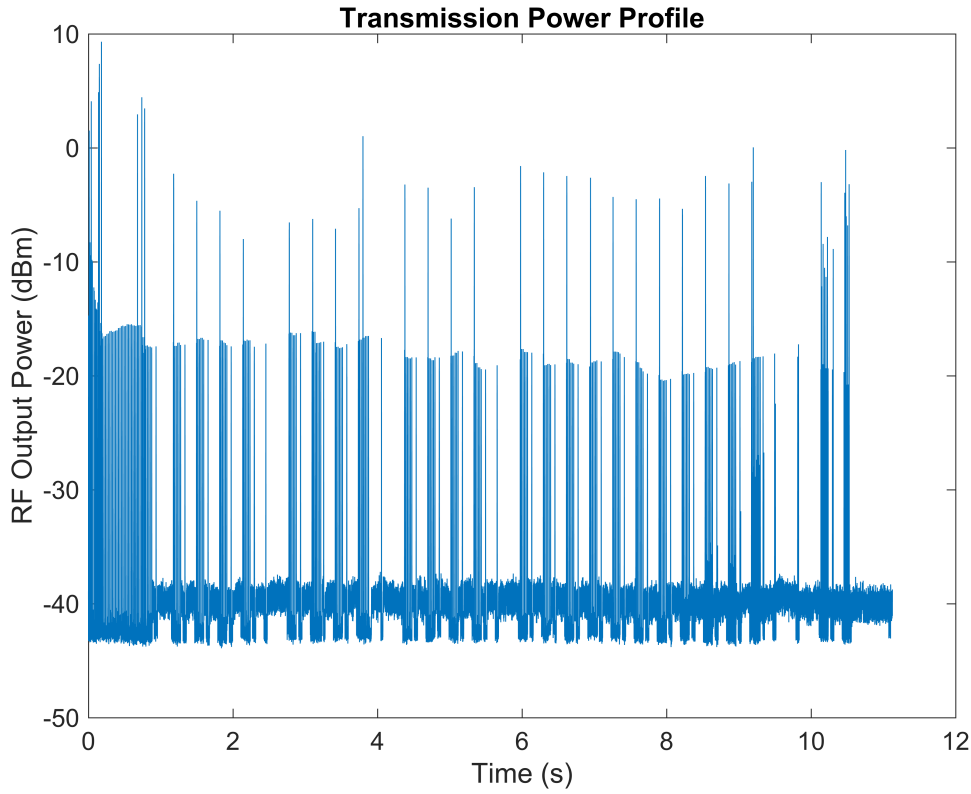


Figure 4.16: Power profile - external network.

also means that measurement of the length of this invariant section can help to ascertain the allocated MCS from the eNB.

Figure 4.19 shows the same measurements, averaged over 10 iterations on a real network deployment. It can be seen that the plot of RF energy versus packet size follows a similar trend to the lab scenario. This is particularly interesting as it suggests that despite the dramatic increase in perceived transmitter activity, and consistent length of this activity, the amount of actual energy transmitted increases proportional to packet size. It can be ascertained that the additional transmissions are short in duration or low in power in comparison with the core packet transmission. Considering the plot of energy consumed overall, this appears to be relatively uncorrelated with packet size; from which we can deduce that while extended duration does not result in a large amount of extra energy being transmitted, the energy consumed by all of the modem processes being active is significant, and results in a distribution of power consumption uncorrelated with packet transmission size.

Verification can be obtained from Figure 4.20 that shows the additional periods of transmission are both at a significantly lower power, which can be observed in Figure 4.16, and are also likely to have a low duty cycle in terms of RF active power. It is possible that the

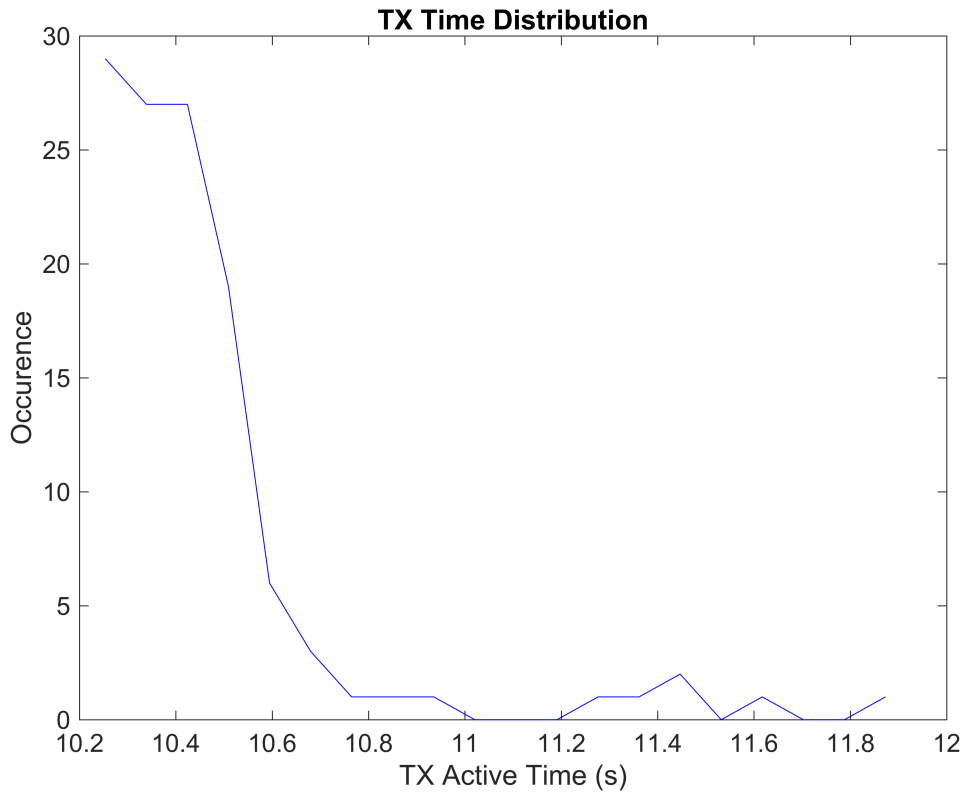


Figure 4.17: Distribution of time spent transmitting.

additional information transmitted is done so at a lower MCS, in order to take advantage of a lower P_{Tx} , intended to save energy.

4.7.5 Conclusion

Using a comparison of experimental results from an emulated lab based LTE network and a real-world deployment, it can be seen there are large differences in system energy consumption whilst transmitting UDP packets of various sizes. The main discrepancy is the addition of a large amount of network communication between the UE and eNB, likely to be related to networks optimisation parameters such as self organising networks and automatic neighbour relations [44], in addition the multitude of possible measurements the UE can be required to make, specified in [45].

Despite the fact that the level and duty cycle of these additional transmissions are low, the effect of the transceiver being active over a much larger interval adds considerably to the overall power consumption of the device. This occurs to such an extent that over the range of UDP packet sizes transmitted, the DC power consumption of the transceiver cannot be accurately modelled in relation to transmission size, but may perhaps be better defined

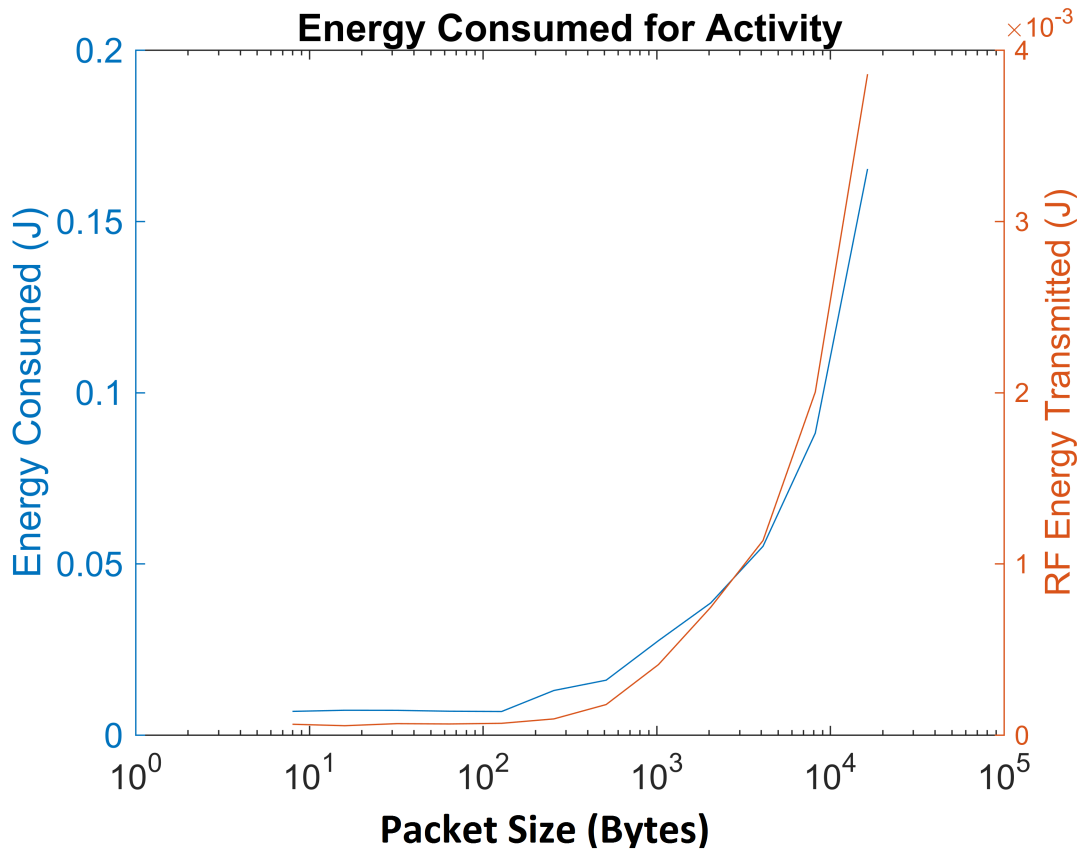


Figure 4.18: Energy used per transmission - lab setup.

by peak transmission power, and a distribution of power consumption associated with this. Discussions with Keysight have reported that when evaluating the performance in their LTE test equipment, some odd behaviour was discovered with some early LTE UEs when DRX performance was evaluated. Bursts of unexplained activity within the UE were observed, and in some cases, the equipment was clearly observed staying active monitoring downlink paging activity for three times longer than was required by DRX specifications.

Additional testing verified that the UDP transmission occurs within a similar initial window as laboratory results. Combined with the restriction on any other outgoing communications, this means that the additional transmissions taking place must be at network level, instigated by the eNB. One plausible explanation for this could be the self organising networks specifications written into the standards. This allows each base station to gain a clearer picture of other, neighbouring base stations and their relative signal levels by polling user equipment. The idea is that this facilitates more optimised handover procedures, especially in dynamic environments, e.g. when temporary base stations are installed for events. It is possible that this polling of user equipment is what is taking place during what should be the DRX periods. Another explanation could be some kind of error in either the UE or

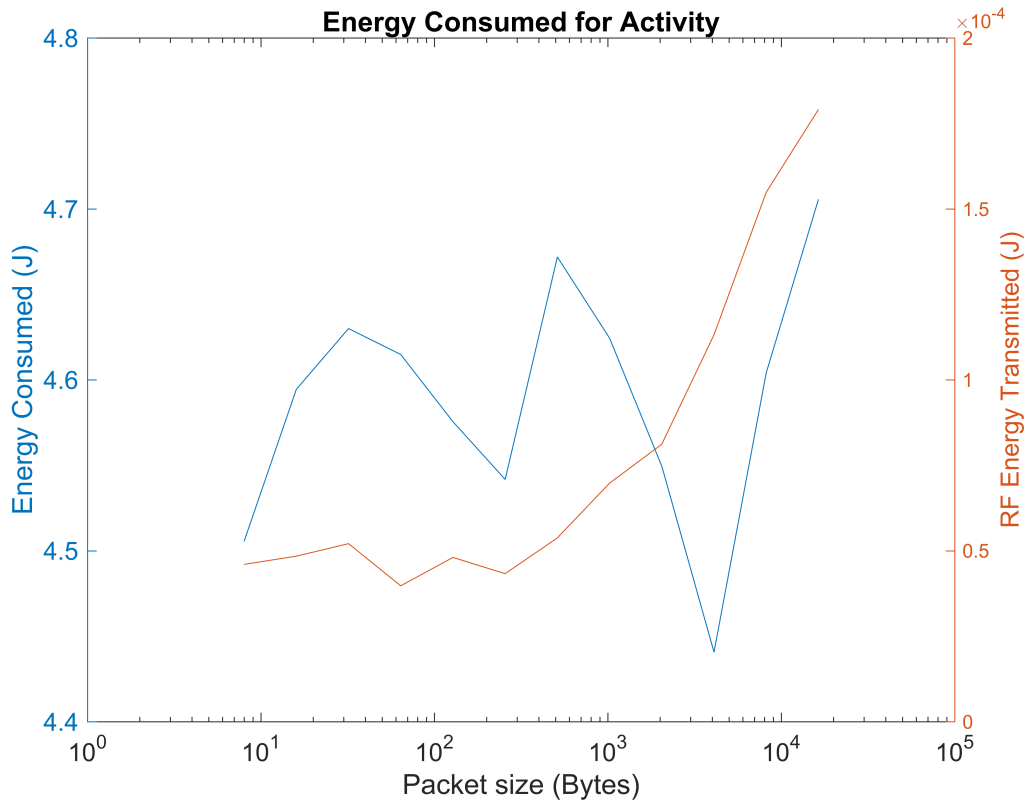


Figure 4.19: Energy used per transmission - network setup.

eNB that causes a particular message to be rejected and re-transmitted over and over until the long DRX timer has expired. This could be an error in the hybrid automatic repeat request (HARQ) process, meaning the UE constantly services a repeat transmission request.

Future versions of this technology; LTE-Cat M and NB-IoT both started with an LTE physical layer and have modified & adapted it to make better use of the LTE spectrum to allow significant power optimization. The goal is to get 10 years of unattended operation from a single Lithium Thionyl Chloride cell. Essentially this means that the power used by the device is as low as the self-discharge current from the battery when averaged over time.

4.8 Sigfox comparison

Once of the most significant contenders to LTE for M2M is Sigfox [46], similar in that the backbone of the Sigfox system is cellular connectivity for low rate and packet size communications. The hardware available for the test was the Arduino MKRFOX1200, a development board consisting of a Microchip SAMD21 Cortex-M0+ microcontroller and an ATA8520E Sigfox module. Sigfox is a low power wide area (LPWA) network.

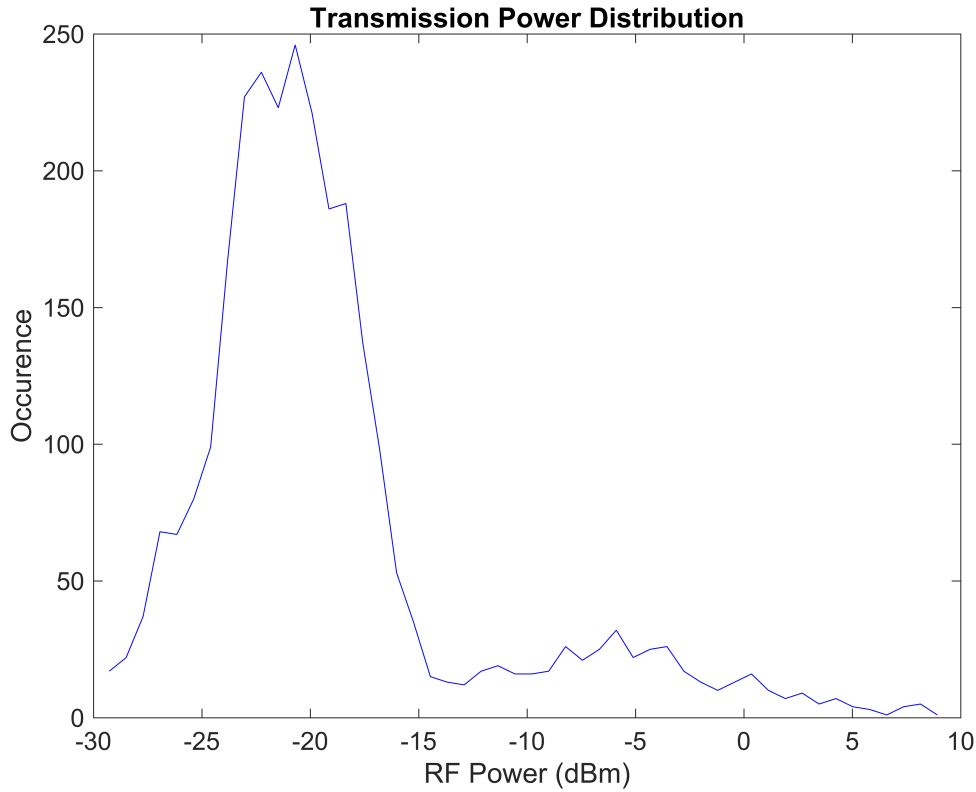


Figure 4.20: TX power distribution - external network.

Sigfox operates within the 868MHz ISM band and claims to have good coverage over the UK and a significant portion of Europe. The protocol is focussed at small pieces of data, with the basic subscription allowing transmission of 140 messages per day for free, however uplink message size is limited to only twelve bytes, with downlink at 8 bytes, which puts it right at the lower end of the M2M usage spectrum

There are two possible modulation schemes used in Sigfox; ultra narrow band (UNB) and orthogonal sequence spread spectrum (OSSS), though UNB is used in this particular implementation, in the 868MHz industrial, scientific and medical (ISM) band. The modulation schemes are binary phase shift keying (BPSK) in the uplink and Gaussian frequency shift keying (GFSK) in the downlink. The bandwidth occupied is 100Hz with data rate of 100 bits per second (bps) uplink and 600 bps downlink. Maximum transmit power is 25mW, and receiver sensitivity must be at least -135dBm. The structure of the packets is shown in Figure 4.21.

Sigfox exploits time and frequency diversity, transmitting a packet on a random frequency within the band, before repeating this on two further random frequencies. Spatial diversity is additionally exploited as the UE is not attached to a particular base station, any base

stations in the area will receive the transmission and pass it on to the core network.

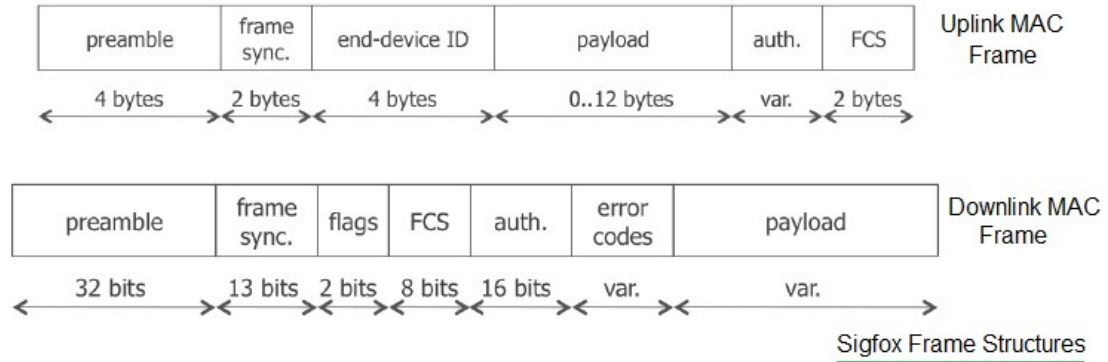


Figure 4.21: Sigfox packet structure [47].

Interestingly there is no MAC layer signalling in the network, to enhance efficiency in the transmission process. As a consequence of this, downlink messages to the device can be more complex. These take the form almost of an acknowledgement (ACK) to an uplink message transmission, thus the process for a device to receive a message involves making an uplink transmission, either useful or dummy, and then waiting for this to pass through the Sigfox network to the appropriate user back end. If a message is waiting or given in response to the uplink stimulus, then this is passed back the the UE as part of the network acknowledgement.

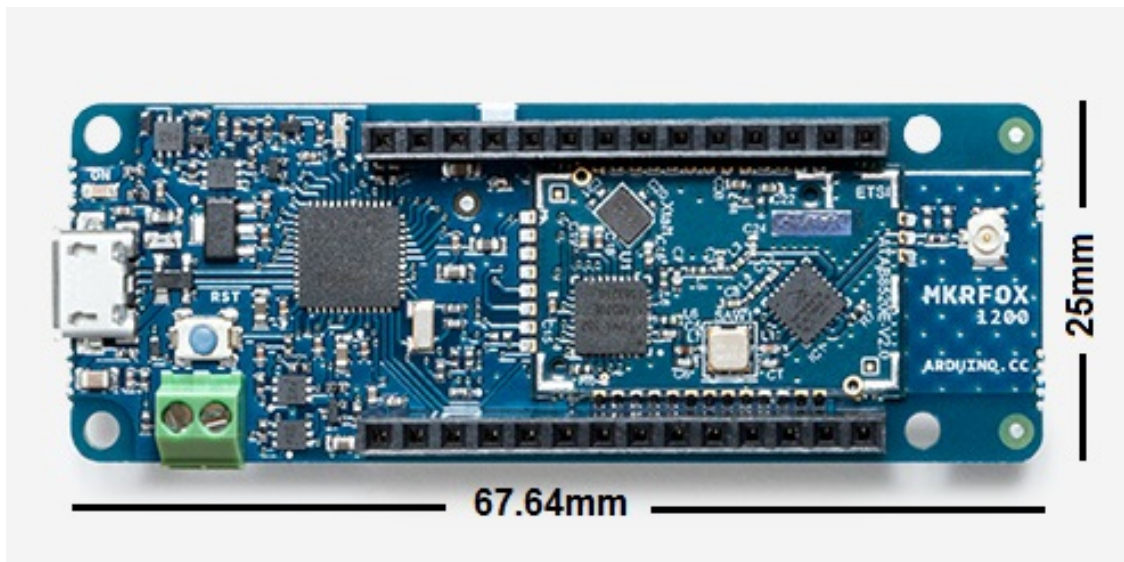


Figure 4.22: MKRFOX1200 board.

As can be seen from Figure 4.22, the development board is reasonably compact and can be powered via a 3V supply through the screw terminals. The concept here is that a battery

life of at least six months can be achieved from a pair of AA batteries in series. This will also provide the perfect place to inject an instrumented power supply in order to test these claims.

4.8.1 Experimental Results

The Sigfox results can be seen below. Figure 4.23 shows the how DC power is consumed for the duration of one packet being sent, the information is summarised in Table 4.6. The time taken for the entire exchange is 10.344 seconds, from the Arduino microcontroller waking up to the transmission exchange completing, and the device returning to the sleep state. Sleep power is 0.05W and average power consumption for the transmission period is 0.139W

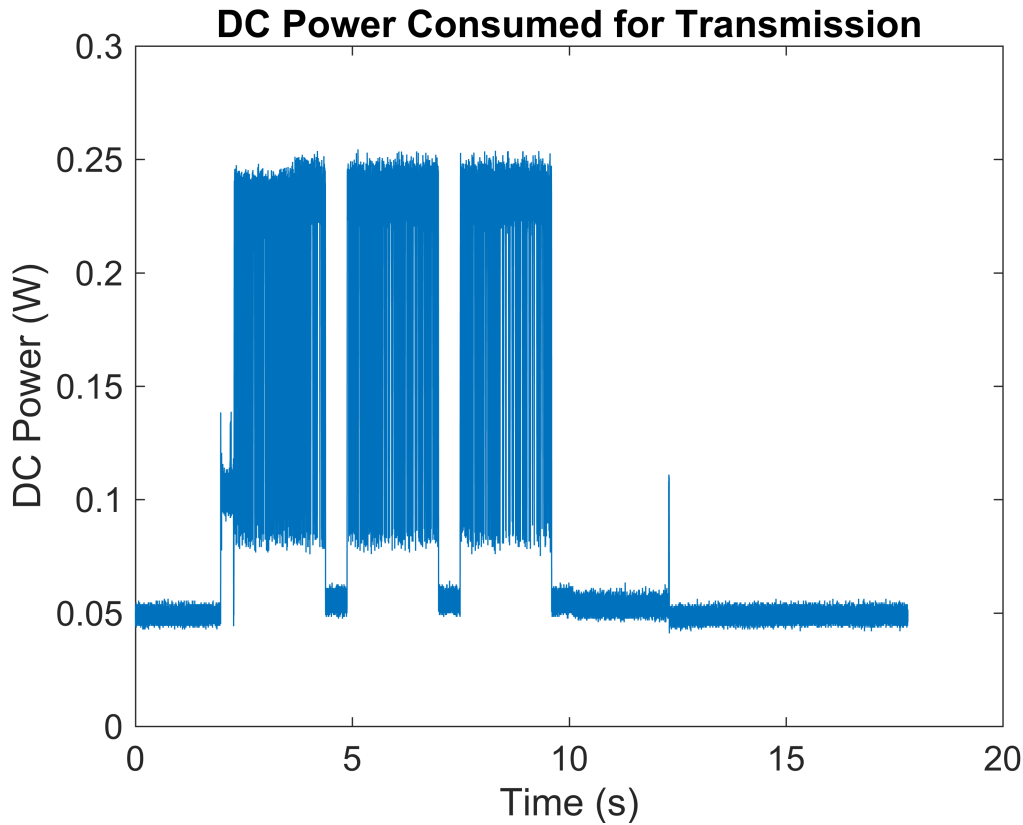


Figure 4.23: MKRFOX1200 5V transmission power profile.

Considering these results, it can be swiftly calculated that the advertised operating time of 6 months on a pair of AA batteries appears wildly optimistic. Further examination of the device schematic was carried out, as even voltage regulator inefficiencies in converting the 5V to 3V supply should not have this poor a performance.

The schematic showed that when the device is powered via the 5V input, an light emitting diode (LED) is lit in order to show this. Given the 330Ω current limiting resistor used,

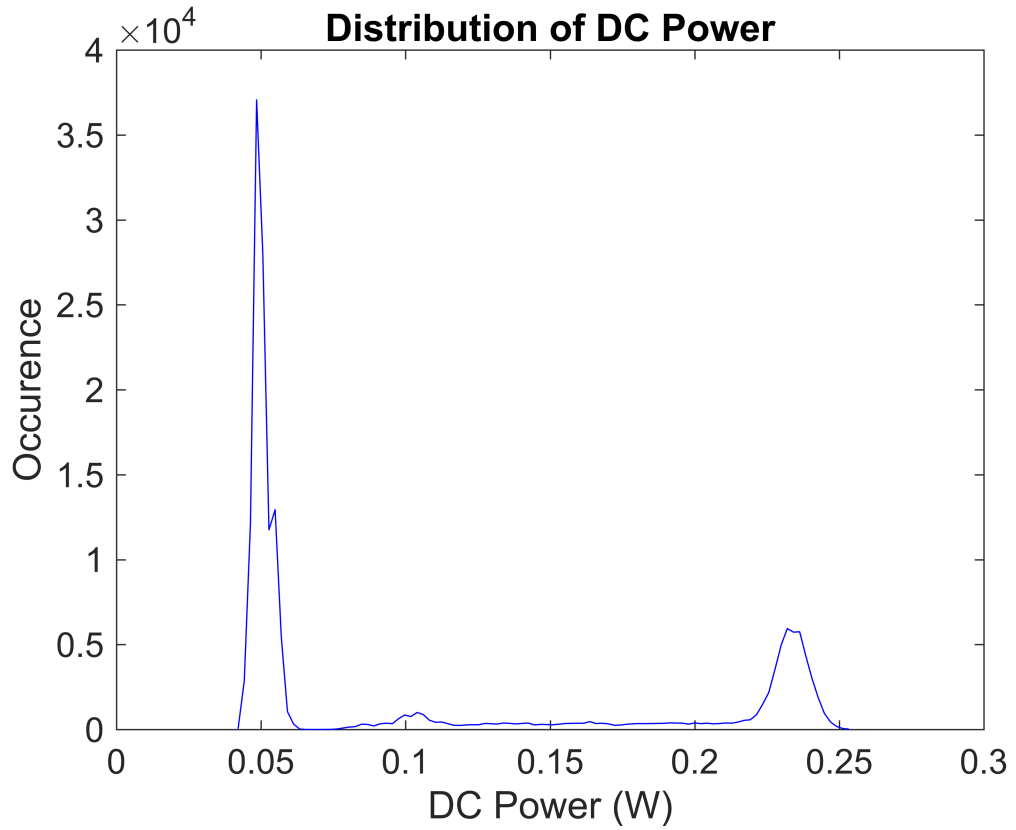


Figure 4.24: MKRFOX1200 transmission power distribution.

Table 4.6: MKRFOX1200 performance.

Idle Power	0.05 W
Transmission Time	10.344 s
Transmission Energy	1.440 J
Mean Transmission Power	0.139 W

this would account for almost all of the 'sleep mode' power consumption, and explain the previously poor efficiency. Experiments were repeated using the 3V supply, which uses no visual indications.

Figure 4.25 illustrated the transmission profile again. A quick comparison with Figure 4.23 shows that despite the process of transmission occupying a similar amount of time, the peak power consumption, generally correlated with RF transmission processes is half of that in the previous experiment.

Figure 4.26 confirms this reduction in power consumption, and also serves as a way to measure the idle power consumption.

Table 4.7 shows the improvement in performance summarised from the distribution shown in Figure 4.26, with idle power consumption down by a factor of almost 40, and

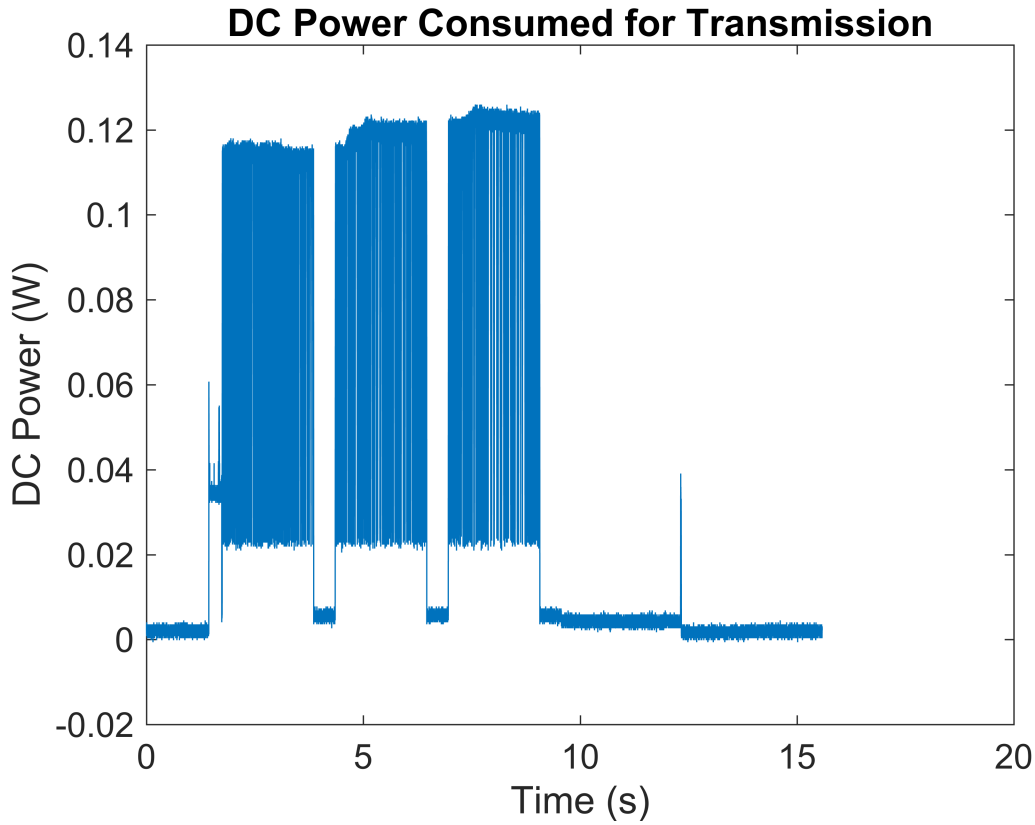


Figure 4.25: MKRFOX1200 transmission power profile.

Table 4.7: MKRFOX1200 performance - 3V supply.

Idle Power	0.00127 W
Transmission Time	10.894 s
Transmission Energy	0.487 J
Mean Transmission Power	0.045 W

even transmission energy consumption is reduced by a factor of three.

4.8.2 LTE Versus Sigfox

To perform a final comparison between these technologies, similar performance attributes are shown in Table 4.8. These can be used to generate a model of energy used per day, based on the number of transmissions per day. This figure is given very simply by Equation 4.10, and in the case of the LTE examples, also includes the times and average powers taken to wake up from a sleep state and connect to the network. Basic comparison parameters for

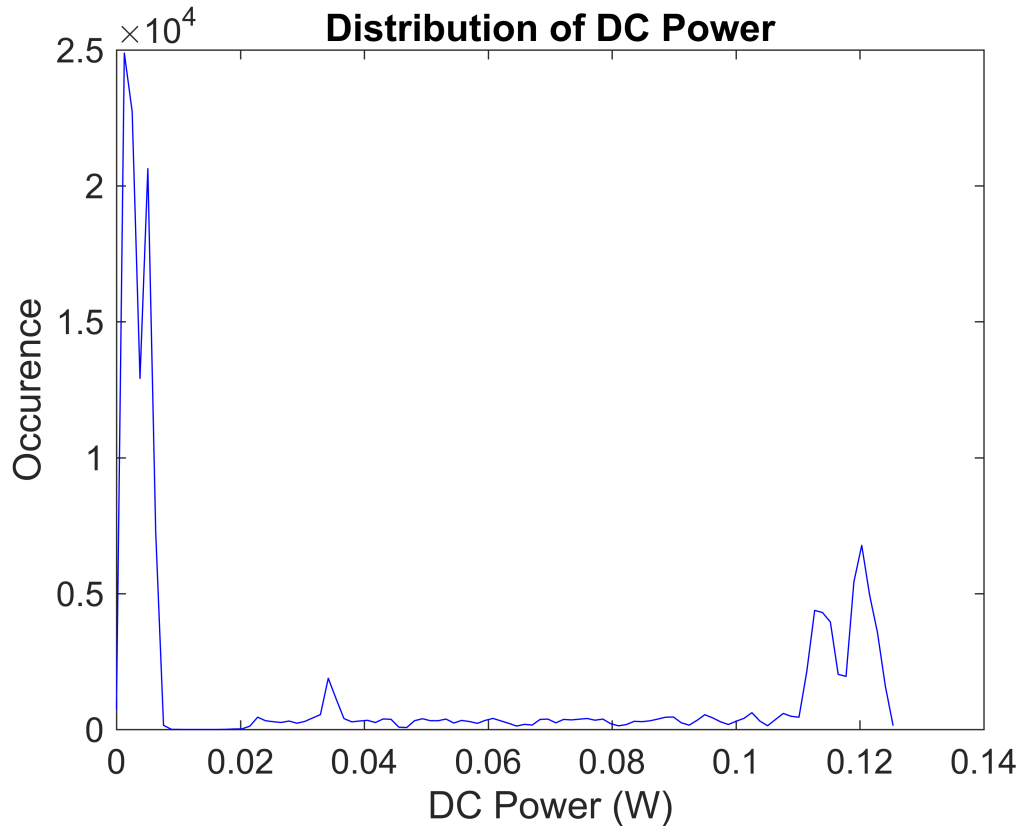


Figure 4.26: MKRFOX1200 3V transmission power distribution.

Table 4.8: Toby L210 performance.

Idle Power	0.166 W
Transmission Time	0.01 s
Transmission Energy	0.007 J
Mean Transmission Power	0.6905 W

the Toby modem are shown in Table 4.8.

$$E_{day} = n((P_{wake} \times t_{wake}) + (P_{TX} \times t_{TX})) + P_{standby} \times (t_{secs.in.day} - (n \times (t_{wake} + t_{TX}))) \quad (4.10)$$

This particular comparison is obviously very application specific, as a fair comparison with SigFox means that packet size is constrained to 12 bytes and the maximum number of transmissions per day is capped at 140, both constraints of the SigFox network. The initial comparison between the SigFox and and LTE, both operating in either active transmitting or 'sleep' modes was so surprising that an additional test was added, with a high latency LTE scenario where the modem is switched off after transmission, and must perform a cold

start and re-connection to the network when it next needs to transmit.

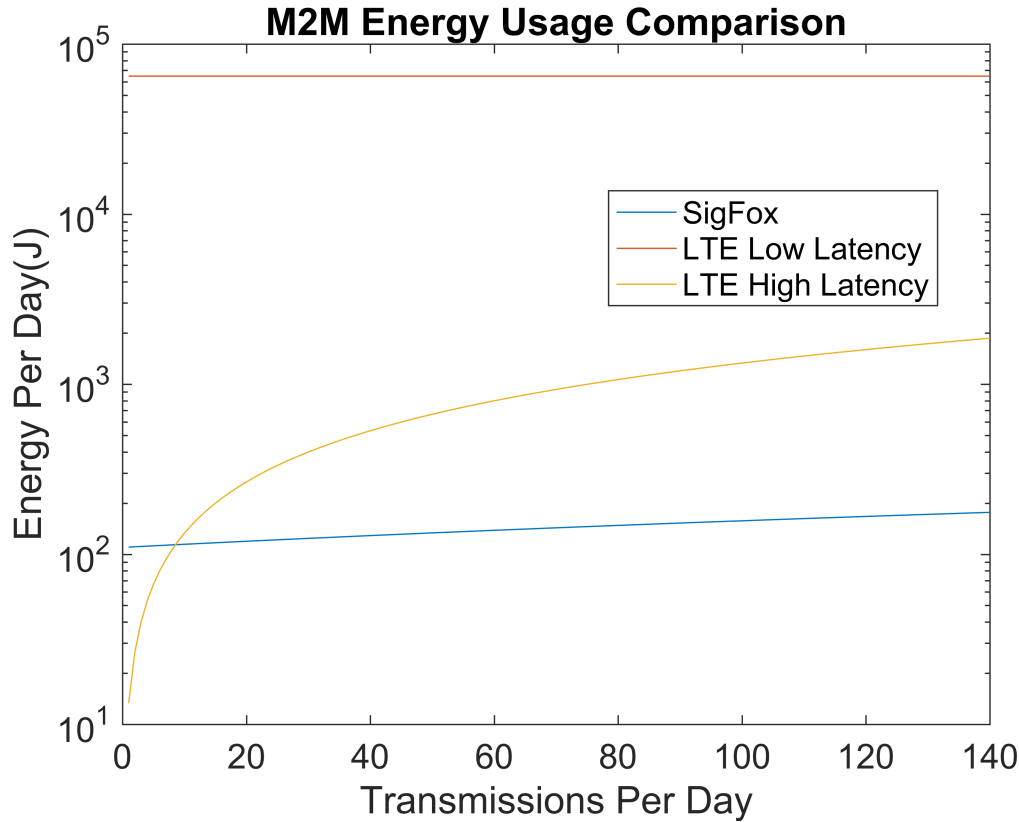


Figure 4.27: Comparison of M2M technologies.

The results of this comparison are shown in Figure 4.27. The baseline performance set by the SigFox modem shows energy consumption of between 100 and 110 Joules per day, over the range of 1 to 140 transmissions per day. By comparison the low latency LTE case shows energy consumption of almost three orders of magnitude higher, due almost entirely to the amount of energy required in keeping the modem in an state where it is able to communicate very rapidly with the network. Finally examining the plot of the high latency case, we can see that LTE manages to gain some ground here, but only because the resting power consumption is zero by virtue of switching the device off. The penalty in this condition is that the time it takes the modem to perform a cold start procedure and reconnect to the network is around 12 seconds at a high power consumption, however in terms of latency, this is not far off what can be achieved with the SigFox equipment; in fact the end to end latency of a SigFox transmission can be between 30 and 60 seconds.

This comparison is obviously a little contrived, in that the LTE functionality is highly constrained in order to provide a fair test. If a packet size of over 12 bytes was required, or more than 140 transmissions per day, then LTE would win hands down by virtue of

being able to fulfil these requirements. LTE has obviously been designed to optimise high data rate transmission and struggles to keep up with more energy efficient competitors, thus the Cat-0, Cat-M and NB-IoT enhancements. What can be seen here is that if latency is not a particularly important comparison, LTE can still be utilised in a reasonable fashion, especially in terms of leverage the large network of coverage.

4.9 Conclusion

This chapter has considered how power has been consumed in an LTE network, predominantly for uplink based transmissions. It has been seen that there are a large amount of factors involved in this process, from the obvious such as the amount of data to be transmitted and distance from the base station, to the more complex, such as the effect of the environment on selection of the modulation and coding scheme, and the density of the surrounding population on resource contention and access grant latency.

Most previous work focusses on the macro aspects of energy consumption, i.e. measuring this over continuous transmissions in response to varying power levels and data rates. This becomes very much less relevant when the energy constrained M2M case is considered. Research has shown that the distribution of power, both transmitted and consumed can be spread wide in comparison with the particular level set by the MAC layer. Once the size of the data packet to be transmitted becomes small in comparison with header data, and periodic with respect to the length of a day then other factors can begin to dominate energy consumption; First and foremost, the idle power consumption is likely to be one of the biggest determining factors on energy consumption. How this is dealt with is mostly down to the latency required by the system. Low latency requirements will inevitably constitute a large sacrifice in terms of energy budget, however if latency is not critical, then it is perfectly possible to develop a fundamentally low power system.

One of the largest confounding variables when modelling how energy in a network is consumed is the way in which resource contention is managed. The reason for this is that the algorithms responsible are usually proprietary, belonging to the eNB manufacturers. In very dense urban environments with many users, this can have a significant effect on the quality of service and the time it takes to transmit a packet of data. Luckily in the case of small packets, the evidence seems to show that the eNB tends to grant the maximum required RB allocation in order to complete the upload in a single subframe, as this is likely to minimise overheads from splitting the packet over multiple subframes, maximising overall eNB throughput. Network measurements have shown that some older generation hardware deals particularly badly with DRX processes, and that the eNB can also be responsible for

over enthusiastic interrogation of the UE about neighbouring networks, leading to power consumption measurements that are not consistent with the amount of data transmitted and presenting a very poor basis for integration in an efficient system.

Recommendations for energy constrained system design depend largely on the specific requirements for performance, particularly frequency of transmission, latency and packet size, however within the scope of this work the common theme is spending only a small portion of time actively transmitting data. This means that for most systems, the energy consumption is to be very heavily influenced by the amount of energy consumed in the idle state. Wherever possible it is crucial to minimise this; if it is possible to switch off a device at the expense of latency, then this is what should be done. Especially regarding LTE, large energy savings can be made by using an upper layer protocol to acknowledge receipt of a UE transmission, at which point the UE can be switched off before going through and additional, unnecessary transactions with the eNB or DRX processes.

An obvious but useful conclusion of this work is that certainly whilst transmitting, the power amplifier is the most prodigious consumer of energy within the modem. This makes the PA one of the most obvious targets for efficiency improvement technologies, which is the subject of the next chapter. Crucially for M2M uses, these improvements must be able to maintain the low cost, small form factor of the device in order to promote usage.

Chapter 5

Power Amplifier Dynamic Load Modulation

THIS chapter is concerned with improving the efficiency of a power amplifier in an energy constrained Long Term Evolution (LTE) system for machine-to-machine (M2M) use cases. Consideration is given to both dynamic power supply and load pull schemes. The information used to control and optimise these schemes is derived only from the medium access control (MAC) layer, in order to reduce cost and complexity. Techniques are demonstrated with real LTE signals, and proposals are made on how to realise these advances on appropriately miniaturised hardware.

5.1 Introduction

The number of connected devices is predicted to increase exponentially over the next few years [48]. Of particular interest is the use of M2M communications. M2M communications can cover a vast array of applications and transmission durations, however of particular interest is the case of wireless sensor networks, which are likely to be remote and battery powered. Consumers have been demanding ever increasing battery lives, driven partly by work suggesting that up to ten years is a possibility [49], which puts intense demand on modem efficiency. The power amplifier and associated components tend to be the most power hungry blocks in the communications system, and thus become prime targets for efficiency enhancement technologies.

There already exists a large range of architectures aimed at increasing PA efficiency, generally modulating supply, as in envelope tracking [50] , [51] or load modulation schemes [52], [53], however these can be complex to implement and expensive in terms of component count. Similarly, lower frequency dynamic power supply (DPS) systems can be employed, albeit with less improvement in performance. Here an alternative method of adaptive load pull, together with supply voltage modulation, is proposed. Similar work has been done in [54], however with wideband signals and still with the need for additional control signal generation and feedback . This system uses MAC layer information for its parameter configuration, removing the need for feedback or high speed analogue to digital converter (ADC)s for sampling and control.

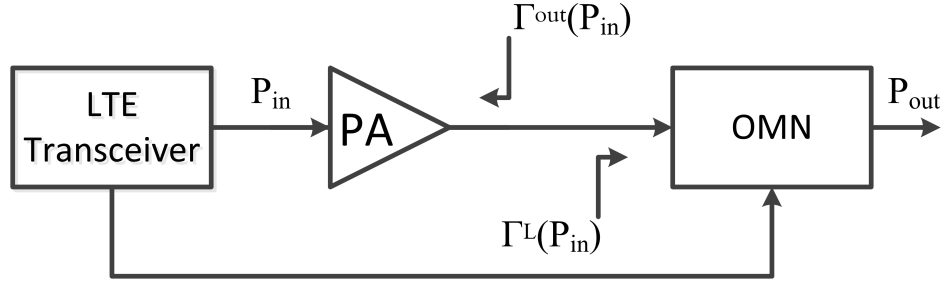
5.2 LTE Physical Layer & Terminology

LTE lends itself to a wide variety of uses due to the highly adaptive nature of the bandwidth, modulation scheme and power output. One of the main advantages of an adaptive link budget, is that due to the use of reference signals and closed loop power control, the radio frequency integrated circuit (RFIC) has knowledge of the power required to be transmitted to a base station, and thus, the amount of power passed into and out of the power amplifier (PA).

LTE power levels are typically updated aperiodically depending on a number of variables, however as they are dependant on the physical downlink control channel (PDCCH) signals, which are updated not more often than each subframe, and thus will not change more than once every millisecond [9]. This knowledge of power level can be used to control the use of both supply modulation and load pull systems in order to reduce power consumption.

When designing RF circuits for optimum power transfer, it is usual to look at the output impedance of the source, and the input impedance of the load. For maximum power transfer

(a)



(b)

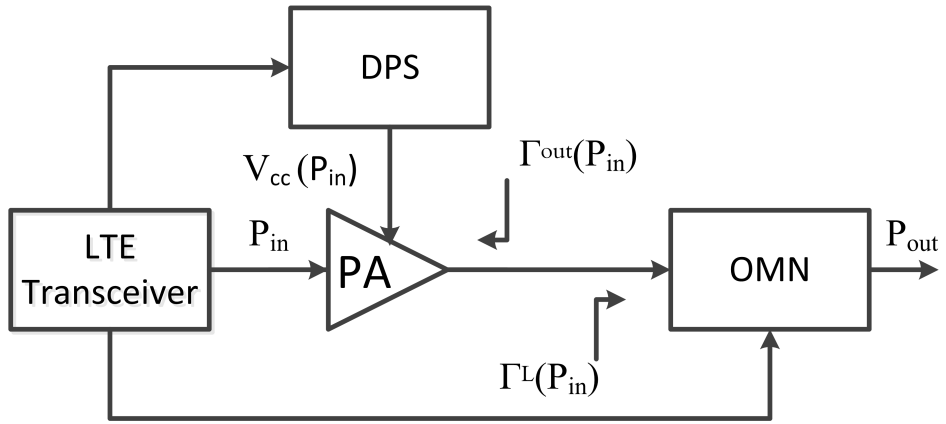


Figure 5.1: Block diagram of proposed schemes; (a) load pull, (b) load pull and DPS.

it is usual to use matching components to make the load appear to have an impedance which is the complex conjugate of the source, this is shown in Figure 5.1. Whilst this may seem like a relatively trivial matter, it is complicated by the fact that the source changes impedance with power level, and thus for optimum operation over a range of output powers, some kind of dynamic matching is required.

Generally most power amplifier units destined for the user equipment (UE) are optimised to be well matched at maximum output power, however this means there is a notable lack in efficiency when operating below this point; An amplifier that operates at 50% efficiency at peak power may be only be 5% efficient when backed off by 15dB, quite a likely scenario particularly in urban locations with many base stations, thus considerable gains to be made by addressing this shortcoming. The principle here is not that the antenna impedance changes with power level, but that as the power amplifier is an active device, and it's output impedance changes with power level and must be matched to the load accordingly.

The optimal solution is for the amplifier to be presented with load that will enable

maximally efficient operation for each particular output power level. Figure 5.1 (a) shows the basic system, where a variable output matching network (OMN) is used to vary reflection coefficient as a function of power level, provided by knowledge of the LTE MAC layer. Load pulling can tend to be a fine balance in a system where power transfer, or insertion loss is a factor. Generally more reactive components added to a matching network will contribute a larger amount of parasitic resistive losses, actually reducing system efficiency. The key here is to balance desired reflection coefficient with acceptable insertion loss.

Figure 5.1 (b) shows a further refinement, where in addition to optimising the output match, the transceiver is also able to control supply voltage as a function of input power. The principle here is quite a simple one. An amplifier requires a certain maximum supply voltage to linearly amplify a signal and its maximum output power. When the amplifier is operating at an output power level below maximum, it no longer requires the maximum value of supply voltage, and in fact, maintaining a constant supply will just contribute to power dissipation and inefficiency. Supply modulation can be slow, such as average power tracking, or fast, such as envelope tracking. The rule here is that the faster the supply is modulated, the higher the gains, but at the expense of system complexity.

Low rate DPS systems have previously been used to good effect in [55], however DPS bandwidth is still high, and requires intensive processing of the baseband signal. Modulating the power supply in the kHz range rather than MHz territory will limit maximum power added efficiency (PAE), however the system will require a minimum of external circuitry, and will also be able to make use of lower bandwidth, more efficient power supplies.

These kinds of methods are particularly appropriate to the work on signals analysis presented in Chapter 3. When setting the operating point of an amplifier, power level and supply voltage are chosen so that the peaks of the signal envelope will not distort due to compression. Whilst the system will be described by the mean power of the signal, the operating point will be adjusted by the signal properties such as peak-average power ratio (PAPR). Using information such as that displayed in Figure 5.2, these signal properties can be derived from the bandwidth and modulation scheme allocated to a UE, and thus enabling an accurate setting of amplifier operating point using only the MAC layer information.

A further possibility for enhancement is that similarly to the load pull case, the output impedance of the power amplifier will change in response to this reduced supply voltage as well as the output power level. This allows the possibility that a tuneable matching network can work in harmony with a dynamic power supply system in order to produce compound gains and maximum efficiency.

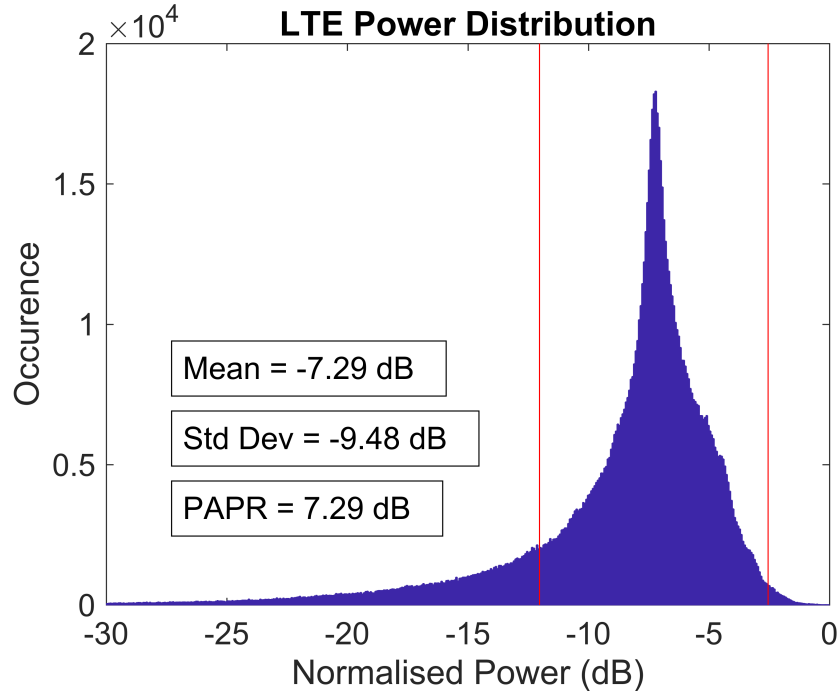


Figure 5.2: Envelope power distribution of a 1.4MHz LTE signal.

5.2.1 A Note on Plotting & Terminology

As most of the material on load pulling incorporates complex RF impedances, a note on how these are displayed is appropriate. All Reflection Coefficient (Γ) values, also referred to as the equivalent parameter S_{11} are displayed on a smith chart, as illustrated in Figure 5.3. The relationship between these values is illustrated in Equation 5.1.

$$\Gamma = \frac{Z_n - 1}{Z_n + 1} = \frac{V_{reflected}}{V_{incident}} \equiv S_{11} \quad (5.1)$$

Due to the mathematics involved in creating the Smith chart, the value of Γ or Reflection coefficient (S_{11}) can be plotted in pure Cartesian form (or polar for that matter), on a traditional axis overlayed onto the Smith chart. The points that are plotted, if read off the displayed Smith chart axes will show the Load impedance (Z_L) looking into a system.

With regard to discussing these S parameters, S_{11} will always be given as a complex value, representing the ratio of reflected voltage to incident voltage, but maybe read from the Smith chart as a complex load impedance as described above. Insertion loss (S_{21}) may be given as either a complex value representing the ratio of transmitted voltage to incident voltage or as a log magnitude to show insertion loss with regard to the power of signals, as

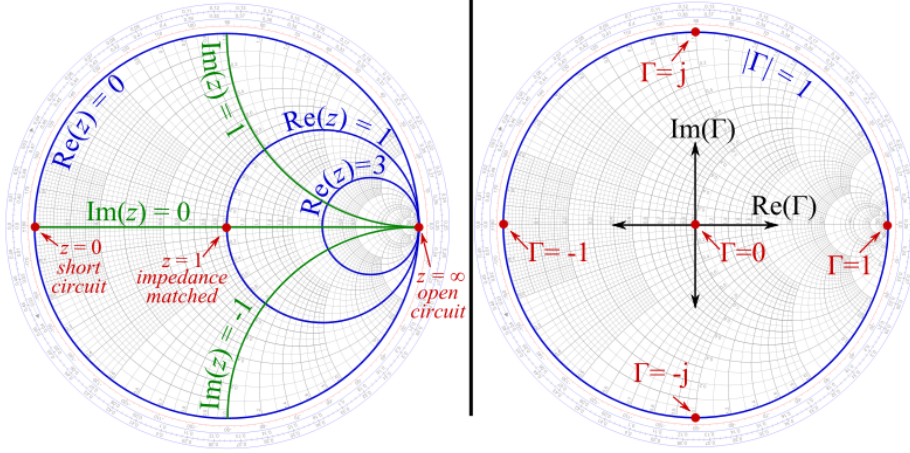


Figure 5.3: Smith chart terminology [56].

shown in the Equation 5.2 below.

$$|S_{21}| = 20 \log_{10} \sqrt{(S_{21_{real}})^2 + (S_{21_{imag}})^2} \quad (5.2)$$

5.3 Current State of the Art

The principle of load pulling a power amplifier is fundamental to effective operation. The concept here is that maximum power transfer will occur when load impedance matches source impedance, when reactive components are involved in the source and load, these should ideally cancel each other out. Whilst this may seem like a trivial problem to overcome, other factors must be considered, such as the fact that impedance will change with frequency of operation, which may be required to be broadband, and also impedance will change with power output, making effective measurement of this quite challenging. Traditional load pulling consists of using mechanical tuners to present various impedances to the input and output of a power amplifier, whilst measuring parameters such as power output or harmonic content. Once the optimum configuration has been ascertained, the tuner settings can be converted back to an impedance via measurement, which can then be formalised into a design via discrete or microstrip components. This is an incredibly time consuming process, and only really optimises performance for one frequency and power level. The focus of this chapter will concern leveraging these principles to provide optimum power transfer at a range of output power levels in a dynamic and miniaturisable way.

Some interesting work on the principle of load pulling was performed in [57]. The motivation for this was a lack of knowledge of transistor impedance data under operating conditions at high power levels. Of course the traditional method of using mechanical tuners at in-

put and output, varied to produce constant gain contours, but this is an incredibly tedious method. This paper evaluated a device under test (DUT) by driving the input with a known signal at the frequency of interest, whilst also supplying this same signal, appropriately phase shifted and attenuated to the output, having the effect of providing an arbitrary reflection coefficient to the device, essentially being able to apply any type of load impedance. A pair of network analysers are used to provide feedback on input and load impedance. It is possible that this could make for an interesting prototype for an active system, certainly enough to warrant calculating how efficient the system might be once losses in splitters and combiners are taken into account.

More advanced load pull techniques have evolved, for example harmonic load pull, as demonstrated in [58]. Whilst most radio frequency (RF) systems are designed to present a well matched load at the fundamental frequency, this is not generally the case at harmonics of the fundamental, which can be of concern. Harmonic load pull techniques can be used to effectively reduce the amount of harmonic content generated or reproduced in a signal in order to increase system efficiency, and more effectively comply with spectrum masks specified in communications standards. This is an important concept, and the paper puts forward an interesting method of measuring this using a circulator combined with frequency selective filtering, mechanical tuners and power meters. The challenge here would be to come up with a more miniaturisable solution, preferably obviating the need for a circulator that could be used adaptively, or perhaps the use of measurement and modelling techniques to predict performance at harmonics whilst an adaptive scheme is in operation. As an aside, with regard to predictions of harmonic performance, [59] uses neural network techniques to predict the load pull performance of field effect transistor (FET) devices using an accurate CAD model, with impressive results.

Some work at a higher power level of 56W in [60] illustrates the concept of combining dynamic power supply operation with load pull techniques. This scenario is kept moderately simple, with only two different supply voltages. As has been previously mentioned, amplifiers are generally tuned to produce optimum PAE at peak power output. Reducing supply voltage for a lower output power level will improve PAE at back-off, but of course this changes the output impedance of the amplifier, giving an upper bound to any PAE improvements. This paper counters this by adjusting the RF match with a varactor diode to provide a variable shunt capacitance on the output. A 20% increase in PAE is shown in the reduced supply voltage case, which verifies the effectiveness of this technique. Whilst not so suitable for the miniaturised case (the varactor diode in this case required a -65V control voltage), it can be seen that DPS and load pull techniques can work well together.

The paper [61] uses dynamic load modulation to achieve an absolute improvement of

10% PAE for a 7W device. This again was a varactor diode, but the amount of Smith chart coverage with this single component was very impressive, from 1.5Ω to almost $0.15 - j0.5\Omega$. Unfortunately, despite the title of the paper suggesting this was all done in a complete dynamic system, a real, higher bandwidth modulating control signal for the varactor diode was not used.

Another varactor based load modulation scheme is presented in [62], though this example is fortunately demonstrated with a real, fast modulation waveform in response to the incident signal's envelope. Whilst the range of back-off power is comparatively small at 10dB, the high bandwidth of 1 - 1.9GHz with 64–79% peak PAE is impressive. Unfortunately varactor control voltages of up to 80V render this rather impractical for UE use, current consumption is very low, but the generation of such high voltages poses a number of problems especially on miniaturised RF devices from an electro-magnetic interference (EMI) perspective.

A more modern approach is shown in [63]. Here a digitally controlled matching network simulation is demonstrated on 40nm complementary metal oxide semiconductor (CMOS) using a digital decoder which responds to signals proportional to the amplitude modulation (AM) of the signal, switching in capacitances in the high fF and low pF range. Peak power is fairly low at 17dBm and the work is simulation only, but the concept is extremely applicable for the low cost mobile scenario, where this could be easily implemented on a PA integrated circuit (IC).

A further investigation of digital load modulation is given in [64]. This is not a simulation, and incorporates micro-electro-mechanical systems (MEMS) devices to switch in capacitances for load pull. Improvements of up to 30 percentage points in drain efficiency are claimed at 10dB back-off. This illustrates that MEMS switched reactances as well as CMOS as becoming useful and miniaturisable for load pull schemes. Previous work from the Institut für Hochfrequenztechnik und Funksysteme in [65] has shown that this technique can also be used at much higher power levels of up to 10W, whilst still offering a 20 percentage point improvement in drain efficiency.

An earlier and more basic work involving MEMS devices is presented in [66]. The principle here is slightly different from the load pull concept, but utilises MEMS devices to switch in appropriate load impedances to produce a triple band amplifier capable of operating at 1.9, 2.4 and 2.6GHz. Whilst the measurements are only taken with continuous wave (CW) signals, a drain efficiencies of 70% at peak power and 60% at 6dB back-off are quite encouraging across the three bands.

In a slightly similar application, [67] shows how similar tuning methods can be used to control antenna tuning capabilities in variable environments. A tuneable RF MEMS capacitor is used to re-tune the antenna in response to mismatch conditions arising from human

body interaction. Using a single series tuneable capacitor yielded an average improvement of 2dB in total radiated power, with a peak improvement of 6.8dB, which is significant. An interesting detection method is used for closed loop performance; feeding the voltage over a series inductor into a phase detector and signal level indicator. This is simple enough that it could be incorporated quite easily into a low cost device.

With regard to supply modulation, the underlying principles do not form the basis novelty in this work, however an excellent overview of dynamic power supply technologies is provided in [51]. Some of the latest developments in envelope tracking technologies are provided in [68]. This explains how when signals of high PAPR are amplified, a linear amplifier must operate in a backed-off region and either accepted the loss in efficiency, or deploy mitigation techniques. Obviously envelope tracking and to a lesser degree, average power tracking form part of these techniques by reducing the amplifier supply voltage when a higher value is not required for linear amplification.

Theoretically speaking, envelope tracking should produce superior results to complementary amplifier techniques such as Doherty [68] in the presence of the high PAPR signals present in LTE systems, superceeded only by envelope elimination and restoration, however these metrics generally do not take into account the efficiency of the regulator supplying the amplifier, or the complexity in actually measuring the envelope and modulating the supply as appropriate.

The advantage of average power tracking implementations in this case is that although the fundamental efficiency improvement of the system is lower, the requirements to using the system in a realistic product are lower in terms of cost and computational overheads. [69] uses an adaptive power supply to both improve efficiency, and also the boost conversion capabilities of the supply to deal with battery droop, whilst claiming a potential 88% increase in battery life due to the reduced energy consumption.

To summarise, there exists a wide range of work targeted at improving the efficiency of the power amplifier in a cellular system, however a lot of this is aimed at the base station, as this is an application that can tolerate, larger, more complex and expensive design solutions. This chapter aims to prove the virtues of dynamic power supplies and load modulation for low cost M2M modems when used in a cost effective, and simple manner, which should also aid commercial uptake.

5.4 Hardware & Measurements

In order to properly validate the degree to which we can improve system performance, a slightly unusual method is undertaken to appropriately instrument the system. If an

entire UE were instrumented for current consumption, we would get a good overall view of system performance, but because there are so many processes occurring within the unit, trying to determine exactly how any efficiency enhancement technologies had taken effect would be quite challenging. The solution in this case is to use the traditional setup of a UE communicating with an evolved node B (eNB), in this case a base station emulator, but add in additional components that can enable measurement of the processes involved. An external power amplifier was selected to be placed in between UE and eNB so that the transmitted power levels from the UE are backed off in closed loop operation, and all appropriate gain is provided by the external amplifier. The advantage here is that the amount of direct current (DC) power being consumed by this device can be easily ascertained, in order to form the basis of comparative measurements for a variety of different performance enhancing technologies, whilst still using real LTE signals.

5.4.1 Circulators & Power Calibration

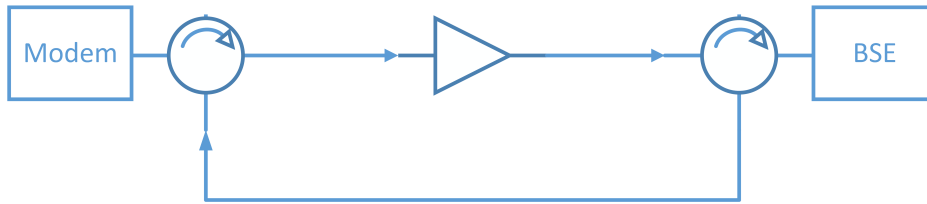


Figure 5.4: Duplexing test arrangement.

The particular test arrangement around the power amplifier is shown in Figure 5.4. The reason for this additional equipment is that the system is a real, hardware in the loop LTE system which requires bi-directional communication for setting up the connection between the UE and eNB. If a power amplifier was connected between the acUE and eNB, the signals produced by the UE would be amplified as appropriate on their way to the eNB, however any signals travelling in the opposite direction would be severely attenuated by the amplifier, due to the non-reciprocal nature of this device. As the basis of an LTE network is highly eNB centric, i.e. the base station is responsible for managing the connection, allocating resources and allowing the UE to transmit, then clearly in this case nothing would happen.

The solution to this is to use a pair of circulators, as illustrated in 5.4. This is a simplification of the final test set-up, but adequately illustrates the principles involved. The purpose of a circulator is to only allow a signal to pass in one direction around the device. Obviously operation is not perfect, but typically there will be a low insertion loss for around 0.5dB from port 1-2, 2-3, 3-1, with a much higher insertion loss of around 30dB with all other port combinations. As can be seen in the diagram, this arrangement ensures that any signal

passing from the UE to the eNB must pass through the power amplifier for appropriate measurement, whilst any signals passing in the opposite direction are free to bypass the amplifier and travel unimpeded to the UE.

5.4.2 Dynamic Power Supply



Figure 5.5: HP 6624A power supply & Agilent E6621A base station emulator.

In order to instrument the amplifier in question, hereafter referred to as the DUT, DC power was provided by 4 output programmable supply, as shown in the top of Figure 5.5. This was tested for calibration before being having three of the outputs connected to the DUT. Two of the outputs are biasing and gain setting voltages for the amplifier, which will consume little power, however the third supply is the main DC source used to power the amplifier. The advantage of this particular power supply is that it is programmable via a general purpose interface bus (GPIB) interface. This means that a Matlab script can be used to set the relevant supply voltages required, set any voltage and current safety limits, and most crucially read back the amount of current consumed by the DUT, providing the basis of a good automated test rig. A further advantage of this control system is that the supply voltage can be manipulated, albeit slowly, in order to form the basis of a DPS system, which will be described further on in the chapter.

Whilst a little old fashioned, the GPIB interface provides an easy way to control instrumentation by manipulating various control strings before sending these over a serial interface. In order to interface this with modern computer control, a universal serial bus (USB) to GPIB converter is used, which can be interfaced with by treating it as a virtual COM port. More details concerning this implementation are placed in Appendix C.

5.4.3 Mechanical Impedance Tuner

In order to present a dynamically varying impedance to the power amplifier, a mechanical tuner is used. This is an automated system whereby a probe is inserted into a low loss, slotted transmission line. Stepper motors are used to vary the distance between the probe and the start of the transmission line, and also the distance between the probe tip and the centre of the transmission line. These two parameters will vary phase and magnitude of the reflection coefficient presented to the output of the power amplifier respectively.



Figure 5.6: Focus 1808 iTuner.

The interface on the mechanical tuner consists of sending new positions in the x and y direction for the tuner to step to, with no direct measurement of reflection coefficient. There are two possible ways to calibrate the tuner; Every possible x,y coordinate could be stepped through, with a 50 Ohm load attached to the out port, and a vector network analyser (VNA) attached to the in port. The VNA can measure S_{11} , which will be our reflection coefficient. Whilst this will work, it will generate a lot of different data points that may not be required for final analysis. A more efficient way is to complete the load pull analysis, noting down any x,y coordinates at positions of interest, such as maximum efficiency, before finally measuring these with a VNA. Calibration using the VNA was also automated, using a Matlab script and an Ethernet interface to the hardware. S_{11} and S_{21} were obtained whilst stepping through the required states for tuneable components.

5.4.4 Power Sensors

Whilst striving towards scientific accuracy, the need for an accurate measurement of RF power is required. The Rohde & Schwarz NRP-Z power sensors are used for this in two parts of the project. As a convenient measure of the amount of RF power entering the

amplifier, for PAE calculations, a power splitter is used to couple off an appropriate portion of power, which can then be fed through a calibration routine to give the actual power entering the amplifier. The portion of power that is coupled off is measured by the power sensor, which has been calibrated regularly enough to be considered a reference device. The second use of the power sensors is to calibrate the power received by the base station emulator. Due to the way all of the test equipment was automated, it is much easier to read the received power level from the base station emulator (BSE), however we cannot be sure that it gives an accurate reading. Similarly to DUT input power, the signal from the DUT is split for calibration, with half fed to the BSE and half fed to the power detector reference, enabling calibration factors to be extracted for future use with the BSE alone. Operation of the R&S power sensors is via direct USB interface, which with appropriately set up drivers, can be configured and interrogated via Matlab scripts for fast operation. Again, further consideration for this is given in Appendix C.

5.4.5 Base Station Emulator

The functionality and use of the base station emulator has been covered comprehensively in Chapter 4, however some of the more advanced operations are used in this piece of work. The requirements of the BSE in terms of functionality are two-fold. Firstly we need the BSE to provide a virtual LTE network in order to stimulate the UE into producing the uplink signals required to validate this work. Secondly, the BSE is used to measure the signals coming from the UE; most important is obviously output power, which is a standard BSE measurement but calibrated with a power sensor.

The other measurements required concern measurements of distortion in the UE signals. This is most significant for the work with dynamic power supplies; when amplifier supply voltage is modulated too low, distortion of the output signal will result. To this end the BSE is used to record two metrics of distortion - error vector magnitude (EVM) and adjacent channel leakage ratio (ACLR). Whilst these parameters are more fully explained in Chapter 2, the basis is that EVM is the magnitude of the distance between an ideal symbol and the symbol that was actually received by a device. ACLR is the relative power level of the transmitted signal, measured within side channels not allocated for the device to use. Both of these parameters can be used to approximate how the transmitter signal is distorted with a reduction in supply voltage for a given output power. Obviously lowering the supply voltage reduces overall power consumption, but there is no point in generating a signal that would not pass LTE specifications; there is a balance to maintain.

The scripts used to automate this testing step through a variety of scenarios. To form the basis of a very simple average power tracking (APT) scheme, appropriate supply voltages

for each output power level are recorded by stepping through each possible output power level, and reducing supply voltage until ACLR and EVM are affected.

5.4.6 UE

Whilst the UE has been well defined in other chapters, there are few unique issues that need to be addressed in this set-up, namely the basis of its physical layer control. When a UE prepares to transmit on a network, it must do so at an appropriate power level that ensures that the signal is powerful enough to be accurately decoded by the eNB, but not so powerful that it risks interfering with equipment in neighbouring cells. This is achieved by the UE measuring the strength of the primary synchronisation signal (PSS) and secondary synchronisation signal (SSS) waveforms from the eNB, and using these to form a basis for the power level that it decides to transmit on.

This has two implications. Firstly on a conventional setup, the power output that the BSE in the lab is set to transmit on should be calculated to take into account the likely output level from the UE, and the power level that it will be required to maintain via physical layer communications. If the BSE power level is set too low, the UE will assume there is a large amount of path loss in the system. and transmit at a level likely to saturate the BSE receiver.

The second implication is that in our test scenario, the algorithm that the UE uses to determine its transmit power will be off by a large amount due to the extra 30dB of gain we have inserted in the form of our power amplifier. The most likely outcome without correction is that the UE will transmit at a sufficiently large power level to saturate the DUT, considerably distorting the output signal to such an extent that the attempt to attach to the simulated eNB is unsuccessful. As no attachment procedure has been performed, there is no MAC layer framework for the eNB to tell the UE it needs to reduce its output power level as part of a closed loop power level control routine. The outcome here is that without intervention the random access channel (RACH) process will never work. Fortunately the solution is simply to increase the output power level of the BSE in line with the gain provided by the DUT. This will increase the received power level at the UE, and cause it to transmit at a correspondingly lower power level. Provided that this initial power level is low enough as not to be distorted by the DUT, the attach procedure will complete, and any further fine tuning of power levels can be completed by the closed loop operation in the MAC layer. Another option would have been to insert an attenuator of equal and opposite value to the gain provided by the amplifier, though this would require additional calibration tables to function accurately

5.4.7 Entire Test Set-up

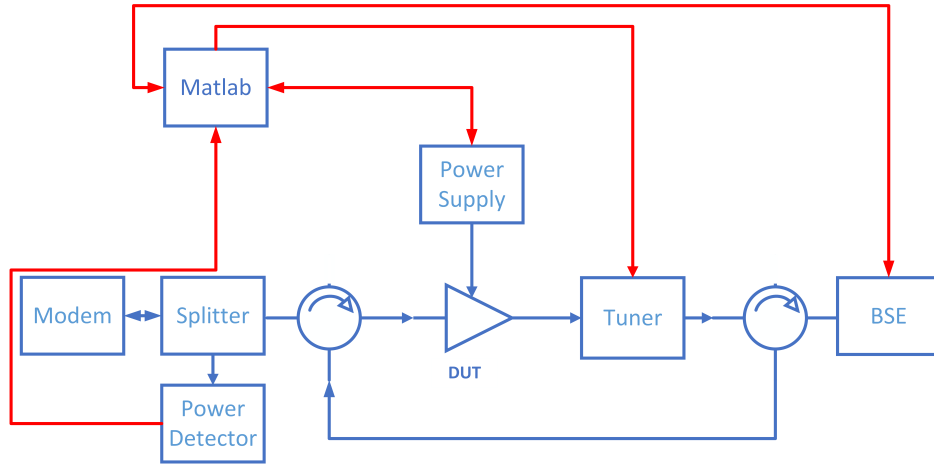


Figure 5.7: Full test set-up.

The diagram above shows the completed test set-up for the load pull and dynamic power supply evaluation. It can be seen that the entire rig is controlled by a laptop running Matlab script. This script interfaces with equipment as described above and records all available and useful parameters for further analysis. Test procedures are documented in subsequent sections.

As accurate measurement of power at both the input and output of the amplifier is crucial to obtain a realistic idea of power added efficiency, the components used for connection, isolation and splitting were all measured for losses and asymmetries so that these could be calibrated out of the final results. These calibrations included taking into account cable loss, splitter asymmetries and circulator insertion loss.

5.5 Practical Attempts at Improvement

The following section details the practical work undertaken to achieve improvements in power amplifier efficiency in a working LTE laboratory system.

5.5.1 What we are trying to achieve

The overarching requirement of this work is to improve efficiency, but how much, and at what cost? The objective of this entire thesis is to improve the efficiency of a communications system, whilst minimising the additional computational or hardware requirements to do this. The two parameters that will be changed in the following experiment will be the supply voltage to the power amplifier and the complex load seen by the PA. To limit overheads,

only existing MAC layer information will be used to change either of these properties. For a full analysis, the efficiency of the dynamic power supply must be taken into account, together with any losses incurred within the load modulation hardware.

5.5.2 Measurement Set-up

In order to create a measurement setup that would provide accurate results with the kind of LTE signals seen on a real system, the uBlox Toby L210 LTE modem is used to generate and receive signals from the BSE. The generated LTE signals are fed through an additional external power amplifier, which can be instrumented in such a way as to measure its DC power consumption, and the RF power in to and out of the device. Whilst using the using an existing piece of LTE hardware to measure signals does make control and analysis easier, it is important to measure distortion in the form of EVM and ACLR over the range of desired output powers, which will become the range of input powers for the external PA (DUT).

Figure 5.8 shows measurements of ACLR and EVM for power levels of -40 dBm to 23dBm measured at the output of the LTE device. This was repeated for bandwidths of 1.4MHz, 10 MHz and 20MHz, and modulation schemes quadrature phase shift keying (QPSK) and 16 symbol quadrature amplitude modulation (16-QAM). These measurements were taken in much the same way as the main work in this chapter; The BSE was calibrated for power measurement, once this was complete, a Matlab script was used to control the BSE, altering UE output power (via the MAC layer, and measuring the actual power level, EVM and ACLR.

The power amplifier under test has a gain of 34dB. The maximum power we need to achieve in any test is 28dBm, which consists of the maximum 23dBm at the antenna allowed by the LTE specifications, plus a margin for losses in switching, filtering and mismatches. It can be assumed that a reasonable minimum required power input into the amplifier would be 0dBm. subtracting the 34dB gain from these two figures gives us the range on input powers supplied by the UE from -34dBm to -6dBm. Referring again to Figure 5.8 we can see that the performance between these limits is generally pretty respectable. EVM remains below 2.5% in all cases, and ACLR below -40dBc.

It would be reasonable to assume that the power amplifier in the Toby modem is introducing very little additional distortion at these output power levels, as it is nowhere near to saturation and there are no dynamic power supply units inside the modem that could also cause compression based distortion. This means that the majority of the signal distortion illustrated in the source plots is likely to be from the baseband modulation in the modem, lending additional validity to our test set-up as it is representative of a real system.

In order to baseline the system, a DUT was selected as the Skyworks SKY77765 Gallium

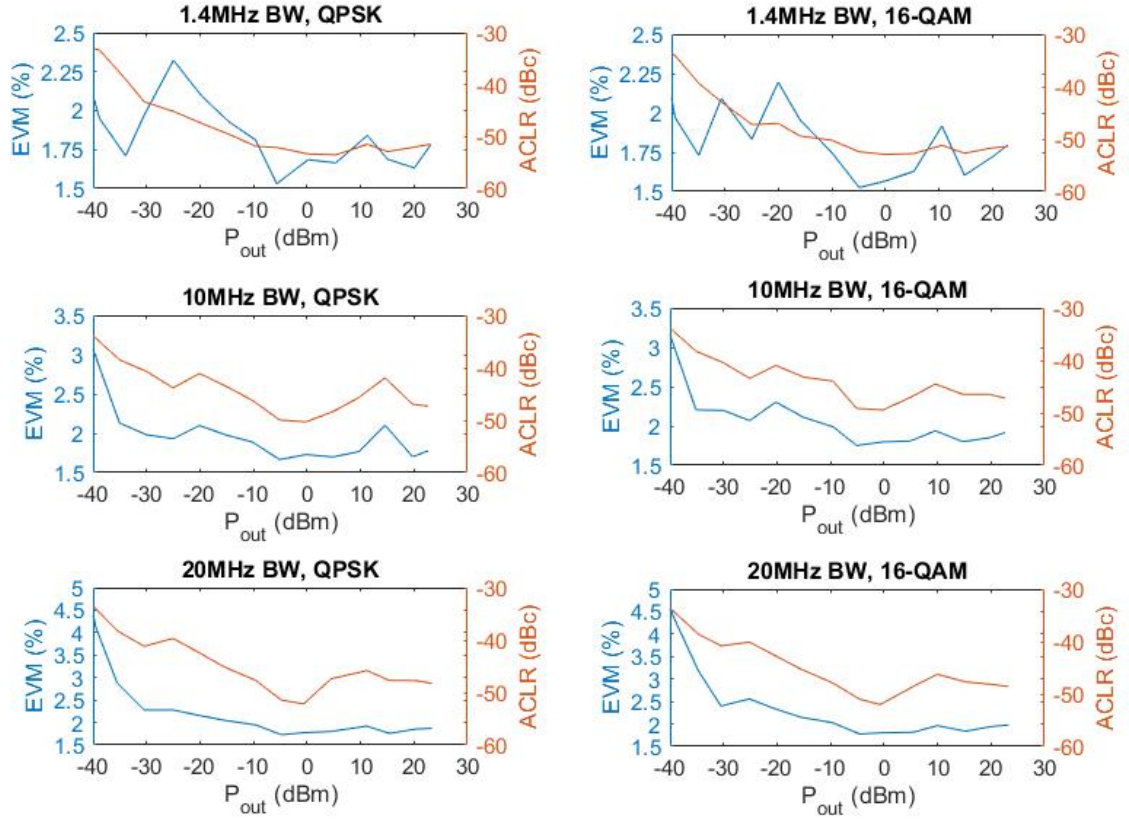


Figure 5.8: Toby measurements as a source.

Arsenide (GaAs) microwave monolithic integrated circuit (MMIC), a basic test was performed over an input power sweep from 0 to 23dBm using QPSK modulation in the shared channel over a 10MHz bandwidth, figures chosen for comparison with datasheet values. Figure 5.9 illustrates that the gain is generally very linear over the power sweep, and the PAE peaks at 48%, which is in good agreement with quoted figures. A photograph of the test bed used for this shown in Figure 5.10.

In order to evaluate the effects of load modulation, a mechanical tuner was used to sweep various trajectories over it's available range of reflection coefficients. The tuner response was swept for each of a range of input power levels until optimum PAE was achieved.

In order to evaluate the DPS case, this was repeated using a supply voltage proportional to the output power required. To obtain a baseline result, an input power sweep was completed. At each power level step PA supply voltage was reduced until adjacent channel leakage ratio increased in excess of -40dBc, a level chosen to exceed LTE UE minimum requirements, PAE was then measured at this point.

Similarly to the first experiment, a load pull sweep was then enacted in order to gauge the effectiveness of the DPS and load pull methods combined. It is important to note that

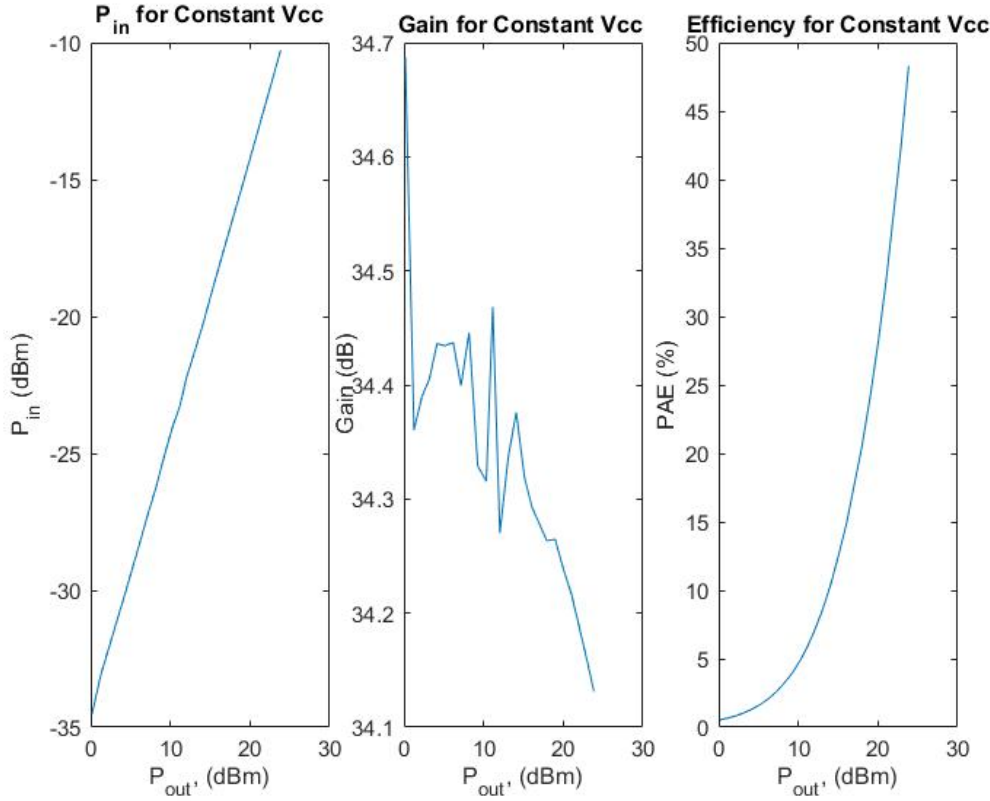


Figure 5.9: Skyworks PA output power sweep - 50 resource blocks.

ACLR and EVM performance were monitored during the tests, and any optimum PAE results were discarded if they would not have passed LTE UE requirements.

5.5.3 Results

Regarding the fixed supply voltage operation in Figure 5.11, improvements in performance using only load pull are generally small at lower output power levels, however significant improvement can be obtained from 15dBm onwards. The 15-25dBm region shows an increase of up to 44% in PAE, with both the standard and optimised traces beginning to converge at peak power, suggesting the amplifier was optimally matched for this level.

The two other traces in figure 5.11 compare PAE for a supply voltage modulation as per subsection 5.5.2, both with and without adaptive load modulation. It can be seen that the largest improvements of the load pull are based around the 10-25dBm region, with a maximum of 27% increase in efficiency over the DPS only case. Slight variation in the trend of the load pull trace are likely to indicate that the granularity of the tuner setting was not sufficiently small to be able to achieve the optimum result.

Figure 5.12 shows the S_{11} values provided by the tuner over the ranges of optimum

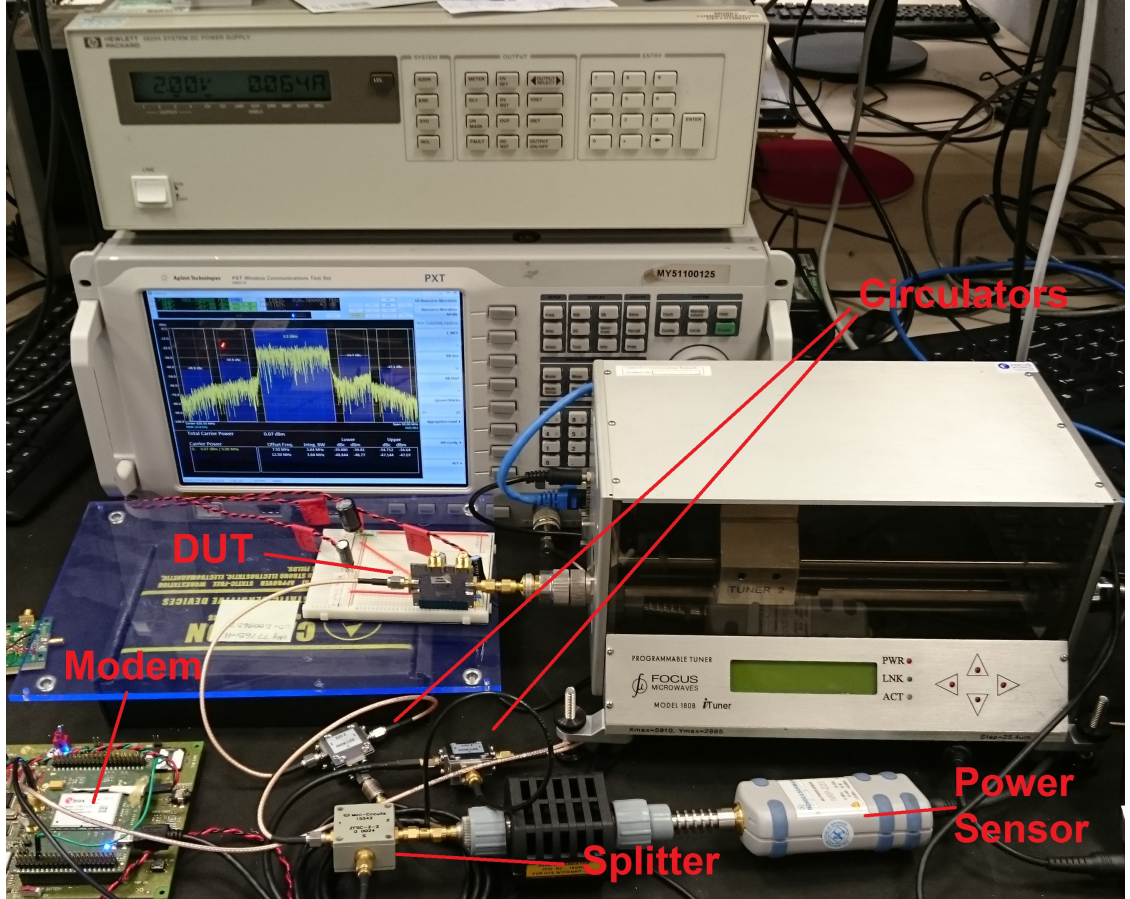


Figure 5.10: Photograph of measurement setup.

operation. The area of the smith chart covered is reasonably small, suggesting there is a large scope for a range of minaturisable technologies that could accomplish similar trajectories.

5.5.4 Discussion

It can be seen from the results that significant increases in PAE can be achieved using low speed techniques governed by information obtained only from the LTE MAC layer, removing the need for any additional signal sampling and processing during operation. Additionally, lower rate modulation of supply voltage and load allow a wider range of candidate technologies to be employed to fulfil this function. Figure 5.12 shows the S_{11} provided by the tuner for both cases.

It is important to note that although the biggest improvements in PAE were not at peak power, the output power at which a device operates at will be based largely on location and environment. It is highly likely that the middle of the operating power range will be most utilised over a range of scenarios and thus will obtain the most benefit.

There are of course limitations to the experimental setup; The response of amplifier PAE

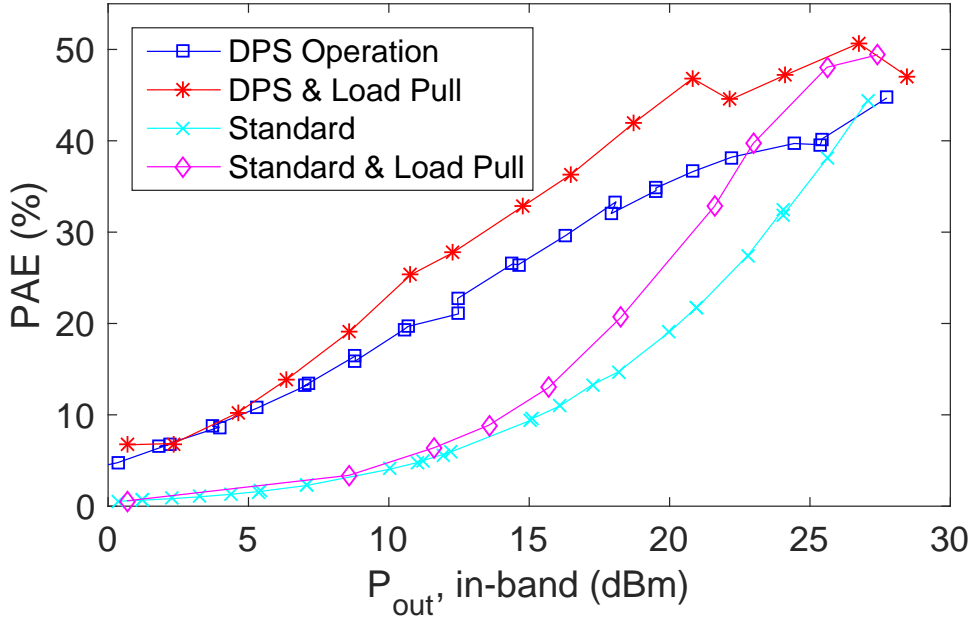


Figure 5.11: Amplifier PAE for an output power sweep.

for a single input power level, over a range of tuner settings exhibited many sharp peaks. Peak PAE often appeared as a single outlier, suggesting that the tuner step size could be reduced in order to further improve results by presenting optimum S_{11} .

One of the main considerations for LTE user equipment is miniaturisation. Further work will focus on the ability to cover similar areas of the Smith chart with techniques such as matching networks incorporating varactor tuning diodes and MEMS capacitors.

5.5.5 Continuous Wave Measurements

In order to 'clean up' the plots of optimum PAE, some continuous wave measurements were made using the existing load pull and DPS techniques. Figure 5.13 illustrates the optimum impedance trajectories required to be seen by the power amplifier at 836.5MHz in order to obtain peak PAE. Obviously these need to be considered in the context that the optimum real-signal solution would consist of taking the probability density function (PDF) of a signal at a certain mean power level and multiplying this by the CW results.

Figure 5.13 shows that the CW trajectories are quite a lot cleaner in terms of showing a trend from high power to low power operation, though unfortunately the trend is not simple enough to use a single tuneable series or parallel reactive component. The plot illustrates

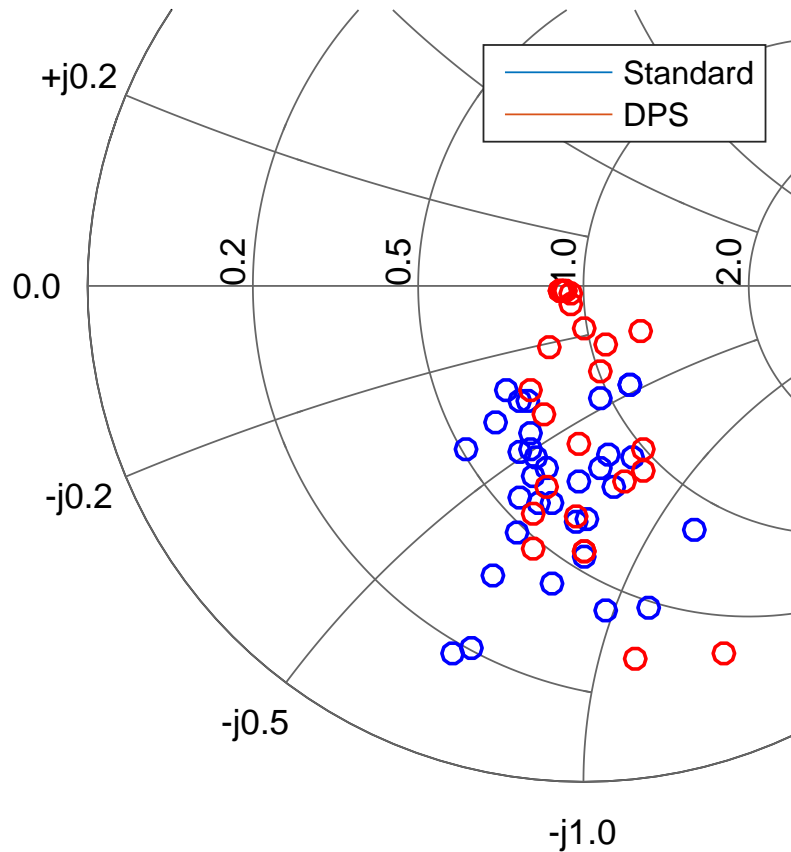


Figure 5.12: Smith chart coverage for standard and DPS load pull.

the need to ideally move in both directions on the Smith Chart in order to obtain optimum performance.

Figure 5.14 shows the insertion loss of these optimum tuner states. It can be seen that the general trend in the lower power states is for an insertion loss of around 3dB. This is higher than expected, however it can be seen as a positive, as any further miniaturised system that is implemented is likely to have a high insertion loss. In order to achieve significant enhancements this only has to be 3dB or better.

5.6 Digital Tuning

In order to gain an greater understanding of the effect of realistic load pull systems, further work has been conducted with digitally tuneable capacitors, in particular those manufactured by Peregrine Semiconductors, chosen due to tuning range, appropriate interface and availability. These devices use CMOS technology to switch banks of on-chip capacitors via

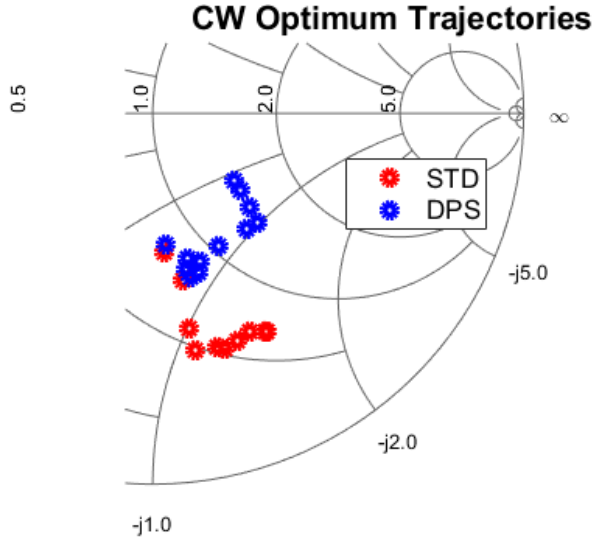


Figure 5.13: Optimum load pull Trajectories for CW operation.

an serial peripheral interface (SPI) interface. There are typically 32 different tuning states, with a range of up to 1.88 - 14.0pF.

It is important to note that there are parasitic elements involved in this process, which are illustrated in Figure 5.15. These need to be properly analysed in order to gain an idea of insertion loss and the limitations of matching network topologies that the digitally tunable capacitor (DTC) technology can be used for. Numeric expressions for the parasitics involved in the model are given in Table 5.1.

Variable	Equation (State = 0:31)	Unit
C_s	$(0.394 \times state) + 1.456$	pF
R_s	$15 / (state + 15 / (state + 0.4)) + 0.4$	Ω
C_{P1}	$-0.0026 \times state + 0.4155$	pF
C_{P2}	$0.0029 \times state + 0.4914$	pF
R_{P1}	4	Ω
R_{P2}	$22000 + 6 \times (state)^3$	Ω
L_s	0.4	nH

Table 5.1: DTC parasitics values [70].

5.6.1 DTC Analysis

A printed circuit board (PCB) was designed to enable analysis of a simple series / parallel combination of DTCs, with appropriate footprints to enable further tuning to reach states

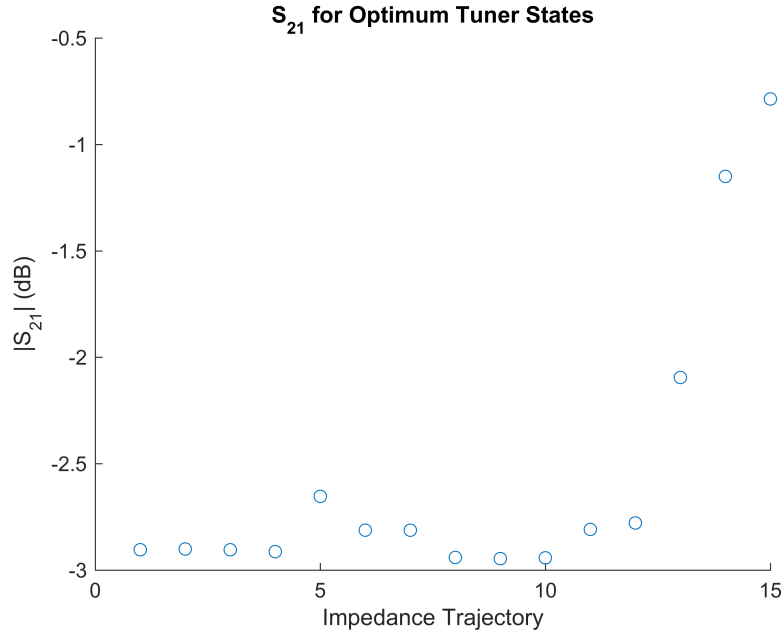


Figure 5.14: Tuner insertion loss for optimum states.

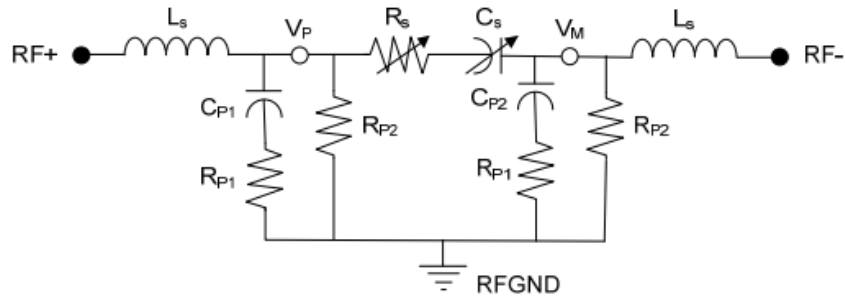


Figure 5.15: DTC parasitics model [70].

on the smith chart indicated as appropriate by previous experiments.

Figure 5.16 shows the prototype PCB for this, incorporating the two DTCs, SMA connectors for RF in and RF out, a screw terminal for DC power input and two pin headers for the SPI control bus for each DTC.

Construction of these devices was technically challenging, due to the incredibly small footprint of the DTC devices, and number of other components in close proximity. A laser cut stainless steel stencil was used to apply solder paste to the appropriate areas, before a hot air surface mount (SMT) rework station was used to melt the solder paste. through hole / end launch components were added later by hand.

Initial experiments consisted of simply measuring the S_{11} and S_{21} for the system. This was done using a PNA-X Vector Network analyser, automated using a MATLAB script to

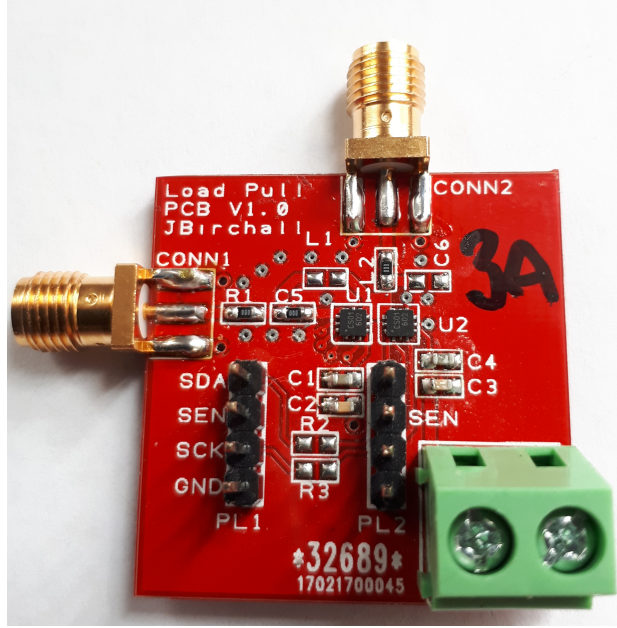


Figure 5.16: DTC initial PCB, populated.

cycle through the states of the tuneable elements, and receive appropriate results from the VNA.

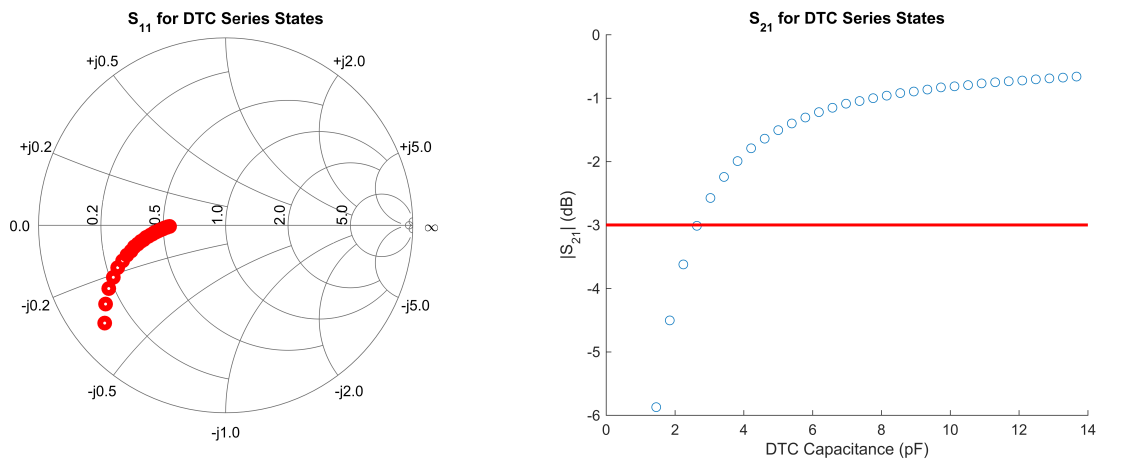


Figure 5.17: DTC series states.

Figure 5.17 shows the response from a single DTC in series between two 50Ω SMA connectors, set up for a two port measurement on the VNA. The Smith chart on the left of the image illustrates the S_{11} characteristics of the device. It can be seen that a good sized arc of coverage is present on the plot. It should be noted that as the tuner state, and thus capacitance increases, the points move from the left of the Smith chart into the centre. Whilst this is not in the locations required for the particular power amplifier, this could be pulled around the chart with additional reactive components.

A further point to note is that the effect of the parasitics within the device can clearly be seen by the shape of the tuning curve. A purely increasing / decreasing capacitive reactance would move only along the lines of constant resistance, however it can clearly be seen that the movement of the tuning states is across two dimensions on the chart, indicating the device parasitics are having a significant effect at this frequency.

Considering the plot on the right hand side of the figure; This illustrates the insertion loss, or S_{21} of the system. It can be seen that in line with expectations the insertion loss decreases with increased series capacitance, and for the majority of the states, the insertion loss is lower than 3dB, which suggests this configuration could be used for a valid load pull system with acceptable increases in system performance.

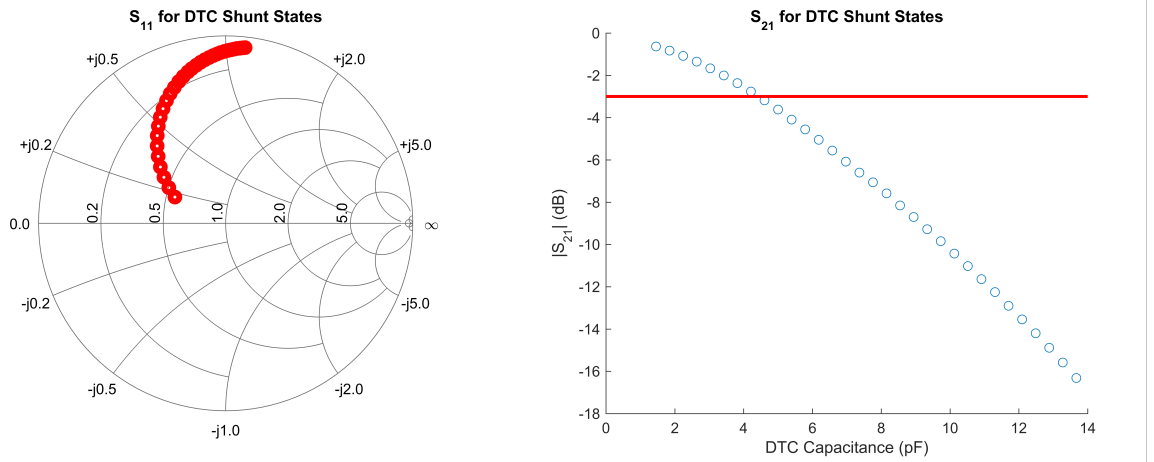


Figure 5.18: DTC shunt states.

Considering the shunt case illustrated in Figure 5.18, it can be seen that the coverage arc over the smith chart is wider than the series case, but is on the opposite portion of the chart to the ideal trajectories we require for the Skyworks amplifier, requiring the addition of a large series capacitance in order to end up where we want, though this would obviously come at the price of an increased insertion loss. The movement of the points with increasing capacitance is from the centre outwards. Taking a look at the S_{21} from the right hand side of the figure, we can see the real problem with this configuration is that perhaps unsurprisingly, this is rather poor, with most states exceeding the -3dB threshold that we require, meaning this is unsuitable for a realistic system to increase efficiency.

As a final consideration, the series / shunt configuration was evaluated. Figure 5.19 shows the results of this. The Smith chart shows that the S_{11} values give a satisfactorily large coverage of the chart, meaning that there is great potential for use in a wide variety of cases, however the S_{21} values illustrate why this is not a viable concept. The majority of the 1024 tuning points are below the -3dB threshold for a realisable improvement in

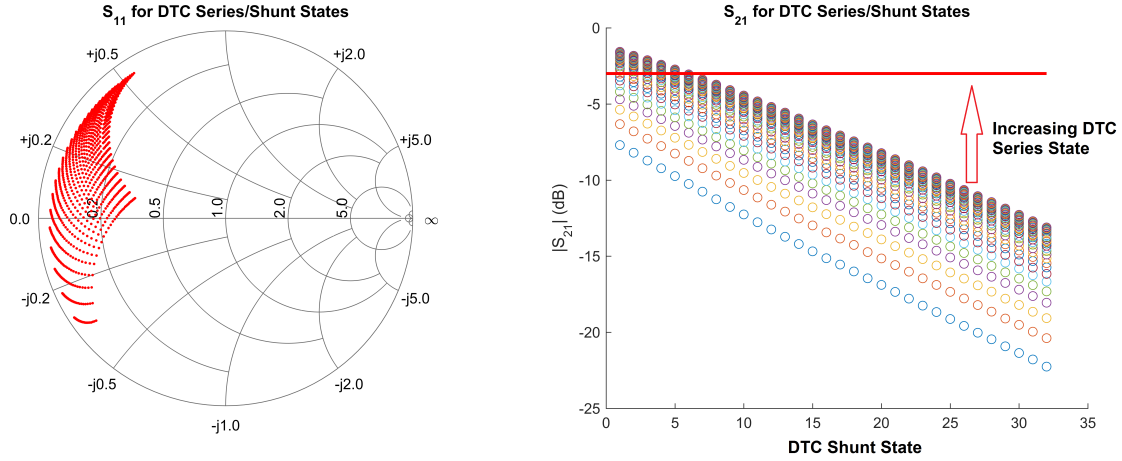


Figure 5.19: DTC series / shunt states.

system efficiency, and this is before additional reactive components are added to move to the required portion of the smith chart.

5.6.1.1 Discussion

It can be seen from initial work with digitally tuneable capacitors that in terms of providing a range of coverage on the Smith chart, there are a lot of options available, especially when combining the devices in series / shunt configurations. The main limitations of the device come with the parasitic components. The series resistance in particular can be a problem in maintaining a reasonable insertion loss. This figure can vary between 0.8Ω and 2.4Ω according to Equation 5.3. Additional resistive parasitics are also present in parallel with the RF ports due to circuit and package parasitics and the biasing networks on the device.

$$R_s = \frac{15}{\frac{\text{state}+15}{\text{state}+0.4}} + 0.4 \quad (5.3)$$

As the plots in this section have shown, S_{21} will likely be the limiting factor in using these devices in an efficiency enhancement design. The series DTC configuration is currently the only one capable of achieving a usable S_{21} , so further work will address pulling the available load into the appropriate regions in the Smith chart.

5.6.2 Contour diagram

When constructing matching networks, it is important to know how the required accuracy will influence the choice of components, and how close the actual match is using real (E.g. E24) values. This principle also help understanding of the required number of degrees of freedom in the system to obtain reasonable results. To illustrate this point, the CW

measurement platform was used again with the mechanical tuner, however a single mid-range optimum trajectory point was chosen, and impedance trajectories around this point were swept whilst measuring PAE. Once all PAE points had been mapped, a contour diagram was constructed to show how PAE falls away with non-optimal trajectories. From this diagram, the contour line describing 95% of the maximum possible PAE was extracted, with the tuner coordinates that give these values. These tuner coordinates were then measured back on the VNA in order that they may be plotted on a Smith chart of S_{11} .

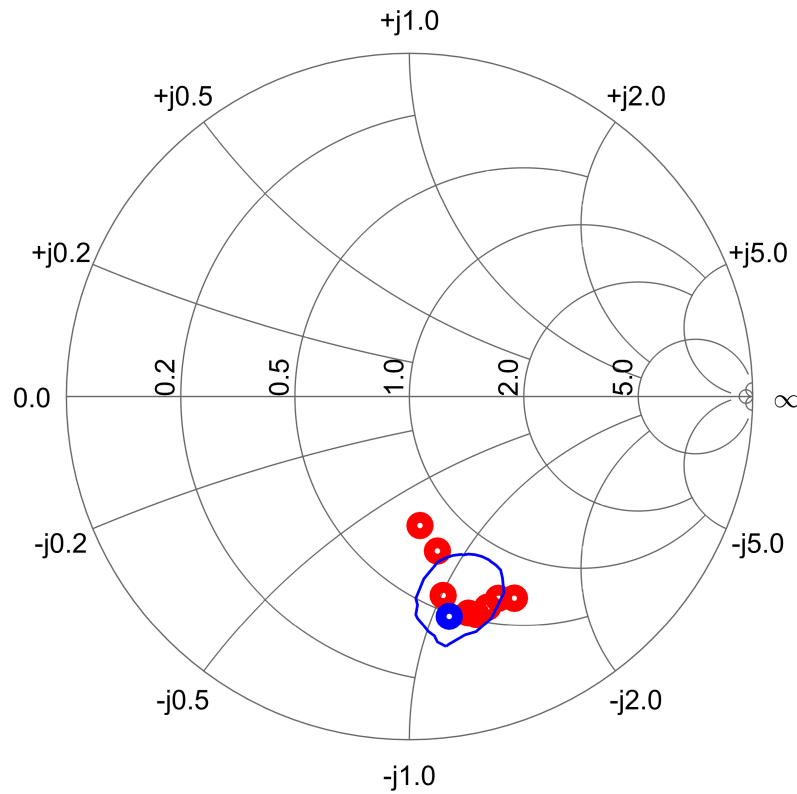


Figure 5.20: 95% peak PAE bounds for a single optimum trajectory.

Figure 5.20 is the resultant plot. Optimum trajectories are shown in red, with the chosen mid range value in blue. The blue ring around this point is the 95% PAE Contour. It can be seen that this is quite large in the context of the other optimum trajectories, which gives scope for achieving a good match with only a single tuneable component, rather than requiring a pair in order to move in two directions over the Smith chart.

5.6.3 Further Tuning

Considering the coordinates for the optimum S_{11} coordinates for the amplifier, it is possible to use movements around the Smith chart to calculate the additional reactive components required to tune the DTC over this range.

After normalisation from 50Ω , the S_{11} values provided by a series DTC alone range from $0.10-0.35j$ to $0.54-0.07j$, and if we consider the set of desired values as an L shape, with the distinct values $0.64-1.41i$, $0.55-1.00i$ and $0.78-0.68i$ it is possible to calculate the required movements to transform one set of impedances into the other. Using an Immitance Smith chart, the required motion around the circles of constant resistance and conductance gives the required movement of $-0.8j\Omega$ around the circle of constant resistance, corresponding to additional series capacitance, followed by a movement of $+0.3jS$ around the circle of constant conductance, corresponding to a shunt inductance. The real value of components required can be calculated as follows:

$$C = \frac{1}{2\pi f X N} = \frac{1}{2\pi \times 836.5 \times 10^6 \times -0.8j \times 50} \quad (5.4)$$

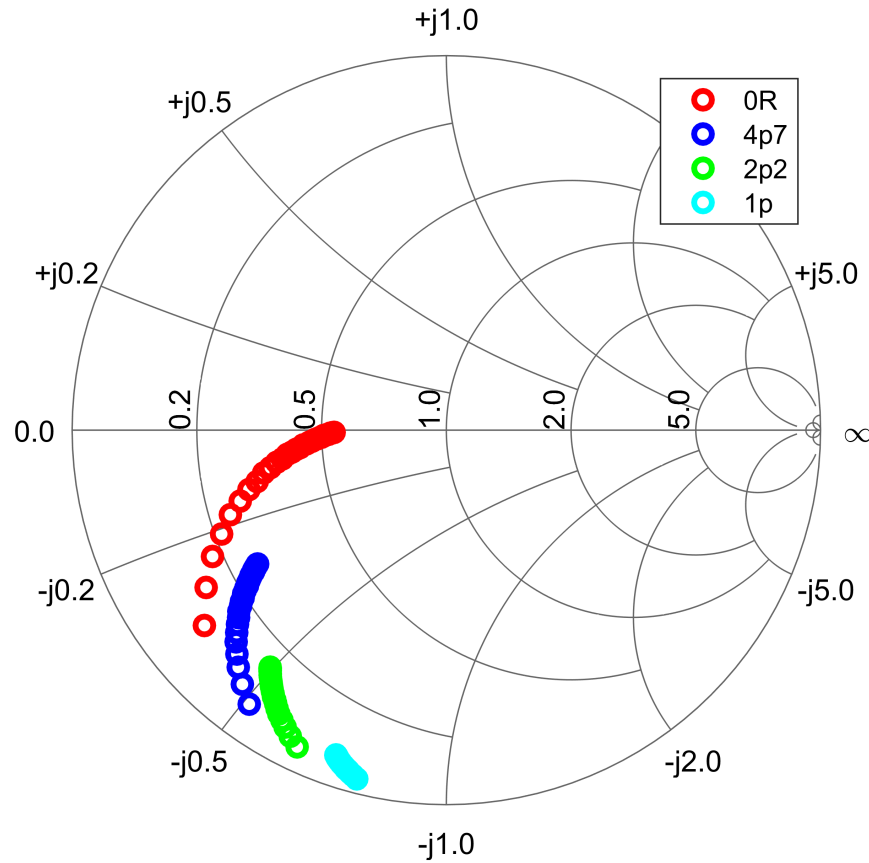
$$L = \frac{N}{2\pi f B} = \frac{50}{2\pi \times 836.5 \times 10^6 \times 0.3j} \quad (5.5)$$

Where Reactance (X), Suceptance (B), and Normalisation factor (N) Take their standard definitions and directions of movement around the chart.

Once these values have been rounded to the nearest available values, moving from the DTC to port 1, a series capacitance of 4.7pF is required, followed by a shunt inductance of 32nH. To ensure that the correct trajectories were being achieved, the series capacitance alone was added before measurement on the VNA.

It can be seen from the results in Figure 5.21 that unfortunately the required results were not observed. To begin with, the additional series capacitance was specified as 4.7pF, as a C0G capacitor in an 0603 package. After measurement across the set of possible DTC tuning values, it was apparent that the S_{11} values were not in the required area. In order to tune this, the fixed series value was decreased, in order to pull the points further anti-clockwise around the chart. The figure illustrates that the range of DTC values are not being pulled around the circle of constant resistance, as would be expected, but in fact with a decrease in series capacitance, the points are being pulled closer together whilst being pushed to the perimeter of the chart, reducing effective tuning range.

Movement towards the perimeter of the chart can be considered slightly confusing, as it implies that while the value of the series capacitance is reduced, the resistive component of S_{11} is also reduced. A possible explanation for this would be because the definition of

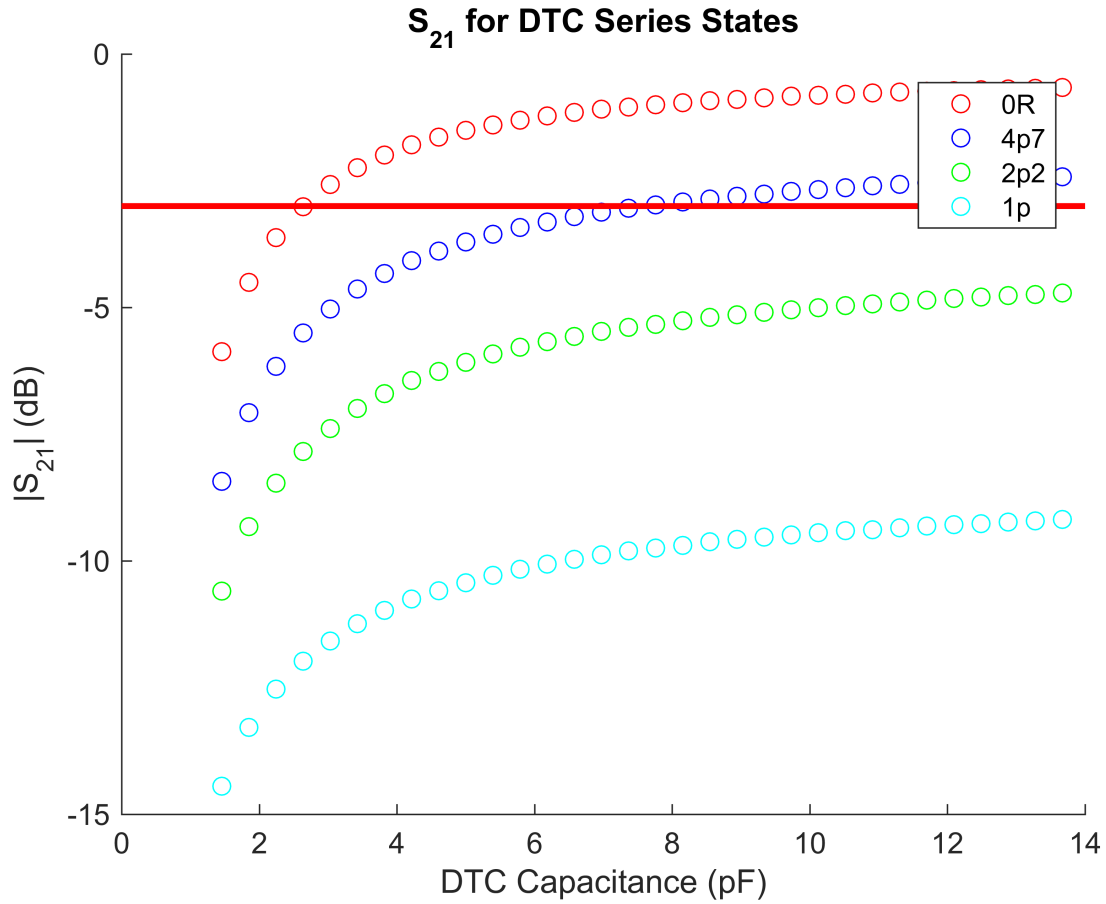

 Figure 5.21: DTI S_{11} with additional series capacitance.

S_{11} is the input reflection coefficient, the ratio between the reflected wave form and the incident waveform. As the points move to the perimeter of the chart, the match effectively becomes poorer, reducing the relative attenuation between the reflected and incident wave. To further analyse why this system will not be viable in its current state, the values of S_{21} are shown in Figure 5.22

It can clearly be seen that even the initial larger capacitance values begin to push half of the DTC tuning states below the -3dB threshold for an efficient system, by the time the value has fallen to 1pF, the insertion loss is completely untenable as a working efficiency enhancement.

5.6.4 Discussion

One area that has not been addressed in this analysis is de-embedding of the PCB mounted SMA connectors, so that the data reflects only that of the tunable components. The calibration of the VNA is effectively done to the ends of the cables used, the effects of not

Figure 5.22: DTI S_{21} with additional series capacitance.

de-embedding the PCB mounted connectors will be twofold. The connectors, in adding effective length to the system will introduce a phase shift, additionally there will be a loss associated with these components. Future work should either use time domain reflectometry, or a reference PCB with a 50ω straight microstrip line to generate measurements that will allow a full calibration to be applied to data.

Given that this analysis was conducted at 850MHz, with a free space wavelength of 35.3cm, it may be suggested that the effect on the phase of the SMA connectors should be fairly minimal. The connectors themselves were rated for use up to 18GHz, which would suggest that operation at less than a 20th of this frequency should not experience any significant losses. Whilst it is unlikely that the connectors would introduce enough loss to suddenly make the DTC devices a tenable solution, it is always important to ensure measurements are as accurate as possible in reflecting the true nature of the device under test, should they be required in the future.

To gain a true idea of the efficacy of a DTC load modulated system, the tunable com-

ponents must be integrated into at least the output matching network. This should achieve two goals; the insertion loss should be lower, due to the fact that we are no longer trying to pull an exiting matching network towards a more efficient state at lower power levels, and additionally the matching network should be more agile, as the entire network can be designed around tuning ability. Trying to pull tunable components that have existing large losses inherent in the device operation results in an overall inefficient system.

5.7 Conclusion

It can be seen from the initial work on load pulling that a definitive benefit can be obtained in terms of amplifier power added efficiency using both pure load pulling and load pull with a dynamic power supply. Initial phase results show that most of the benefit of these techniques is to be found within the middle of the range of likely output powers, this is due to the fact that most amplifier RFICs are designed to give peak efficiency at maximum output power. The caveat here is that with LTE being a system that uses an adaptive transmit power, there is little likelihood of permanently operating at maximum output power, unless in the case of a static unit right on the edge of coverage, and certainly not within urban environments where cell diameters are continually shrinking.

The techniques demonstrated required no more sampling of the LTE signal than would normally be available at the MAC layer of the RFIC, leading to a reduced component cost. Since the average RF channel power is updated at a maximum sub kHz rate, simpler power supply and output tuning may be employed with ease in order to realise these benefits. It is believed that these techniques may also be employed in future communications systems using similar power control methods.

Regarding more realistic implementations of a load pull hardware setup, there are two main points to take away from this; Firstly that it is important to design tuneable reactive components into the amplifier matching network. Using an integrated RFIC or MMIC with a digitally tuneable capacitor system will not produce the efficiency enhancements required to make the system worthwhile. Secondly, further analysis should be performed on different types of tuneable components. Whilst varactor based systems should be discounted due to the requirement for high control voltages, there are other such possibilities such as MEMS packages that might be able to offer lower losses.

Finally, there are other fringe benefits associated with load pull systems. There is a high likelihood that placing tuneable components within the PA matching network will enhance the frequency agility of the device. At a time where modern LTE modems use multiple amplifier packages in order to cover the large amount of available bands worldwide, this can

only lead to benefits, especially in terms of cost.

Chapter 6

Further Power Amplifier Design Techniques

DURING the course of this work, I have become involved in several other methods of increasing the efficiency of radio frequency (RF) power amplifier in collaboration with colleagues. The exploits that have yielded publications are detailed in the following chapter, together with a description of my contributions. The topics covered are sweet spot biasing, multi-band power amplifier (PA) operation and asymmetrical outphasing.

6.1 Introduction

Whilst the main theme of this thesis has been around exploiting knowledge of signal envelope characteristics to enhance power amplifier efficiency, there are of course many other methods that have been used to achieve this aim. The first method involves analysing the bias point of the amplifier and optimising this together with harmonic terminations in order to maximise efficiency whilst minimising harmonic distortion. A power added efficiency (PAE) of 44% was demonstrated in a two tone test at a level of -30dBc third order intermodulation product (IMD3), representing very reasonable performance for a simple, low component count design. Modern communications devices are often required to operate over a wide range of frequencies, generally requiring multiple transmission amplification paths in order to operate efficiently. The second body of work in this chapter concerns the design of a power amplifier designed to operate efficiently in multiple frequency bands without using multiple semiconductor devices; Peak power added efficiencies of between 58% and 70% were demonstrated over 3 distinct and well separated bands. More exotic PA topologies can also be used, albeit generally in base stations due to the increased physical size. Asymmetrical outphasing is one such technique where two power amplifiers effectively load modulate each other to achieve optimum efficiency over a range of signal envelope excursions. The final additional piece of work describes the use of this technique to realise a 15% increase in drain efficiency over a normal class B amplifier.

6.2 Publications

6.2.1 Hitting The Sweet Spot

One of the first additional pieces of work came from a decision to enter the power amplifier design competition at the 2016 International Microwave Symposium in San Francisco, USA. We were fortunate enough to win the competition, with part of the prize being the opportunity to write up the design and testing process in IEEE Microwave magazine, the article in [3].

The criteria for the competition was to design an amplifier between 1 and 10 GHz that produces a CW output power of at least 36dBm with an input power of less than 24dBm. The competition also requires that the amplifier should produce a saturated output in a two-tone test with less than 22dBm per tone, with the overall figure of merit for the amplifier given by an operating frequency weighted PAE measured when IMD3 reaches -30dBc.

The principle for our entry was to exploit so-called class AB 'sweet spots' in a design incorporating a third harmonic termination. This basically means that the biasing conditions

of the amplifier are optimised to improve the linearity of the amplifier. In addition to this, the input and output adjusting networks are adjusted such that the presence of the third harmonic component is minimised, which according to theory and simulations, corresponds to maximum PAE due to minimising the overlap between the drain-source voltage and drain current waveforms, effectively reducing real power consumption.

My main efforts in this project were the manufacture, optimisation and testing of a prototype and the competition entry. Construction involved producing the PCBs from gerber files on the Rogers substrate using a laser milling technique. A piece of aluminium was then milled to size using conventional equipment, together with slot being cut to bring the transistor down to an appropriate level on the board. This proved to be somewhat of an issue, as simply surface mounting the transistor to a PCB would likely not have offered sufficient heat sinking performance. The transistor was soldered to a small strip of copper, which was then mechanically attached to the aluminium heat sink / backplane at a depth sufficient to solder the drain and gate tabs to the appropriate matching network PCBs. The aluminium heatsink was drilled and tapped for screws to attach the PCBs, the input DC power connectors and the flanged SMA connectors for signal input and output.

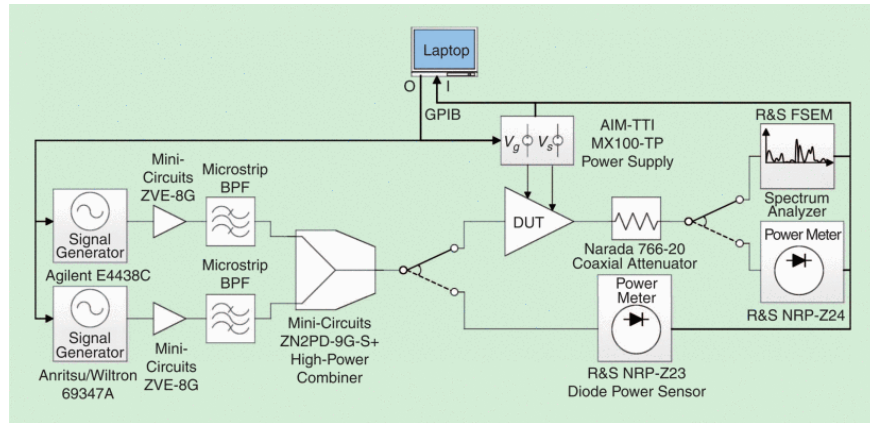


Figure 6.1: Optimisation block diagram.

The main body of work was involved with automated optimisation of the amplifier operating point. This proved to be quite challenging due to the limitations in available equipment to work at this frequency and power level. The block diagram of the equipment used is shown in the publication and reproduced in Figure 6.1, and consists of two signal generators, one for each tone, each with a reference power amplifier to provide the requisite 22dBm per tone. As this was close to the maximum power output of the reference amplifiers, two microstrip bandpass filters were designed and EM optimised in AWR microwave office before being fabricated and used to eliminate any harmonic distortion from the input stages. The signals were then combined, before the generators were calibrated between displayed power, and

power apparent at the input of device under test (DUT).

The direct current (DC) power into the DUT was measured from the calibrated DC source, whilst output power was measured using a spectrum analyser, so that power could be measured at the tones of interest, and also at the levels of the intermodulation distortion components. The spectrum analyser was calibrated against a reference power sensor. This entire system was controlled using a Matlab script, which would perform an input power sweep at a range of gate bias voltages. An excerpt of the plot, as published in [3] is shown in Figure 6.2. It can be seen that the gate bias voltage of -2.85V yields the optimally minimal value of IMD3, which will enable the maximisation of the competition figure of merit of PAE and -30dBc IMD3. It is worth noting that with a field effect transistor (FET) device such as this with no internal protection circuits, the control software must ensure the gate bias voltage is applied prior to the drain source voltage, to avoid a potentially damaging DC current flowing through the device.

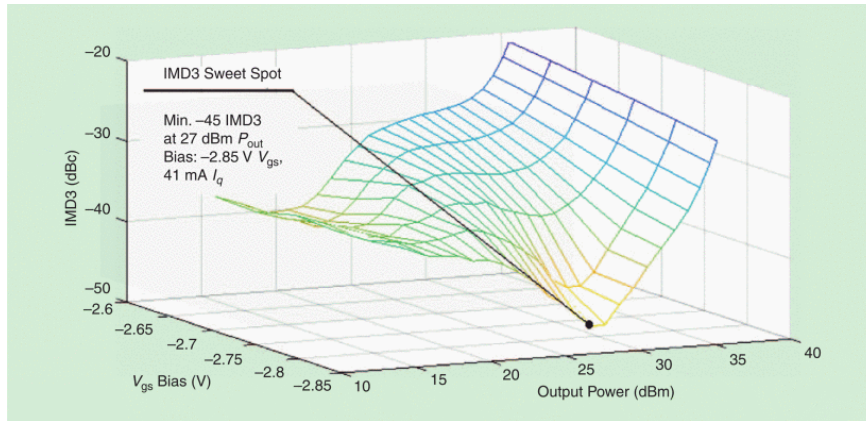


Figure 6.2: Optimisation results.

Relevant points from this exercise are that a simple amplifier topology can often yield good performance statistics with a sensible design. The previous four years winners had all used a complex Doherty topology with multiple technology, whereas our design uses a single device, which is cheaper, due to the reduction in active components, and reduction in supply voltages. Uses of harmonic terminations can simply and cheaply increase amplifier performance in the context of unwanted spectral emissions, whilst taking the time to truly optimise operating points can maximise these advantages.

6.2.2 Triple Band Power Amplifier

With the massive increase in the amount of operational bands, particularly for 4th generation mobile communications (4G) systems, there is always an incentive to design and build multi-band operation into a power amplifier. Conventional techniques generally use multiple

amplifiers and matching / filtering components, which are switched into the transmission path as appropriate. Not only does this take up a large amount of PCB real estate, it is not particularly efficient either.

The work presented in [4] surrounds the design of a power amplifier for operation in three bands - 0.8, 1.8, and 2.4GHz. Class B operation is used, and an output matching network using two L-section is proposed, which required optimisation of the impedance and length of each of the four sections of microstrip in the matching network. This gives 8 degrees of freedom for optimisation in the model. Mathematical optimisation procedures are used to maximise performance at the three frequencies of interest.

My contribution to this project was again to design and automate the testing procedure for the evaluation of the completed design. In a similar fashion to previous efforts, Matlab scripts are used to interface with signal generation and power measurement hardware. This particular case was fairly simple, requiring some basic calibration, followed by frequency sweeps at a constant level of drive power, measuring PAE, gain and output power. These measurements were taken over a frequency sweep of width 2GHz, in each of the three bands of interest. Strong results were obtained, offering a good agreement with simulations, and desirable overall performance of 70%, 60% and 58% peak PAE in each of the three respective bands, with an average gain of 11.5dB.

This work shows that it is possible to limit the amount of active devices present in a transceiver with a large amount of bands to cover, whilst still offering good performance characteristics. Whilst this work covers power levels more applicable to evolved node B (eNB) operation, the fundamental principles can be applied to any power levels. Additionally at the higher frequency bands proposed in future 5th generation mobile communications (5G) systems, the use of microstrip matching within devices is likely to become much more ubiquitous due to the reduction in geometries required.

6.2.3 Asymmetrical Outphasing

Outphasing is another concept within PA design that attempts to provide high efficiency, though this method maintains high linearity too. The idea here is that in the presence of an input signal with a variable amplitude envelope, a power amplifier may provide gain efficiently but with low linearity, or linearly at the expense of efficiency. Outphasing addresses this problem by splitting the variable envelope signal into two constant envelope streams which can be amplified efficiently and linearly before being combined back into the original signal, obviously at a higher power, this is well described in [71].

The asymmetrical outphasing presented in [5] uses two different PA branches, rather than the identical branches in conventional outphasing systems. This concept here is that, simi-

larly to the load pull material that forms the bulk of this chapter, each of the power amplifier in the pair applies the required optimum conjugate load to its opposite number.

As this is a complex system to produce, the practical verification of the concept was achieved using a single branch of the amplifier system, with the load pull effects of the second amplifier being applied using a mechanical tuner. My contribution in this work was to automate the test bed that applied a variable impedance load through a power combiner, whilst sweeping output power to assess the efficacy of the design. As usual, Matlab scripts were used to calibrate power measurement devices, before sweeping input power and load trajectory to obtain maximum drain efficiency. It was found that using Class J biasing with this scheme obtained a 15% improvement in drain efficiency over the normal Class B case.

Whilst these principles are most likely too complex to end up in low cost user equipment very soon, with advances in transistor technology and miniaturisation, there is every chance this will happen in the future. Again, although the output power levels in this work are larger than general user equipment (UE) use, the principles should scale linearly with power level, providing the same advantages.

6.3 Conclusions

It has been shown that a variety of different techniques can be deployed to enhance power amplifier efficiency, each with their own merits and drawbacks. Following on from the theme of this thesis, the most relevant are those that maintain a simple and physically small profile so that they may be deployed in a small and low cost unit, enhancing the potential uptake in industry. The capacity for using well thought out biasing methods and harmonic terminations in order to increase efficiency or reduce multi-amplifier designs cannot be overstated.

Chapter 7

Conclusions & Further Work

7.1 Conclusions

The over arching theme of this thesis has been the use of Long Term Evolution (LTE) communications systems to enable machine-to-machine (M2M) data exchanges, and how best to achieve a high degree of efficiency whilst doing this. The often mentioned figure of merit is being able to achieve 10 years battery life; whilst this obviously does not address constraining factors such as battery size, or any of the requirements of a system such as transmission size, frequency or latency, it is not hard to see that achieving this with any kind of wireless system is an extreme challenge, due to the high demands in communicating with a base station that may be anywhere up to 35km away.

In order to achieve these requirements, sensible operation is required from at least four separate stakeholders; standards bodies, network operators, base station equipment vendors, and user equipment (UE) manufacturers. Only the combination of sensible standards, a well organised and distributed network and efficient user equipment will together achieve the required aims. The following chapter summarises the implications of the good, the bad and the unhelpful engineering discovered and developed over the course of the work in this thesis.

7.1.1 Summary of Research Contributions

Chapter 3 considers the degrees of freedom present in an uplink LTE signal with regard to factors relevant to the biasing of the most energy hungry subsystem of the modem; the power amplifier. It was demonstrated that in addition to the obvious factors, such as depth of modulation scheme, the bandwidth also has an effect on signal metrics such as peak-average power ratio (PAPR), as demonstrates in Table 3.2, meaning that if not the absolute value,

but at least the distribution of PAPR can be predicted using only knowledge of constraints in the medium access control (MAC) layer. Additionally, it is possible to leverage features in a particular modulation scheme such as regularly occurring demodulation reference signals, that possess a lower peak signal excursion that may be leveraged for optimisation, illustrated in Figure 3.20. Illustrating differences in average PAPR, between modulation schemes, of up to 2dB means that a power amplifier could effectively reduce its backoff by the same amount, resulting in a dramatic drop in required supply voltage and the associated power requirement for a transmission. The work in Section 3.4 helps to describe how PAPR is not actually the most appropriate way to describe signals in terms of methods of amplification; Comparisons between hardware measurement and software simulation show differences mainly due to the PAPR metric being heavily susceptible to infrequent outlying data points.

It has been shown in Chapter 4 that much effort has been put in to the optimisation of mobile communications with regard to efficiency, however this is rarely with regard to how the energy is actually being used in a realistic system. Figure 4.16 shows how the total time taken for transmitting very small packets of data can deviate significantly from that suggested by both analysis of protocols and lab simulation. This can be at least partly attributed to the increasing use of dynamically organised networks, that utilise users to sense network topology. A comparison of laboratory and network measurements shows that for a large user datagram protocol (UDP) packet, laboratory results have a power consumption of 0.2J for the transmission, though this is closer to 4.6J for the network measurement. This represents a significant variation, which would dramatically alter the power budget and potential lifetime for a system if not taken into account.

Delving further into the modem itself, it can be seen from Figures 4.11 and 4.10 that whilst the power amplifier dominates power consumption in the transmit phase, as expected, both data rate and received signal power level have a significant effect on receive power consumption. It is always important to keep in mind there are other communications systems available, which maybe considered alongside LTE with appropriate latency requirements being considered, as demonstrated in Figure 4.27.

In Chapter 5, work was completed to show how dynamic efficiency enhancement schemes can be implemented using only information in the MAC layer, as postulated in Chapter 3. Figure 5.11 shows that both dynamic power supply and dynamic load modulation schemes can be controlled by this information only, and achieve significant benefits. The peak increase of 44% in power added efficiency (PAE) means that the most energy hungry part of the system, the power amplifier, is operating up to 44% more efficiently, thus saving power with every transmission, and offering the system designer the opportunity of using smaller, cheaper batteries. Similarly with the dynamic power supply (DPS) and load pull

techniques, a 27% increase in PAE is demonstrated over the DPS alone setup, which overall results in significant energy savings. Further more, the improvements in efficiency are in a wide band in the middle of the likely range of power amplifier (PA) output power, raising PAE from negligibly small figures, to between 10 and 40% depending on the configuration and power level. This means that significant energy savings can be easily obtained in real world systems.

Further on in the chapter, load modulation using realistically miniaturisable components is considered. Figure 5.20 shows that whilst a moderate coverage of the Smith chart is required for optimum efficiency across the range of possible UE output powers, good improvements can be seen without having to present the perfect reflection coefficient, and in fact, a relatively coarse load modulation would probably still deliver significant enhancements. Figure 5.22 shows that whilst complementary metal oxide semiconductor (CMOS) switched reactive components can give good Smith chart coverage, the associated parasitics generally mean that insertion losses negate any efficiency enhancements.

Chapter 6 covers additional methods for enhancing the efficiency of the radio frequency (RF) power amplifier. It has been demonstrated that very respectable increases in this performance metric can be achieved using simple methods such as sweet spot analysis to optimise bias point, and hybrid matching networks to achieve multi band operation with only a single active device. More exotic methods such as asymmetrical outphasing are shown to achieve strong results, albeit using multiple devices, more appropriate for physically larger and more power hungry equipment.

7.1.2 Relevance to 5G / NB-IoT

Whilst this body of work has concentrated on mainstream deployments of 4th generation mobile communications (4G), two key technologies for the future are narrow band internet of things (NB-IoT) and of course 5th generation mobile communications (5G). At the time of writing, no specifications for 5G have been set in stone, though a wider range of frequency bands has been suggested, together with targets for lower latency, higher speeds, capacities and efficiency. NB-IoT has been standardised, and includes higher latency, lower data rates and a narrow bandwidth, all aimed at increasing efficiency. Whilst these standards have been written, there is currently only one available UK NB-IoT deployment available, owned by Vodafone and Huawei, and with UE modems hard to obtain, this prohibits experimentation.

Regarding the main contributions of this work; using MAC layer information to control efficiency enhancement schemes for the power amplifier, it is absolutely possible that these will be applicable to both 5G and NB-IoT. 5G would likely be the main benefactor, as the increased data rates will likely involve highly PAPR variable signals, able to benefit

from these power amplifier techniques. NB-IoT is in theory, a specification already tailored towards efficiency, so the benefits of adaptive load pull techniques may be smaller. However as long as the communications system has an adaptive link budget, where transmit power may vary, then the power amplifier will still find advantage in being provided with a range of supply voltages and load impedances.

7.2 Recommendations to Communications Stakeholders

There are a number of stakeholders with a potential interest in some of the topics covered in this thesis. The following section consists of recommendations for the main interested parties aimed at increasing the efficiency of the cellular communications system.

7.2.1 Standards Bodies

The first recommendation made is not to manufacturers of cellular communications equipment, but to the organisations responsible for creating the rules and regulations that govern the communications standards. Whilst some of this is superseded by the NB-IoT standards, there still exists missed opportunities to have further optimise items such as the modulation schemes involved. Figure 3.21 shows how it would have been possible to remove higher order modulation schemes from low rate systems, which particularly in low cost equipment would have provided ample opportunities for a more efficient power amplifier biasing point.

7.2.2 Base Station Vendors / Networks

Regarding manufacturers of cellular base stations, observations have shown that there are also significant enhancements that can be made here. Whilst trying to understand exactly the processes occurring at these base stations is incredibly hard, as the algorithms that govern operation are proprietary, some of the work in Chapter 4 has shown that some quite unexpected and inefficient effects can result under error conditions. This seemed to be due to the use of the self organising networks principle. To recap, this is where base stations gain knowledge of their neighbour base stations on the same network by polling user equipment in order to ask what other stations they are receiving signals from. The principle for this is quite sensible, as it allows adaptive handover maps to be dynamically modified with any addition of cell towers, whether due to planned infrastructure development or the positioning of temporary towers, e.g. for a festival. The problem with this process is that nothing comes for free, and the transmissions from the UE obviously require an energy expenditure, reducing

the efficiency of the whole transmission process. In extreme circumstances, as has been demonstrated, this self organising networks principle can significantly extend transmission duration, which causes models developed with laboratory equipment to be no longer relevant, and system efficiency to drop catastrophically.

7.2.3 UE Manufacturers

Regarding UE manufacturers, there are similarly important recommendations to make. This advice comes mainly from the work in Chapter 5 on PA optimisation. The focus here is generally on the power amplifier and supporting systems as this is the most energy hungry part of the system for the transmit process.

When making comments on the optimisation of power amplifier operation, it is important to keep in mind the final application that this technology might end up in. To this end, it has always been a consideration that proposals for new technologies can be implemented as part of a low cost, low volume / PCB real-estate solution, with the idea that it might end up in cheap, low power M2M devices deployed en masse. For this reason, high speed techniques such as envelope tracking are not covered, as they are complex and expensive to implement. What has been covered is the use of lower speed techniques for both power supply and PA load modulation. Whilst these techniques are not novel, the basis of controlling them with MAC layer information, which requires virtually no signal processing overheads to work is.

The core premise behind these techniques is that the average power amplifier is likely to be optimally matched at peak power output, and less optimally matched when operating at a lower output power level, due to proximity to a base station. This can be optimised dynamically using switched capacitor systems, with optimum operating points based on knowledge of amplifier characteristics and knowledge of the signal input into the amplifier. As far as use cases are concerned, the basis for this technique is applicable to all forms of wireless communication that use adaptive modulation schemes and bandwidths, however peak efficiency was shown to be most evident in cases where the power output of the device is less than the peak output power

7.3 Future Work

Whilst this piece of work has attempted to address as many of the factors pertinent to efficiency in M2M systems as possible, there are of course areas which merit further work, the most relevant being related to network measurements and adaptive load pull systems.

7.3.1 Network Measurements

One of the really important measurements for future work with networks is to begin to develop a knowledge of the distribution of output power for the range of environments that M2M communications are likely to occur, for example a coarse generalisation of urban, suburban and rural. The reason for the importance of this is due to the relationship between distance to cellular base station, path loss exponent (related to the environment) and power consumed by the device. In addition to this, the different types of environment will likely have slightly different densities of base stations, relating this to population density and perceived demand for cellular capacity.

This data could be incredibly useful in modelling activities, both to assess power consumption likely for a device in a particular environment, and also to form an idea of the potential benefit of any efficiency enhancement technologies. An example of this is given in Chapter 5, where the improvements in efficiency are fairly minimal at amplifier peak power output, however these techniques can offer significant benefits if used in the middle of the amplifiers output power range. By applying the knowledge of likely distribution of output power for a particular environment, these techniques can be quantitatively analysed for benefit.

7.3.2 Load Pull

The future research directions taken from Chapter 5 on adaptive load pull systems are quite easy to see. To begin with, a discrete power amplifier design is required. At this stage the choice of device / technology is fairly insignificant, as long as it is capable of producing the required output power levels representative of a piece of UE equipment. The reason a discrete design is required, is that the work in Chapter 5 was based on an amplifier-on-chip device that incorporated matching components into the package. With each additional reactive component added in between the amplifier output and the antenna connector, there will be an associated loss. The work on load pull added additional reactive components in order to change the impedance presented to the amplifier. If the additional components were built in to the transistor output matching network from the start, a much more efficient design could be achieved.

Further work is absolutely required to further identify and characterise tunable reactive components. As demonstrated, the CMOS switched solution had a high insertion loss due to parasitic elements. Some micro-electro-mechanical systems (MEMS) switched devices are making their way to the market, and should in theory be much more suitable for a low loss tunable solution. It may even be worth revisiting a varactor diode solution, to gauge

whether any recent work has brought the generation of the required high control voltages in to an efficient and small package.

A final subject worth considering would be the additional benefits unlocked when using a dynamic load pull system, namely the possibility of increasing the frequency agility of the system. Traditional cellular communications modems use multiple power amplifiers in order to efficiently cover the multitude of different bands required for communication. This is typically due to the requirement for each amplifier to be optimally matched at a particular frequency, with wideband matching always being a trade-off. With the ability to dynamically vary output matching, it is possible that one tunable device could replace multiple fixed frequency devices, achieving not only a cost saving, due to the lack of required semiconductors, but also a substantially larger increase efficiency, as using multiple power amplifiers requires many switches and filters to route signals properly, each with their respective insertion losses. The benefit of potentially removing such a quality of additional loss cannot be overstated.

7.4 Final Comments

Whilst producing generalised solutions for M2M communications is certainly very challenging, the most important piece of advice is to not take anything for granted when producing a functional system. It is always critically important to measure power consumption at high temporal resolution and pay attention to exactly what is happening when wireless transmission and reception is taking place, and particularly with reference to the environment in which a device is deployed; Distance from base station, competition for resources, and network specific activity will all have an effect. When writing embedded code to control cellular modems, it is beneficial to bear in mind requirements such as transmission frequency and latency. If neither of these requirements is particularly stringent, then simply ensuring all wireless devices are turned completely off rather than taking advantage of a convenient sleep mode can give great benefits in terms of increasing battery life. The recent explosion in cellular operating bands has provided many challenges for UE manufacturers, and it is all too easy to address these by paralleling up frequency selective transceiver (TRX) chains, whereas in fact there is significant benefit to exploring new work on frequency agile devices.

Appendix A

Labview Data Acquisition

In order to interface with the National Instruments hardware described in Chapter 4, appropriate software was required to acquire a stream of high speed data and trigger recording for the required duration; this is shown in Figure A.1.

The flow of data here is from left to right via the appropriate blocks. The 'Sample Clock' generates the timing pulse required for data acquisition based on knowledge of the task required, buffer size, sample rate and continuous or one-shot data acquisition. This task is then passed to the 'Start Task' block, which initialises the data capture process before is it passed into the while loop indicated by the grey outline. The first block within the while loop is 'Analog 1D Wfm, NChan NSamp' which controls the acquisition of data from appropriately sized buffer packets. In this example there are four possible inputs from the analogue to digital converter (ADC) in addition to a time series reference, these are illustrated in Table A.1. All quantities are recorded in volts, although obviously calibration factors are applied in post processing to obtain Amps and dBm for channels 1 and 2 respectively.

Once the data has been set streaming within the while loop, it is first passed on to a waveform chart, to be displayed on screen, before having one of the components separated off for triggering acquisition. As we only want to record waveforms produced from the transition of the device under test (DUT) from sleep mode into an active transition, channel 2 - current consumption is extracted from the data flow and the magnitude data is compared with a threshold value. Once this has been exceeded, the 'Write to Measurement File' case structure is activated to log the ADC values. Additional triggering is used to make sure

Channel	0	1	2	3
Signal	Supply Voltage	Current	RF Power	Unused

Table A.1: ADC Input Signals

that data for an entire process is logged even if it dips back below the threshold value at an intermediate stage. This is accomplished by introducing a 'monostable' like timing routine, which stops data acquisition only if the current waveform dips below the threshold for more than a specified duration. Any additional data points recorded after the final drop below the threshold value are removed in post processing. Additional controls at the top of the diagram are used to ensure the resulting measurement file is appropriately titled with time & date and stored in the correct location.

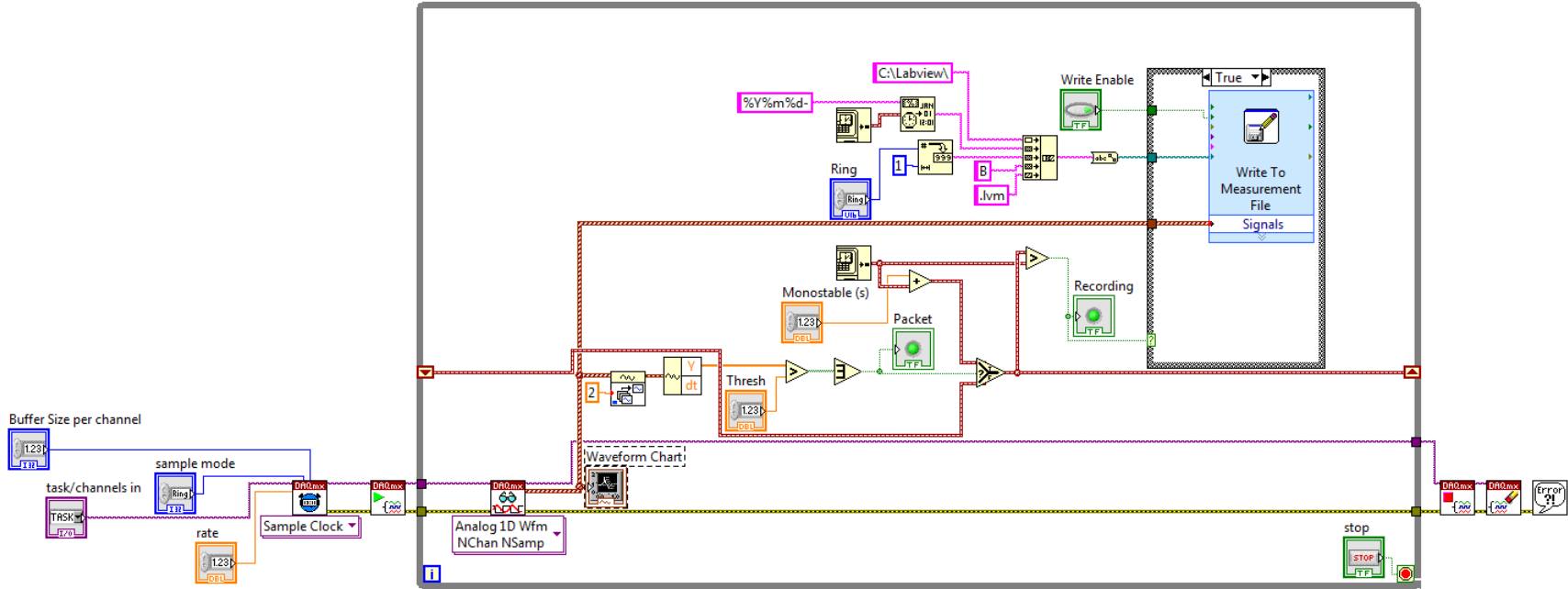


Figure A.1: LabVIEW Data acquisition flow

Appendix B

Python Code for Network Measurements

As a large part of this project has comprised of work with the Raspberry Pi computer, the relevant code was developed in Python. The relevant code may be obtained on Github using the following URL:

<https://github.com/JBirchall186/Python>

B.1 GUI

The code for the graphical user interface (GUI) forms the basis of the work in Chapter 4, and generates appropriately sized packets of UDP data that may be transmitted on the cellular network.

Prerequisites:

- Python running in an appropriate environment
- Tkinter GUI library installed
- uBlox Toby modem connected via USB

Once the above software has been obtained, the python scripts may simply be run, and should interface with the modem to generate data in the packet size required.

B.2 MQTT

Some initial work involved the evaluation of a popular protocol, MQTT to send M2M style data via the uBlox Toby modem. The following software sends data to a pre-configured

server.

Prerequisites:

- Python running in an appropriate environment
- Device running Mosquitto as an MQTT server
- uBlox Toby modem connected via USB

As long as the hardware is connected correctly, the server IP address should be configured as required, and data packets may be generated, with the modem being woken and put to sleep as needed.

Appendix C

Matlab Code

The three core technical chapters all contain functions involving code written in Matlab. The code may be found at the following URL:

<https://github.com/JBirchall186/Matlab>

The next three sections detail hardware / software required and basic instructions for use. More detailed information is available in code comments.

C.1 Signal Power Simulations

This is the code required for the work in Chapter 3 LTE signal analysis.

Prerequisites:

- Matlab
- Matlab LTE Toolbox

Provided the above software is available, the code may be simply run and the outputs used as required. Range of modulation schemes / resource block allocations may be modified as the user desires.

C.2 Network Deployment Power Consumption

This is the code required for the work in Chapter 4 on power consumption measurements.

Prerequisites:

- Matlab
- Data gathered from measurements in lvm files.

The code may simply be run in Matlab to process data of the appropriate format into plots. Further and more relevant information will be given in comments.

C.3 Load Modulation Experiments

This is the code required for the work in Chapter 5 on load modulation.

Prerequisites:






















- Matlab
- Keysight hardware interface drivers
- R&S Interface Drivers
- USB to GPIB conversion hardware
- Hardware as described in Chapter 5
- USB - SPI interface drivers if DTC functionality required

Hardware should be connected as indicated in the chapter, and any relevant calibration values updated as appropriate. Measurements for determining optimum reflection coefficient may take a long time to run, and data should be saved on each iteration to prevent loss in the case of a crash.





















Appendix D

Project Plan

A broad summary of the tasks and durations of the various sub-projects involved in this research is provided on the following pages.

		Name	Duration	Start	Finish	Predecessors	Resource Names
1		Literature review	69 days	11/09/14 08:00	16/12/14 17:00		James Birchall
2		Phase I Power Measurement	70 days	28/02/17 08:00	05/06/17 17:00	1	
20		Design power measurement hardware	20 days	09/05/17 08:00	05/06/17 17:00	1	James Birchall
4		Learn to operate BSE	30 days	28/03/17 08:00	08/05/17 17:00	3	James Birchall
5		Initial connectivity measurements	10 days	14/03/17 08:00	27/03/17 17:00	3;4	James Birchall
6		Analysis of measurements	10 days	28/02/17 08:00	13/03/17 17:00	5	James Birchall
7		LTE Toolbox Work	220 days	26/04/16 08:00	27/02/17 17:00	2;6	
8		Learn LTE toolbox	60 days	06/12/16 08:00	27/02/17 17:00	6	James Birchall
9		Simulate LTE Waveforms	60 days	13/09/16 08:00	05/12/16 17:00	8	James Birchall
10		Process Data	30 days	02/08/16 08:00	12/09/16 17:00	9	James Birchall
11		Capture real data from BSE	25 days	28/06/16 08:00	01/08/16 17:00	10	James Birchall
12		Analysis & writeup	45 days	26/04/16 08:00	27/06/16 17:00	11	James Birchall
13		IMS PA Design Competition	92 days	18/12/15 08:00	25/04/16 17:00	7;12	
14		Design	30 days	18/12/15 08:00	28/01/16 17:00	12	James Birchall
15		Build	4 days	29/01/16 08:00	03/02/16 17:00	14	James Birchall
16		Analysis	20 days	04/02/16 08:00	02/03/16 17:00	15	James Birchall
17		Write article	10 days	12/04/16 08:00	25/04/16 17:00	16	James Birchall
18		Supporting PA Joint Work	60 days	26/04/16 08:00	18/07/16 17:00	13;17	
19		Enhance testbed	30 days	26/04/16 08:00	06/06/16 17:00	16	James Birchall
20		Testing for multi-band PA	15 days	07/06/16 08:00	27/06/16 17:00	19	James Birchall

PhD - page1

		Name	Duration	Start	Finish	Predecessors	Resource Names
21		Testing for load pull PA	15 days	28/06/16 08:00	18/07/16 17:00	20	James Birchall
22		Phase I Load Pull	94 days	19/07/16 08:00	25/11/16 17:00	18;21	
23		Design testbed	20 days	19/07/16 08:00	15/08/16 17:00	21	James Birchall
24		Calibrate	4 days	16/08/16 08:00	19/08/16 17:00	23	James Birchall
25		Measurements	30 days	22/08/16 08:00	30/09/16 17:00	24	James Birchall
26		Analysis & write paper	40 days	03/10/16 08:00	25/11/16 17:00	25	James Birchall
27		Phase II Power Measurement	110 days	28/11/16 08:00	28/04/17 17:00	22;26	
28		Adapt hardware for live network	10 days	28/11/16 08:00	09/12/16 17:00	26	James Birchall
29		Scripts to run modem	10 days	12/12/16 08:00	23/12/16 17:00	28	James Birchall
30		Measurements	40 days	26/12/16 08:00	17/02/17 17:00	29	James Birchall
31		Analysis & write paper	40 days	20/02/17 08:00	14/04/17 17:00	30	James Birchall
32		Sigfox comparison	10 days	17/04/17 08:00	28/04/17 17:00	31	James Birchall
33		Phase II Load Pull	80 days	01/05/17 08:00	18/08/17 17:00	27;32	
34		DTC design	25 days	01/05/17 08:00	02/06/17 17:00	32	James Birchall
35		DTC test & analysis	35 days	05/06/17 08:00	21/07/17 17:00	34	James Birchall
36		Write up findings	20 days	24/07/17 08:00	18/08/17 17:00	35	James Birchall
37		Write Up Thesis	280 days	21/08/17 08:00	14/09/18 17:00	33	
38		Writing	250 days	21/08/17 08:00	03/08/18 17:00	33;36	James Birchall
39		Proof reading	30 days	06/08/18 08:00	14/09/18 17:00	38	James Birchall

Bibliography

- [1] J. Birchall, P. Enrico de Falco, K. Morris, and M. Beach, “Efficiency enhancement of M2M communications over LTE using adaptive load pull techniques,” in *2017 IEEE Radio and Wireless Symposium (RWS)*. IEEE, jan 2017, pp. 26–28. [Online]. Available: <http://ieeexplore.ieee.org/document/7885935/>
- [2] J. Birchall, K. Morris, and M. Beach, “M2M Communications over LTE - Evaluating Energy Consumption Models,” in *13th International Wireless Communications and Mobile Computing Conference (IWCMC)*. Valencia, Spain: IEEE, 2017, pp. 1–5. [Online]. Available: <http://ieeexplore.ieee.org/stamp/stamp.jsp?tp={&}arnumber=7986342{&}isnumber=7986245>
- [3] P. E. de Falco, J. Birchall, and L. Smith, “Hitting the Sweet Spot: A Single-Ended Power Amplifier Exploiting Class AB Sweet Spots and Optimized Third Harmonic Termination,” *IEEE Microwave Magazine*, vol. 18, no. 1, pp. 63–70, jan 2017. [Online]. Available: <http://ieeexplore.ieee.org/document/7779279/>
- [4] E. Arabi, P. Enrico de Falco, J. Birchall, K. A. Morris, and M. Beach, “Design of a triple-band power amplifier using a genetic algorithm and the continuous mode method,” in *2017 IEEE Topical Conference on RF/Microwave Power Amplifiers for Radio and Wireless Applications (PAWR)*. IEEE, jan 2017, pp. 48–51. [Online]. Available: <http://ieeexplore.ieee.org/document/7875570/>
- [5] P. Enrico de Falco, J. Birchall, S. Ben Smida, K. Morris, K. Mimis, and G. Watkins, “Asymmetrical outphasing: Exploiting conjugate continuous modes of operation,” in *2017 IEEE Topical Conference on RF/Microwave Power Amplifiers for Radio and Wireless Applications (PAWR)*. IEEE, jan 2017, pp. 18–21. [Online]. Available: <http://ieeexplore.ieee.org/document/7875562/>
- [6] GSMA Intelligence, “Cellular M2M forecasts and assumptions : 2010 – 2020,” no. September, 2014. [Online]. Available: <https://www.gsma.com/iot/wp-content/uploads/2016/09/GSMA-Intelligence-Cellular-M2M-forecasts-2010-2020.pdf>

-
- [7] Embedded Computing Design, “The fast-growing M2M market presents a series of wireless design challenges,” 2015. [Online]. Available: <http://www.embedded-computing.com/embedded-computing-design/the-fast-growing-m2m-market-presents-a-series-of-wireless-design-challenges>
 - [8] M. Rumney, “De-mystifying Single Carrier FDMA The New LTE Uplink,” 2010. [Online]. Available: <https://pdfs.semanticscholar.org/4a50/06d2898ad3afe163ce95dce3ef3d50506209.pdf>
 - [9] *LTE and the Evolution to 4G Wireless*. Wiley, 2013.
 - [10] M. Rumney, Ed., *LTE and the Evolution to 4G Wireless: Design and Measurement Challenges*. Agilent Technologie, 2013. [Online]. Available: <http://www.amazon.co.uk/Books-LTE-Evolution-Wireless-Measurement-Challenges/dp/1119962579/ref=sr{ }1{ }1?ie=UTF8{ }&qid=1455200342{ }&sr=8-1{ }&keywords=lte+rumney>
 - [11] “Single-carrier FDMA.” [Online]. Available: <https://en.wikipedia.org/wiki/Single-carrier{ }FDMA>
 - [12] 3GPP Group, “3gpp ts 36.101,” 2007.
 - [13] X. Fan, Y. Li, M. Li, and X. Zhang, “Analysis and comparison of different SC-FDMA schemes for 3GPP LTE,” *2007 International Conference on Wireless Communications, Networking and Mobile Computing, WiCOM 2007*, pp. 787–790, 2007.
 - [14] X. Yu, M. Wei, Y. Song, Z. Wang, and B. Chi, “A PAPR-Aware Dual-Mode Sub-GHz CMOS Power Amplifier for Short Range Wireless Communication,” *IEEE Transactions on Circuits and Systems II: Express Briefs*, vol. 7747, no. c, pp. 1–1, 2015. [Online]. Available: <http://ieeexplore.ieee.org/lpdocs/epic03/wrapper.htm?arnumber=7279106>
 - [15] B. Thomas and J. Johnson, “N ew RF M etrics for the S martphone - centered W orld,” no. January, 2011.
 - [16] H. Ochiai, “Peak-to-average power ratio distribution analysis of single-carrier FDMA signals,” *European Wireless, 2012. EW. 18th European Wireless Conference*, no. 2, pp. 1–5, 2012.
 - [17] 3GPP, “Evolved Universal Terrestrial Radio Access (E-UTRA); User Equipment (UE) conformance specification; Radio transmission and reception; Part 1: Conformance testing.” [Online]. Available: <https://www.etsi.org/deliver/etsi{ }ts/136500{ }136599/13652101/13.01.00{ }60/ts{ }13652101v130100p.pdf>

- [18] Mathworks, “Matlab LTE Toolbox,” 2018. [Online]. Available: <https://uk.mathworks.com/products/lte-system.html>
- [19] 3GPP, “3GPP - The Mobile Broadband Standard.” [Online]. Available: <http://www.3gpp.org/release-13>
- [20] ETSI, “Physical layer procedures (3GPP TS 36.213 version 13.0.0 Release 13),” *3Gpp, Ts 36.331*, vol. Sep, 2011. [Online]. Available: <http://www.etsi.org/standards-search>
- [21] A. R. Jensen, M. Lauridsen, P. Mogensen, T. B. Sørensen, and P. Jensen, “LTE UE Power Consumption Model: For System Level Energy and Performance Optimization,” in *2012 IEEE Vehicular Technology Conference (VTC Fall)*, sep 2012, pp. 1–5.
- [22] B. Dusza, C. Ide, and C. Wietfeld, “Measuring the Impact of the Mobile Radio Channel on the Energy Efficiency of LTE User Equipment,” in *2012 21st International Conference on Computer Communications and Networks (ICCCN)*, jul 2012, pp. 1–5.
- [23] A. Simonsson and A. Furuskar, “Uplink Power Control in LTE - Overview and Performance, Subtitle: Principles and Benefits of Utilizing rather than Compensating for SINR Variations,” in *2008 IEEE 68th Vehicular Technology Conference*, sep 2008, pp. 1–5.
- [24] “3GPP TS 36.213 V14.1.0,” 650 Route des Lucioles – Sophia Antipolis Valbonne – France, dec 2016.
- [25] LTE Encyclopedia, “TE Radio Link Budgeting and RF Planning.” [Online]. Available: <https://sites.google.com/site/lteencyclopedia/lte-radio-link-budgeting-and-rf-planning>
- [26] A. T. Koc, S. C. Jha, R. Vannithamby, and M. Torlak, “Device power saving and latency optimization in LTE-a networks through DRX configuration,” *IEEE Transactions on Wireless Communications*, vol. 13, no. 5, pp. 2614–2625, 2014.
- [27] B. Dusza, C. Ide, L. Cheng, and C. Wietfeld, “An Accurate Measurement-Based Power Consumption Model for LTE Uplink Transmissions,” *2013 IEEE Conference on Computer Communications Workshops (INFOCOM WKSHPS)*, pp. 5–6, apr 2013.
- [28] P. J. Chen, G. Y. Lin, and H. Y. Wei, “Experiment-Based Smartphone Traffic Modeling and Power Saving Performance Analysis for LTE DRX Mechanism,” in *2014 IEEE International Conference on Internet of Things (iThings), and IEEE Green Computing and Communications (GreenCom) and IEEE Cyber, Physical and Social Computing (CPSCoM)*, sep 2014, pp. 597–603.

- [29] S. Fowler, "Study on power saving based on radio frame in LTE wireless communication system using DRX," in *2011 IEEE GLOBECOM Workshops (GC Wkshps)*, dec 2011, pp. 1062–1066.
- [30] G. C. Madueño, J. J. Nielsen, D. M. Kim, N. K. Pratas, Č. Stefanović, and P. Popovski, "Assessment of LTE Wireless Access for Monitoring of Energy Distribution in the Smart Grid," *IEEE Journal on Selected Areas in Communications*, vol. 34, no. 3, pp. 675–688, mar 2016.
- [31] F. Ghavimi and H. H. Chen, "M2M communications in 3GPP LTE/LTE-A networks: Architectures, service requirements, challenges, and applications," *IEEE Communications Surveys and Tutorials*, vol. 17, no. 2, pp. 525–549, 2015.
- [32] A. Rico-Alvariño, M. Vajapeyam, H. Xu, X. Wang, Y. Blankenship, J. Bergman, T. Tirronen, and E. Yavuz, "An overview of 3GPP enhancements on machine to machine communications," *IEEE Communications Magazine*, vol. 54, no. 6, pp. 14–21, 2016.
- [33] R. Ratasuk, A. Prasad, Z. Li, A. Ghosh, and M. A. Uusitalo, "<Recent advancements in M2M communications in 4G networks and wvolution towards 5G.pdf>," no. c, pp. 52–57, 2015.
- [34] M. Z. Sha, L. Ji, S. Member, A. X. Liu, J. Pang, and J. Wang, "Large-Scale Measurement and Characterization of Cellular Machine-to-Machine Traf fi c," vol. 21, no. 6, pp. 1960–1973, 2013.
- [35] E. Soltanmohammadi, K. Ghavami, and M. Naraghi-Pour, "A Survey of Traffic Issues in Machine-To-Machine Communications over LTE," *IEEE Internet of Things Journal*, vol. 3, no. 6, pp. 865–884, 2016.
- [36] R. C. D. Paiva, R. D. Vieira, and M. Säily, "Random access capacity evaluation with synchronized MTC users over wireless networks," *IEEE Vehicular Technology Conference*, 2011.
- [37] L. Tello-Oquendo, I. Leyva-Mayorga, V. Pla, J. Martinez-Bauset, J. R. Vidal, V. Casares-Giner, and L. Guijarro, "Performance Analysis and Optimal Access Class Barring Parameter Configuration in LTE-A Networks with Massive M2M Traffic," *IEEE Transactions on Vehicular Technology*, vol. XX, no. XX, p. 1, 2017. [Online]. Available: <http://ieeexplore.ieee.org/document/8119564/>

- [38] K. Edemacu and T. Bulega, “Resource sharing between M2M and H2H traffic under time-controlled scheduling scheme in LTE networks,” *Proceedings of 2014 8th International Conference on Telecommunication Systems Services and Applications, TSSA 2014*, 2015.
- [39] a. Rice and S. Hay, “Decomposing power measurements for mobile devices,” *Pervasive Computing and Communications (PerCom), 2010 IEEE International Conference on*, pp. 70–78, 2010.
- [40] UBlock, “TOBY-L2-MPCI-L2 System Integration Manual,” 2014.
- [41] Analog Devices, “AD625 Datasheet,” 2000.
- [42] IPerf, “iPerf - The ultimate speed test tool for TCP, UDP and SCTP.” [Online]. Available: <https://iperf.fr/>
- [43] Raspberry Pi Foundation, “Raspivid.” [Online]. Available: <https://www.raspberrypi.org/documentation/usage/camera/raspicam/raspivid.md>
- [44] “3GPP TS 32.511 V13.0.0,” 650 Route des Lucioles – Sophia Antipolis Valbonne – France, jan 2016.
- [45] “3GPP TS 36.331 V14.2.2,” 650 Route des Lucioles – Sophia Antipolis Valbonne – France, apr 2017.
- [46] Sigfox, “Sigfox Connect.” [Online]. Available: <https://www.sigfox.com/en>
- [47] RF Wireless World, “SigFox Frame Structure — SigFox MAC Frame Downlink, Uplink.” [Online]. Available: <http://www.rfwireless-world.com/Tutorials/Sigfox-frame-structure.html>
- [48] Newgenapps, “21 Big Data Statistics & Predictions on the Future of Big Data,” 2018. [Online]. Available: <https://www.newgenapps.com/blog/big-data-statistics-predictions-on-the-future-of-big-data>
- [49] S. Andreev, “Understandaing the IoT Connectivity Landscape: A Contemporary M2M Radio Technology Roadmap,” *Risk Management*, vol. V, no. September, pp. 1–9, 2006.
- [50] J. Jeong, D. F. Kimball, M. Kwak, C. Hsia, P. Draxler, and P. M. Asbeck, “Modeling and Design of RF Amplifiers for Envelope Tracking WCDMA Base-Station Applications,” *IEEE Transactions on Microwave Theory and Techniques*, vol. 57, no. 9, pp. 2148–2159, sep 2009.

-
- [51] *Dynamic Power Supply Transmitters*. Cambridge University Press, 2015.
 - [52] H. M. Nemati, A. L. Clarke, S. C. Cripps, J. Benedikt, P. J. Tasker, C. Fager, J. Grahn, and H. Zirath, “Evaluation of a GaN HEMT transistor for load- and supply-modulation applications using intrinsic waveform measurements,” in *Microwave Symposium Digest (MTT), 2010 IEEE MTT-S International*, may 2010, pp. 509–512.
 - [53] H. Jang, Y. Ko, P. Roblin, C. K. Yang, and H. D. Park, “Pulsed load-pull based optimal load-modulation PA design methodology for average efficiency enhancement,” in *Microwave Measurement Symposium (ARFTG), 2011 78th ARFTG*, dec 2011, pp. 1–6.
 - [54] K. Mimis, S. Wang, and G. T. Watkins, “A load-modulated low-power amplifier with average power tracking,” in *Microwave Conference (EuMC), 2015 European*, sep 2015, pp. 88–91.
 - [55] J. Jeong, D. F. Kimball, M. Kwak, C. Hsia, P. Draxler, and P. M. Asbeck, “Wide-band Envelope Tracking Power Amplifiers With Reduced Bandwidth Power Supply Waveforms and Adaptive Digital Predistortion Techniques,” *IEEE Transactions on Microwave Theory and Techniques*, vol. 57, no. 12, pp. 3307–3314, dec 2009.
 - [56] Sbyrnes321, “Mobius Transformation.” [Online]. Available: https://en.wikipedia.org/wiki/Mobius_transformation#/media/File:Smith_chart_explanation.svg
 - [57] G. E. Brehm, J. W. Trippett, and D. W. Jenkins, “Session xiii: microwave oscillators, power combiners and measurement techniques,” in *IEEE International Solid-State Circuits Conference*. San Francisco, CA, USA, USA: IEEE, 1978, pp. 1–2.
 - [58] R. B. Stancliff and D. B. Poulin, “Harmonic load-pull,” in *... Symposium Digest, 1979 IEEE MTT-S ...*. Orlando, FL, USA, USA: IEEE, 1979, pp. 185–187. [Online]. Available: http://ieeexplore.ieee.org/xpls/abs_all.jsp?arnumber=1124014
 - [59] J. I. Upshur, C. White, J. Bayne M.E., B. Davis, J. Walker L., M. Reece, I. Thompson W.L., S. Cheng, R. E. Wallis, J. Bayne, M.E., B. Davis, J. Walker, L., M. Reece, I. Thompson, W.L., S. Cheng, and R. E. Wallis, “Advanced non-linear model for accurate prediction of harmonically terminated power amplifier performance,” *2004 IEEE MTT-S International Microwave Symposium Digest (IEEE Cat. No.04CH37535)*, vol. 2, pp. 1077–1080, 2004.

-
- [60] S. Kelz, M. Schmidt, N. Wolff, M. Berroth, W. Heinrich, and O. Bengtsson, "A 56 W power amplifier with 2-level supply and load modulation," *GeMiC 2016 - 2016 German Microwave Conference*, pp. 185–188, 2016.
- [61] H. M. Nemati, S. S. Member, C. Fager, U. Gustavsson, S. S. Member, R. Jos, H. Zirath, and S. S. Member, "Design of Varactor-Based Tunable Matching Networks for Dynamic Load Modulation of High Power Amplifiers," vol. 57, no. 5, pp. 1110–1118, 2009.
- [62] K. Chen and D. Peroulis, "Design of Adaptive Highly Efficient GaN Power Amplifier for Octave-Bandwidth Application and Dynamic Load Modulation," *IEEE Transactions on Microwave Theory and Techniques*, vol. 60, no. 6, pp. 1829–1839, jun 2012.
- [63] Q. Liu, V. Adrian, B.-h. Gwee, S. Member, J. S. Chang, and S. Member, "A Class-E RF Power Amplifier with a Novel Matching Network for High-Efficiency Dynamic Load Modulation," pp. 2–5, 2017.
- [64] S. Probst, L. Berkemann, L. Bernard, B. Geck, and D. Manteuffel, "Investigation of the Dynamic Load Modulation of an Inverse Class-F Power Amplifier with an Adaptive Matching Network," pp. 20–22, 2018.
- [65] S. Probst, B. Luers, and B. Geck, "Load modulation with an adaptive matching network based on MEMS for efficiency enhancement of an inverse class-F power amplifier," *GeMiC 2016 - 2016 German Microwave Conference*, pp. 181–184, 2016.
- [66] A. M. Mahmoud Mohamed, S. Boumaiza, and R. R. Mansour, "Reconfigurable doherty power amplifier for multifrequency wireless radio systems," *IEEE Transactions on Microwave Theory and Techniques*, vol. 61, no. 4, pp. 1588–1598, 2013.
- [67] M. A. De Jongh, A. Van Bezooijen, K. R. Boyle, and T. Bakker, "Mobile phone performance improvements using an adaptively controlled antenna tuner," *IEEE MTT-S International Microwave Symposium Digest*, pp. 3–6, 2011.
- [68] X. Ruan, Y. Wang, and Q. Jin, "A Review of Envelope Tracking Power Supply for Mobile Communication Systems," vol. 2, no. 4, pp. 277–291, 2017.
- [69] B. Sahu, S. S. Member, G. A. Rincón-mora, and S. S. Member, "A High-Efficiency Linear RF Power Amplifier With a Power-Tracking Dynamically Adaptive Buck-Boost Supply," vol. 52, no. 1, pp. 112–120, 2004.
- [70] Peregrine Semiconductor, "Product Specification," Tech. Rep., 2012. [Online]. Available: <http://www.psemi.com/pdf/datasheets/pe64102ds.pdf>

- [71] T. Barton, “Not Just a Phase: Outphasing Power Amplifiers,” *IEEE Microwave Magazine*, vol. 17, no. 2, pp. 18–31, 2016.